PHASE DIAGRAM FOR THE S EQUALS ONE-HALF AND J EQUALS THREE-HALVES KONDO LATTICE MODEL

A Dissertation
Submitted to
the Temple University Graduate Board

In Partial Fulfillment
of the Requirements for the Degree
DOCTOR OF PHILOSOPHY

---

by
Miguel J. Abele
December 2018

Examining Committee Members:

Peter Riseborough, Advisory Chair, Dept. of Physics
Maria Iavarone, Temple University Dept. of Physics
Andreas Metz, Temple University Dept. of Physics
Spiridoula Matsika, External Member, Temple University Dept. of Chemistry

ABSTRACT

A Kondo lattice Hamiltonian for arbitrary total angular momentum J is formulated using a pseudofermion representation and without addition of RKKY interaction terms. An Hartree-Fock treatment is applied, and both variational and Green's function methods are used to calculate physical quantities from the linearized Hamiltonian. The Kondo phase is represented by finite hybridization. Magnetic ordering is examined via ordering vectors, but coexistence with the Kondo phase is not allowed. Phase diagrams are produced in S=1/2 and J=3/2 with second-order transitions at Kondo-paramagnetic and magnetic-paramagnetic boundaries, and first order transitions between Kondo and magnetic phases. Various coupling strengths are explored. Magnetic phases found include antiferromagnetism, ferromagnetism, and spin-density wave ordering of both commensurate and incommensurate varieties. In S=1/2, the magnetic phase exhibits a spike in critical temperature at half-filling. In J=3/2, the Kondo phase is reentrant at weaker coupling but not at stronger coupling.

This work is dedicated to Lisa and Lillian

ACKNOWLEDGMENTS

This research was supported by the US Department of Energy, Office of Basic Energy Sciences, Materials Science through award no. DF-FG02-01ER45872. This research includes calculations carried out on Temple University's HPC resources and thus was supported in part by the National Science Foundation through major research instrumentation grant number 1625061 and by the US Army Research Laboratory under contract number W911NF-16-2-0189.

Insightful conversations with Sergio Magalhães of the Universidade Federal do Rio Grande do Sul, Brazil, were made possible by the American Physical Society and the Sociedade Brasileira de Física.

I would like to express my gratitude to the following individuals, all of whom have either supported me in or enabled my pursuit of education in Physics: Christopher and Barbara Schmidt, Tom Kiely, and Peter Riseborough.

TABLE OF CONTENTS

LIST OF FIGURES

LIST OF TABLES

CHAPTER 1

INTRODUCTION

1.1 A Brief History of the Kondo Model

In the 1934, de Haas, de Boer, and Van den Berg measured the resistivities of several metals as a function of temperature [4]. Specifically for two gold samples, an unexpected behavior was observed: at low temperatures, the samples each exhibited minima in their resistivities. The occurrence of such minima puzzled researchers for decades. By the 1960's, it was believed that the phenomenon was related to impurities in metal samples. Further evidence of this was seen, for example, in the work of Van den Berg and de Nobel [5] on silver wires with manganese impurities, where the resistivity minima only appeared at low concentrations of manganese. Indeed, in 1964 Jun Kondo published an "s-d exchange" model with which he showed, via perturbation expansion, the occurrence of a minimum. In particular he calculated a resistivity due to spin contributions of

$$\rho \propto c\rho_M(1+\frac{3zJ}{\varepsilon_f}\mathrm{Ln}T) \tag{1}$$

where c is the concentration of the impurity and T is the temperature of the sample. In other words, he produced a resistivity which showed a minimum with respect to temperature. He also phenomenologically calculated the position of the minimum with respect to temperature as being proportional to $c^{1/5}$. Over time, Kondo's contribution to this mystery has led

to the resistivity minimum, as well as other related observable behaviors, to be dubbed the Kondo effect.

Kondo's s-d exchange Hamiltonian describes interactions between conduction band spins and a single impurity spin. Likewise, it does not describe impurity-impurity interactions. In total, this model applies to dilute magnetic alloys: when the concentration of impurities is very low, one may neglect impurity-impurity interactions and thereby treat only a single impurity. The model itself is related to the Anderson model. In the limit of strong coupling, or large U, Schrieffer and Wolff showed that the Kondo model could be reached from the Anderson model via transformation [6]. The large-U limit corresponds to localization of the impurity spin, and it has since been shown that not only do transformations exist which do not require the large-U limit [7], but also that the Schrieffer-Wolff transformation holds for the periodic Anderson and lattice Kondo models [8, 9, 10].

An important point about the perturbative treatment of the Kondo model is that the logarithmic dependence of the resistivity upon the temperature persists down to zero-temperature. This logarithmic divergence is unphysical and was referred to as the Kondo problem. However, in the decades to follow, greater understandings of the Kondo effect and the Kondo problem have been reached. The Kondo effect can be said to result from the formation of a many-body resonance at the Fermi level. This is an Abrikosov-Suhl resonance, or, for systems exhibiting the Kondo effect, the Kondo resonance. The width of this resonance is $k_B T_K$. T_K, or the Kondo temperature, is a characteristic temperature for the system. Importantly, the Kondo model describes a system where, at temperatures above T_K, the interaction between conductions spins and the impurity spin is weak, but at temperatures below T_K, the interaction is strong. That the interaction is strong for temperatures below T_K leads to the failure of the perturbation method and thus to the appearance of a logarithmic divergence in the resistivity.

The Kondo problem was resolved in 1975 when Wilson showed, through his numerical renormalization group method [11], that the divergence in the resistivity did not occur and was an artifact of the analyses theretofore used. By 1980, exact solutions for the model had been produced by Andrei [12] and Wigman [13] using the Bethe ansatz. The year 1980 does not signal the cessation of active interest in the Kondo model, however.

The lattice Kondo model, which is the subject of this work, was introduced in 1977 by Doniach [14]. Doniach described a necklace of interacting impurities; he used a one-dimensional lattice with an impurity in each unit cell. With an impurity spin in each unit cell, this model necessarily does not describe a dilute magnetic alloy, but rather a dense one. With a dense alloy, the neglect of impurity-impurity interactions is inappropriate. To treat this interaction, Doniach used the Ruderman-Kittel-Kasuya-Yosida (RKKY) interaction, through which he explored a competition between two behaviors: the magnetic ordering of the impurity spins via the RKKY interaction; and the screening of the impurity spins, and hence non-magnetism, via the Kondo interaction.

For several decades, the phase diagram for the single-impurity Kondo model has continued to be a matter of some interest due, in part if not entirely, to its behavior below its characteristic temperature, T_K. As mentioned above, at temperatures below T_K, perturbative methods for solution fail. Most notably, below this temperature, the specific heat becomes remarkably large [15]. In a concentrated magnetic alloy, modeled by a lattice, there are two possible scales, T_K, which marks the formation of singlet states, and T^*, which marks the onset of a coherent Fermi liquid [16]. Analagous to the behavior of a dilute magnetic alloy at $T < T_K$, a concentrated alloy at $T < T^*$ displays heavy fermion behavior [15]. This behavior is still of interest today, not only in superconducting systems but in topological systems as well [17, 18].

The competition between the magnetic phase and the non-magnetic suggests an either-or solution. However, as researchers have either discovered or fabricated materials that can

be classified as dense alloys describable by Kondo lattices, many heavy fermion materials have been found to exhibit small magnetic moments. $CeCu_6$, for example, is non-magnetic, although evidence suggests a Néel temperature of 2 mK [19]. When it is doped with gold, it shows Fermi liquid characteristics [20, 21] as well as an ordered moment of .1 to .15 μ_B [21] despite that the free moment of Ce^{3+} is 2.56 μ_B. $CePd_2Al_3$ is another Kondo material [22] with an usually small ordered moment of .47 μ_B [23]. URu_2Si_2, rather infamous for its so-called hidden order phase, has an ordered moment in the normal state of .03 μ_B for its $5f$ electron [24]. However, it has a large-moment antiferromagnetic (AFM) phase in which the moment has been measured at .4 μ_B [25, 26]. A final example is $YbCu_3Al_2$, which has been found to have an integer valence, a Néel temperature of 2 K, and an ordered moment of 2.1 μ_B [27] which is much reduced from the Yb^{3+} moment of 4.54 μ_B [28]. In many of these materials, it has been supposed that the Kondo effect suppressed the ordered moments, or, in other words, that Kondo-type screening of the magnetic moment is present but incomplete.

The richness of the questions of crossovers and instabilities to magnetic ordering only increases. Recently there has been work in quantum critical points through the study of the Hall effect [29] in $YbRh_2Si_2$. In this material and others, the system under study is a heavy fermion material where there exists a continuous transition which can be pushed to $T = 0$. In particular, for $YbRh_2Si_2$, the transition is an magnetic one, and there have been questions surrounding the Kondo breakdown around this critical point [30].

1.2 Subjects of Interest to This Work

The primary goal of this work is to provide a phase diagram for the Kondo lattice model. Doniach studied a one-dimensional lattice [14] and visited the matter of the correspondence between his pseudospin chain and a Coulomb gas via the Yuval-Anderson transformation

[31]. One-dimensional phase diagrams were produced by Ueda *et al* in 1993 [32] and also by Fazekas and Müller-Hartmann in 1991 as a part of a larger examination [33]. In two dimensions, quantum critical point research led to a phase diagram by Li *et al* in 2015 [2]. In 2017, Costa *et al* treated classical spin averages and two dimensions in their diagram [3]. Notably, Lacroix and Cyrot published their three-dimensional lattice phase diagram in 1979 [1].

This work will study a three-dimensional lattice in the Hartree-Fock method. Overall, comparisons with one-dimensional diagrams will not be made in this work, but will be made with two- and three-dimensional ones. In this work, two sets of phase diagrams will be produced: one in S=1/2, and one in J=3/2. While the S=1/2 phase diagram will allow for comparison with other works, such as the diagram of Lacroix and Cyrot, it is the set of J=3/2 diagrams reported here which is, to the author's knowledge, a new finding.

Among the questions that arose from the lattice model was that of conduction electron exhaustion [34]. In the picture of a single impurity, conduction electrons are bound to the local magnetic moment and form a magnetic singlet state. For a system with a Kondo temperature T_K, these compensating or screening electrons come within $k_B T_K$ of the Fermi level. If in the lattice this screening happens at every magnetic site and T_K is low, there may not be enough electrons to compensate every local spin. Is there some threshold in the conduction occupation above which the moments are screened and below which the conduction electrons are exhausted before screening is be complete? It was shown in 2000 [16] that the exhaustion problem does not arise, and that T^* and T_K are indeed the same length scale. Nevertheless, exhaustion is a question that this work touches upon.

Trends in the phase diagrams of this work will also be discussed in connection with the spin-orbit degeneracy of a magnetic alloy. As the degeneracy of states, $N = 2J + 1$, grows large, an expansion can be made in terms of the small quantity $1/N$ [35]. If one examines the stability of the Kondo phase against magnetic ordering, where the conduction electrons

are coupled to the local moments via coupling constant $\mathcal{J}$, and where the conduction band density of states at the Fermi level is ρ, one finds that $\mathcal{J}\rho$ of order $1/(2J+1)$ is required [36]. The $1/N$ expansion shows that, as temperature increases, even as the lattice correlations are destroyed, the system still behaves as a system of isolated impurities as N grows large [37]. In this work, systems of $S = 1/2$ and $J = 3/2$ are considered with respect to coupling strengths as well as to phase boundaries with paramagnetism (PM). In examining the critical temperature of the magnetically-ordered phase and T_K for the Kondo phase, this work provides support to the argument that increasing degeneracy leads to increasing stability of the Kondo phase.

As mentioned in the previous section, several dense alloy, or concentrated Kondo systems, have been identified wherein small ordered moments coexist with heavy-fermion behavior. This work will examine first-order transitions between the Kondo and magnetically-ordered (MO) phases but will not consider coexistence of phases. However, coexistence is considered by Li *et al* [2] and Costa *et al* [3] for their diagrams in two-dimensional systems.

Towards producing the phase diagrams in this work, and in order to provide a strong foundation for an exploration of nearly-filled and nearly-empty conduction bands, it is necessary to address the matter of the conduction band density of states. In both the phase diagram of Lacroix and Cyrot [1] and the $1/N$ expansion of Coleman [36], the conduction band density of states is taken to be constant or featureless. This dissociates their work from a specific crystal lattice. In the slave-boson approach to the $1/N$ expansion, Burdin *et al* [16] use a semi-circular density of states, but their focus is on the scales T^* and T_K. Ohashi *et al* [38] and Li *et al* [2] both use tight-binding dispersion relations for the conduction electrons which lead to non-flat densities of states. However, the use of tight-binding approximations complicates model calculations and thereby leads to numerical computation. In this work, in which a tight-binding approximation is used, this complication is especially important when an ordering vector is introduced.

1.3 Aims and Outline

Several methods will be combined in this work to produce a new diagram in J=3/2. For S=1/2, a phase diagram has already been done for three dimensions [1] and a phase diagram has already been done in a self-consistent mean-field treatment [2]. In S=1/2, this work may be thought of as a bridge between them: this work will use neither AFM sublattices nor a flat density of states, yet it will take the tight-binding and mean-field approximations to three dimensions; it will not use classical spin averages, but will not examine the coexistence of hybridization and magnetic ordering.

This work will explore magnetic-ordering without the addition of an local-itinerant spin-exchange interaction necessary to produce an RKKY interaction. A Kondo-type Hamiltonian is used here which can produce magnetic ordering solely through the application of an ordering vector. Altogether, this work examines the following phases both by variation and by Green's function methods: the normal paramagnetic (PM) phase, the Kondo phase, and the magnetically-ordered (MO) phase, which includes spin density wave (SDW) magnetism and ferromagnetism (FM). The coherent Fermi-liquid phase is not examined.

This dissertation is presented as follows. In chapter 2, the Hamiltonian is presented. In chapter 3, linearization of the Hamiltonian is performed and assumptions stated so that the Kondo phase may be explored first at finite temperature and then at zero temperature. In chapter 4, a similar linearization is performed so that the magnetic phase may be explored. In chapter 5, the numerical implementation, algorithms, and challenges are summarized, and finally, the phase diagram is presented along with a discussion of results. The appendix and other materials follow after.

CHAPTER 2

THE MODEL

2.1 The Hamiltonian

The lattice Kondo model will be expressed with the following Hamiltonian:

$$H = H_0 + H_{int}\,. \tag{2}$$

For the noninteracting portion of the Hamiltonian,

$$H_0 = -t \sum_{i,i',j} c^{\dagger}_{i,j} c_{i',j}, \tag{3}$$

where $c_{i,j}$ ($c^{\dagger}_{i,j}$) destroys (creates) a particle in the conduction band (or an itinerant moment) at site i with total angular momentum J and a J_z-value of j. Terminology regarding the conduction band and itinerant moments will be used interchangeably in this work. The tight-binding dispersion relation for the conduction electrons in a simple cubic lattice, with only nearest-neighbor terms retained, is

$$\varepsilon_{\mathbf{k}} = -2t \sum_{\mathbf{k}} \left(cos(k_x a_x) + cos(k_y a_y) + cos(k_z a_z) \right). \tag{4}$$

such that in (4) the coordinate c-operators are replaced by their momentum-space counterparts, which destroy or create said moments with Bloch momentum $\mathbf{k}$. Lattice spacing is

chosen here so that $a_x = a_y = a_z = 1$, and

$$\sum_{\mathbf{k}} = N. \tag{5}$$

In this work, $\mathbf{k}$ is restricted to the first Brillouin zone. The bandwidth of the conduction electrons is $12t$. For the interacting portion of the Hamiltonian,

$$H_{int} = \mathcal{J} \sum_i \hat{\mathbf{S}}_i \cdot \hat{\mathbf{M}}_i \tag{6}$$

where $\mathcal{J}$ represents the interaction potential, and the summation is over lattice sites, i. $\hat{\mathbf{S}}$ and $\hat{\mathbf{M}}$ represent the total angular momentum operators of the itinerant and local moments:

$$\begin{aligned} \hat{\mathbf{S}}_l &= \sum_{j,j'} c^\dagger_{i,j} \hat{\mathbf{s}}_{jj'} c_{i,j'}\,, \\ \hat{\mathbf{M}}_l &= \sum_{j,j'} f^\dagger_{i,j} \hat{\mathbf{m}}_{jj'} f_{i,j'}\,. \end{aligned} \tag{7}$$

The above has been expressed in a pseudofermion representation with the operator, $f_{\mathbf{k},j}$, destroying a local (or impurity) moment in a manner analogous to the c-operator and the itinerant moments. The operators c and f satisfy the anticommutator ($[..]_+$) relations,

$$\begin{aligned} \left[c_{\mathbf{k},j}, c^\dagger_{\mathbf{k}',j'}\right]_+ &= \delta(\mathbf{k}-\mathbf{k}')\delta_{j,j'} \\ \left[f_{\mathbf{k},j}, f^\dagger_{\mathbf{k}',j'}\right]_+ &= \delta(\mathbf{k}-\mathbf{k}')\delta_{j,j'} \\ \text{All others} &= 0. \end{aligned} \tag{8}$$

A Lagrange multiplier is added to the Hamiltonian (2) to provide the constraint upon the dynamics that any impurity site is only singly occupied:

$$\lambda \sum_{\mathbf{k},j} \left(f^{\dagger}_{\mathbf{k},j} f_{\mathbf{k},j} - 1 \right), \text{ or, per particle,}$$
$$\lambda \left(\frac{1}{N} \sum_{\mathbf{k},j} f^{\dagger}_{\mathbf{k},j} f_{\mathbf{k},j} - 1 \right). \tag{9}$$

As a further constraint, transverse interaction terms will account for J_z-changes of unity only, i.e., $\Delta J_z = \pm 1$.

Writing out (2) in momentum-space representation and using the expressions of (3) through (9):

$$\begin{aligned} H = & \sum_{\mathbf{k},j} \varepsilon_k c^{\dagger}_{\mathbf{k},j} c_{\mathbf{k},j} + \lambda \left(\sum_{\mathbf{k},j} f^{\dagger}_{\mathbf{k},j} f_{\mathbf{k},j} - N \right) \\ & + \frac{\mathcal{J}}{N} \sum_{\mathbf{k},\mathbf{k}',j,j'} j j' c^{\dagger}_{\mathbf{k},j} c_{\mathbf{k},j} f^{\dagger}_{\mathbf{k}',j'} f_{\mathbf{k}',j'} \\ & + \frac{\mathcal{J}}{N} \sum_{\mathbf{k},\mathbf{k}',\mathbf{q},j,j'} \frac{r_j r_{j'}}{2} c^{\dagger}_{\mathbf{k},j+1} c_{\mathbf{k}+\mathbf{q},j} f^{\dagger}_{\mathbf{k}'+\mathbf{q},j'} f_{\mathbf{k}',j'+1} \\ & + \frac{\mathcal{J}}{N} \sum_{\mathbf{k},\mathbf{k}',\mathbf{q},j,j'} \frac{r_j r_{j'}}{2} c^{\dagger}_{\mathbf{k}+\mathbf{q},j} c_{\mathbf{k},j+1} f^{\dagger}_{\mathbf{k}',j'+1} f_{\mathbf{k}'+\mathbf{q},j'} \end{aligned} \tag{10}$$

The interaction terms (second through fourth lines) of (10) are gotten by expressing the dot-product of (6) as

$$\hat{\mathbf{S}}_i \cdot \hat{\mathbf{M}}_i = \hat{S}^z_i \hat{M}^z_i + \frac{1}{2} \left(\hat{S}^+_i \hat{M}^-_i + \hat{S}^-_i \hat{M}^+_i \right), \tag{11}$$

and in this manner, the r-constants are seen to represent the matrix elements of the rotation operator for the total angular momentum, or,

$$r_j = \sqrt{J(J+1) - j(j+1)}. \tag{12}$$

In the magnetic ordering analysis of chapter 4 below, the z-component will be taken as the longitudinal one.

2.2 The Hartree-Fock Method

The Hartree-Fock method involves several approximations and assumptions, the overall effect of which has been reached historically in several different ways, from partial summations of diagrams [39] to self-consistent approximations. Involved in the method are: a) the Born-Oppenheimer approximation; b) the neglect of relativistic effects; c) a variational solution formed from a finite, nearly-complete basis set; d) eigenfunctions built from a Slater determinant of anti-symmetrized single-particle wave functions; and e) the mean-field approximation.

That item (a) has been fulfilled already is evident from the formulation of the model Hamiltonian in section 2.1, above, wherein the electrons and moments have been referenced by site indices. This implies that the ions in the lattice are fixed, or rather that the lattice is rigid, and that, hence, the Born-Oppenheimer approximation has been made.

Item (b) is fulfilled through less obvious means. The Kondo model can be reached via Schrieffer-Wolff transformation from the Anderson model [6]. Under this transformation, the weak interaction limit of the Kondo model corresponds to the large-U limit of the Anderson model [10]. In this way, the impurity moment is completely localized. Hence, the transformation implies an integer occupation of the valence electron at the impurity site. The Hamilton of (10) meets this criterion through both its Lagrange multiplier (9) and its conservation of J_z-number in H_{int}. With this connection established, the Anderson model can be discussed. In particular, the terms in the Anderson model do not include relativistic effects [40]. Hence, the absence of these effects is carried over via transformation to the Kondo model.

Item (e) is fulfilled by the linearization of the Hamiltonian in the sections to follow, which amounts to neglect of fluctuations and thus a mean-field treatment.

Finally, in this work the Hamiltonian is linearized into terms built from operator pairs. Two routes are then taken. First, the Hamiltonian is varied and extremized in order to produce an expression for the canonical free energy as well as self-consistency equations. Second, fermionic single-particle Green's functions are written and solved with the equation of motion method. From these Green's functions are calculated various quantities, including self-consistency equations. In each case, the two routes lead to the same results, as is pointed out by Roth [41]. Moreover, the basis set of operators, as also described by Roth, are the c- and f-operators which are used to construct the Green's functions. Hence, items (c) and (d) are satisfied.

CHAPTER 3

THE KONDO PHASE

3.1 Mean-Field Approximation

The Hamiltonian will be linearized by taking two-operator pairs and replacing them with their thermodynamic averages. This is done in the interaction terms, where there are four operators. The result is a variety of terms consisting of an average multiplied by two remaining operators, plus one term consisting of two average values which must be adjusted for double-counting. In the Kondo phase, the quantities of interest will be the hybridization constants,

$$V_j = \frac{1}{N}\sum_k \langle c^\dagger_{\mathbf{k},j} f_{\mathbf{k},j} \rangle \,, \tag{13}$$

which will be examined as nonzero only in this phase. The thermodynamic average is defined, for an arbitrary operator O,

$$\langle O \rangle = \frac{\mathrm{Tr}[e^{-\beta H} O]}{\mathrm{Tr}[e^{-\beta H}]}. \tag{14}$$

Moreover, in the Kondo phase, it is assumed that no magnetization is present. A simple way to enforce this condition, expressed as

$$n_{\chi,j} - n_{\chi,j'} = 0 \quad \forall j \neq j' \quad \text{and} \quad \chi \in c, f,$$

where the itinerant and local moment occupation numbers are defined as

$$\begin{aligned} n_{c,j} &= \frac{1}{N}\sum_{\mathbf{k}} \langle c^{\dagger}_{\mathbf{k},j} c_{\mathbf{k},j} \rangle = \langle c^{\dagger}_{j} c_{j} \rangle \\ n_{f,j} &= \frac{1}{N}\sum_{\mathbf{k}} \langle f^{\dagger}_{\mathbf{k},j} f_{\mathbf{k},j} \rangle = \langle f^{\dagger}_{j} f_{j} \rangle, \end{aligned} \tag{15}$$

is to set all occupation numbers equal. In other words,

$$\begin{aligned} n_{c,j} &= n_c, \quad \text{and} \\ n_{f,j} &= n_f \quad \forall j. \end{aligned} \tag{16}$$

It follows that, in the linearization of the Hamiltonian,

$$\sum_j j \langle c^{\dagger}_{j} c_{j} \rangle = \sum_j j \langle f^{\dagger}_{j} f_{j} \rangle = 0. \tag{17}$$

The condition of zero net magnetization will also be enforced by taking the staggered averages to be zero:

$$\frac{1}{N}\sum_{\mathbf{k}} \langle f^{\dagger}_{\mathbf{k}-\mathbf{q},j+1} f_{\mathbf{k},j} \rangle = \frac{1}{N}\sum_{\mathbf{k}} \langle c^{\dagger}_{\mathbf{k}-\mathbf{q},j+1} c_{\mathbf{k},j} \rangle = 0. \tag{18}$$

Applying the above considerations, the linearized Hamiltonian becomes

$$\begin{aligned} H = &\sum_{\mathbf{k},j} \varepsilon_k c^\dagger_{\mathbf{k},j} c_{\mathbf{k},j} + \lambda \left(\sum_{\mathbf{k},j} f^\dagger_{\mathbf{k},j} f_{\mathbf{k},j} - N \right) \\ &- \mathcal{J} \sum_{\mathbf{k},j} \left(j^2 V_j f^\dagger_{\mathbf{k},j} c_{\mathbf{k},j} + \frac{r_j^2}{2} V_j f^\dagger_{\mathbf{k},j+1} c_{\mathbf{k},j+1} + \frac{r_j^2}{2} V_{j+1} f^\dagger_{\mathbf{k},j} c_{\mathbf{k},j} \right) \\ &+ \text{H.C.} + \text{constant terms.} \end{aligned} \tag{19}$$

The three interaction terms simplify if, in the second line, j is shifted down by one unit. Performing this shift, the interaction terms become

$$j^2 V_j f^\dagger_{\mathbf{k},j} c_{\mathbf{k},j} + \frac{r_{j-1}^2}{2} V_{j-1} f^\dagger_{\mathbf{k},j} c_{\mathbf{k},j} + \frac{r_j^2}{2} V_{j+1} f^\dagger_{\mathbf{k},j} c_{\mathbf{k},j}. \tag{20}$$

As a result of the hybridization definition (13) as well as the zero-value assumption (18), the mean-field expression (20) contains no terms involving J_z changes; every pair of operators involves the same j. The only instances where two different j values are present in the same term are in the interaction terms, between the hybridization constants and the operators. This suggests that by dropping the J_z-dependence of V, the Hamiltonian might be reduced to $2J+1$ mutually non-interacting subsystems, which is a situation in and of itself self-consistent with a J_z-independent hybridization. Hence, a major assumption will now be made that the hybridized interaction is isotropic.

With the assumption of isotropy, $V_j \to V$, and, recalling the definition (12),

$$j^2 + \frac{r_{j-1}^2}{2} + \frac{r_j^2}{2} = J(J+1). \tag{21}$$

This, in the pseudofermion framework, is consistent with the spin-rotational invariance one would expect from a single particle of spin $S = J$ and orbital angular momentum $L = 0$. Use of (21) permits the simplication of the interaction terms in (19) as well as the constant

terms, which will now be explicitly shown.

$$\begin{aligned}
&\mathcal{J}N\sum_j j^2\frac{1}{N}\sum_{\mathbf{k}}\langle c^\dagger_{\mathbf{k},j}f_{\mathbf{k},j}\rangle\frac{1}{N}\sum_{\mathbf{k}'}\langle f^\dagger_{\mathbf{k}',j}c_{\mathbf{k}',j}\rangle\\
&+\mathcal{J}N\sum_j \frac{r_j^2}{2}\frac{1}{N}\sum_{\mathbf{k}}\langle c^\dagger_{\mathbf{k},j}f_{\mathbf{k},j}\rangle\frac{1}{N}\sum_{\mathbf{k}'}\langle c^\dagger_{\mathbf{k}',j+1}f_{\mathbf{k}',j+1}\rangle\\
&+\mathcal{J}N\sum_j \frac{r_j^2}{2}\frac{1}{N}\sum_{\mathbf{k}}\langle c^\dagger_{\mathbf{k},j+1}f_{\mathbf{k},j+1}\rangle\frac{1}{N}\sum_{\mathbf{k}'}\langle c^\dagger_{\mathbf{k}',j}f_{\mathbf{k}',j}\rangle\\
&=2N\mathcal{J}J(J+1)(2J+1)|V|^2, \qquad (22)
\end{aligned}$$

where the extra (2J+1) comes from summing over the J_z states. After adjustment for double-counting, the Hamiltonian becomes, altogether,

$$\begin{aligned}
H=&\sum_{\mathbf{k},j}\varepsilon_k c^\dagger_{\mathbf{k},j}c_{\mathbf{k},j}+\lambda\left(\sum_{\mathbf{k},j}f^\dagger_{\mathbf{k},j}f_{\mathbf{k},j}-N\right)\\
&-\mathcal{J}J(J+1)\sum_{\mathbf{k},j}\left(Vf^\dagger_{\mathbf{k},j}c_{\mathbf{k},j}+V^\dagger c^\dagger_{\mathbf{k},j}f_{\mathbf{k},j}\right)\\
&+N\mathcal{J}J(J+1)(2J+1)|V|^2. \qquad (23)
\end{aligned}$$

In (23) and the steps leading up to it, the value of J has been left unspecified. Unlike for the magnetically-ordered phase, the equations for the Kondo phase can be written and solved with an arbitrary, integer or half-integer J. Further demonstration of this appears below in the use of the variational method.

3.2 Finite Temperature

Variational Method

Due to the assumption of isotropy and the resulting creation of $2J+1$ mutually non-interacting subsystems, each J_z subsystem may be represented by its own Hamiltonian, so

that the sum is

$$H = \sum_{\mathbf{k},j} H_{\mathbf{k},j}, \tag{24}$$

with

$$\mathbf{H}_{\mathbf{k},j} = \begin{pmatrix} \varepsilon_{\mathbf{k}} & -\mathcal{J}J(J+1)V^{\dagger} \\ -\mathcal{J}J(J+1)V & \lambda \end{pmatrix}. \tag{25}$$

One immediately sees that (25) does not contain any J_z-dependence on the right-hand side. Then, using the vector representation,

$$\phi^{\dagger}_{\mathbf{k},j} = \left[c^{\dagger}_{\mathbf{k},j} f^{\dagger}_{\mathbf{k},j}\right], \tag{26}$$

the Hamiltonian can be expressed as

$$H = E_0^K + \sum_{\mathbf{k},j} \phi^{\dagger}_{\mathbf{k},j} \mathbf{H}_{\mathbf{k},j} \phi_{\mathbf{k},j}\,, \tag{27}$$

where

$$E_0^K = NJ(J+1)(2J+1)\mathcal{J}|V|^2 - N\lambda\,. \tag{28}$$

The Hamiltonian in (27) can be written in an equivalent fashion by replacing the four 2×2 matrices and four 2×1 column vectors in the summation with a single $2(2J+1)\times 2(2J+1)$ matrix and a $2(2J+1)\times 1$ column vector. The matrix will be block diagonal, and the vector will be the original 2×1 vectors stacked one upon the other. Rewriting the Hamiltonian in this way may make the multiplicity of the eigenvalues much more obvious, but will otherwise add nothing to the conversation.

The matrix (25) has eigenvalues and associated bands of

$$w^{\pm}(\mathbf{k}) = \tfrac{\varepsilon_{\mathbf{k}}+\lambda}{2} \pm \sqrt{\left(\tfrac{\lambda-\varepsilon_{\mathbf{k}}}{2}\right)^2 + J^2(J+1)^2\mathcal{J}^2|V|^2} \tag{29}$$

For the free energy of the system, the diagonalized Hamiltonian is written out using the new operators, W,

$$H' = E_0^K + \sum_{\mathbf{k},j} w^+(\mathbf{k}) W^\dagger_{\mathbf{k},j,+} W_{\mathbf{k},j,+} + \sum_{\mathbf{k},j} w^-(\mathbf{k}) W^\dagger_{\mathbf{k},j,-} W_{\mathbf{k},j,-}\,. \tag{30}$$

The free energy for a canonical ensemble is

$$\begin{aligned} \mathcal{F} &= -\beta^{-1}\,\mathrm{Ln}\,\mathrm{Tr}\,\mathrm{e}^{-\beta H'}\text{, or} \\ &= \langle E\rangle - TS, \end{aligned} \tag{31}$$

where β is the thermodynamic variable, $(k_B T)^{-1}$. As demonstrated in appendix A, the free energy can be rewritten as

$$\begin{aligned} \mathcal{F} = NE_0^K &+ \sum_{\mathbf{k},j} w^+(\mathbf{k}) f\left(w^+(\mathbf{k})\right) + \sum_{\mathbf{k},j} w^-(\mathbf{k}) f\left(w^-(\mathbf{k})\right) \\ &+ \beta^{-1}\sum_{\mathbf{k},j} f\left(w^+(\mathbf{k})\right)\,\mathrm{Ln}\, f\left(w^+(\mathbf{k})\right) + \beta^{-1}\sum_{\mathbf{k}j} f\left(w^-(\mathbf{k})\right)\,\mathrm{Ln}\, f\left(w^-(\mathbf{k})\right) \\ &+ \beta^{-1}\sum_{\mathbf{k},j} \left[1-f\left(w^+(\mathbf{k})\right)\right]\,\mathrm{Ln}\,\left[1-f\left(w^+(\mathbf{k})\right)\right] \\ &+ \beta^{-1}\sum_{\mathbf{k},j} \left[1-f\left(w^-(\mathbf{k})\right)\right]\,\mathrm{Ln}\,\left[1-f\left(w^-(\mathbf{k})\right)\right], \end{aligned} \tag{32}$$

where $f()$ is a suggestively chosen function which is, ultimately, determined by variation to be the Fermi-Dirac function (see appendix A),

$$f(x) = \left(\mathrm{e}^{\beta(x-\mu)}+1\right)^{-1}, \tag{33}$$

with μ representing the chemical potential. However, in the above expression summations over j must be carried out. Because the eigenvalues w do not depend on j, this allows $\mathcal{F}$ to be written in a slightly more explicit fashion:

$$\begin{aligned}(2J+1)^{-1}\mathcal{F} = {} & N^2 J(J+1)\mathcal{J}|V|^2 - (2J+1)^{-1}N\lambda \\ & + \sum_{\mathbf{k}} w^+(\mathbf{k}) f\left(w^+(\mathbf{k})\right) + \sum_{\mathbf{k}} w^-(\mathbf{k}) f\left(w^-(\mathbf{k})\right) \\ & + \beta^{-1}\sum_{\mathbf{k}} f\left(w^+(\mathbf{k})\right) \operatorname{Ln} f\left(w^+(\mathbf{k})\right) + \beta^{-1}\sum_{\mathbf{k}} f\left(w^-(\mathbf{k})\right) \operatorname{Ln} f\left(w^-(\mathbf{k})\right) \\ & + \beta^{-1}\sum_{\mathbf{k}} \left[1 - f\left(w^+(\mathbf{k})\right)\right] \operatorname{Ln}\left[1 - f\left(w^+(\mathbf{k})\right)\right] \\ & + \beta^{-1}\sum_{\mathbf{k}} \left[1 - f\left(w^-(\mathbf{k})\right)\right] \operatorname{Ln}\left[1 - f\left(w^-(\mathbf{k})\right)\right] . \end{aligned} \tag{34}$$

Minimizing (34) with respect to V^+ or V^-, a self-consistency equation is obtained:

$$\frac{1}{\mathcal{J}} = \frac{J(J+1)}{2N}\sum_{\mathbf{k}} \frac{f\left(w^-(\mathbf{k})\right) - f\left(w^+(\mathbf{k})\right)}{\sqrt{\left(\frac{\lambda - \varepsilon_{\mathbf{k}}}{2}\right)^2 + J^2(J+1)^2\mathcal{J}^2|V|^2}}. \tag{35}$$

Satisfaction of (35) requires that $\mathcal{J} > 0$.

Green's Function Method

The single-particle temperature Green's function is defined as, for arbitrary fermionic operators a and b, and for imaginary time $\tau = it$,

$$\begin{aligned}\langle\langle a_{\mathbf{k},j}(\tau)|b^\dagger_{\mathbf{k}',j'}(\tau')\rangle\rangle &= -\langle \mathcal{T}\left[a_{\mathbf{k},j}(\tau)b^\dagger_{\mathbf{k}',j'}(\tau')\right]\rangle \\ &= -\frac{\operatorname{Tr}\mathcal{T}\left[e^{-\beta H}a_{\mathbf{k},j}(\tau)b^\dagger_{\mathbf{k}',j'}(\tau')\right]}{\operatorname{Tr} e^{-\beta H}}\end{aligned} \tag{36}$$

and $\tau, \tau' \in [0, \beta]$. $\mathcal{T}$ is the ordering operator which is defined, here, for fermions with the Heaviside function Θ, to be

$$\mathcal{T}\left[a(\tau)b(\tau')\right] = \Theta(\tau-\tau')a(\tau)b(\tau') - \Theta(\tau'-\tau)b(\tau')a(\tau) \tag{37}$$

Without loss of generality, τ' is set to 0, which effectively sets the relevant domain of the function to be $\tau \in [-\beta, \beta]$. The above Green's functions, as defined for fermions, are antiperiodic:

$$\langle\langle a_{\mathbf{k},j}(\tau)|b^{\dagger}_{\mathbf{k}',j'}(0)\rangle\rangle = -\langle\langle a_{\mathbf{k},j}(\tau)|b^{\dagger}_{\mathbf{k}',j'}(\beta)\rangle\rangle \tag{38}$$

Using the equation of motion method, the Green's function may be differentiated with respect to τ. For the above arbitrary Green's function,

$$\begin{aligned}\partial_\tau\langle\langle a_{\mathbf{k},j}(\tau)|b^{\dagger}_{\mathbf{k}',j'}(0)\rangle\rangle &= -\partial_\tau\Theta(\tau)\langle a_{\mathbf{k},j}(\tau)b^{\dagger}_{\mathbf{k}',j'}(0)\rangle \\ &\quad + \partial_\tau\Theta(-\tau)\langle a_{\mathbf{k},j}(\tau)b^{\dagger}_{\mathbf{k}',j'}(0)\rangle \\ &\quad - \langle T\left[\partial_\tau a_{\mathbf{k},j}(\tau)b^{\dagger}_{\mathbf{k}',j'}(0)\right]\rangle,\end{aligned} \tag{39}$$

or,

$$\begin{aligned}\partial_\tau\langle\langle a_{\mathbf{k},j}(\tau)|b^{\dagger}_{\mathbf{k}',j'}(0)\rangle\rangle &= -\delta(\tau)\langle\left\{a_{\mathbf{k},j}(\tau), b^{\dagger}_{\mathbf{k}',j'}(0)\right\}\rangle \\ &\quad - \langle T\left[\left[H(\tau), a_{\mathbf{k},j}(\tau)\right]_+ b^{\dagger}_{\mathbf{k}',j'}(\tau)\right]\rangle.\end{aligned} \tag{40}$$

Four single-particle Green's functions from combinations of c and f operators will be examined. Their four equations of motion constitute a dependent set of equations which, in frequency-space, is a linear system. The Fourier transform of the Green's function is

introduced as

$$\langle\langle a_{\mathbf{k},j}(\tau)|b^{\dagger}_{\mathbf{k}',j'}(0)\rangle\rangle = -\frac{1}{\beta}\sum_n \mathrm{e}^{-i\Omega_n\tau}\langle\langle a_{\mathbf{k},j}|b^{\dagger}_{\mathbf{k}',j'}\rangle\rangle_{i\Omega_n}$$
$$\text{where} \quad \Omega_n = \frac{(2n+1)\pi}{\beta} \quad \text{for n} \in \mathbb{Z}. \tag{41}$$

Application of this transformation to the Green's functions leads to Matsubara-type Green's functions.

The four equations of motion are:

$$\begin{aligned}
(i\Omega_n-\lambda)\langle\langle c_{\mathbf{k},j}|c^{\dagger}_{\mathbf{k}',j'}\rangle\rangle_{i\Omega_n} &= \delta(\mathbf{k}-\mathbf{k}')\delta_{j,j'} - \mathcal{J}J(J+1)V\langle\langle f_{\mathbf{k},j}|c^{\dagger}_{\mathbf{k}',j'}\rangle\rangle_{i\Omega_n},\\
(i\Omega_n-\lambda)\langle\langle f_{\mathbf{k},j}|c^{\dagger}_{\mathbf{k}',j'}\rangle\rangle_{i\Omega_n} &= -\mathcal{J}J(J+1)V^{\dagger}\langle\langle c_{\mathbf{k},j}|c^{\dagger}_{\mathbf{k}',j'}\rangle\rangle_{i\Omega_n},\\
(i\Omega_n-\lambda)\langle\langle f_{\mathbf{k},j}|f^{\dagger}_{\mathbf{k}',j'}\rangle\rangle_{i\Omega_n} &= \delta(\mathbf{k}-\mathbf{k}')\delta_{j,j'} - \mathcal{J}J(J+1)V\langle\langle c_{\mathbf{k},j}|f^{\dagger}_{\mathbf{k}',j'}\rangle\rangle_{i\Omega_n},\\
(i\Omega_n-\lambda)\langle\langle c_{\mathbf{k},j}|f^{\dagger}_{\mathbf{k}',j'}\rangle\rangle_{i\Omega_n} &= -\mathcal{J}J(J+1)V^{\dagger}\langle\langle f_{\mathbf{k},j}|f^{\dagger}_{\mathbf{k}',j'}\rangle\rangle_{i\Omega_n}.
\end{aligned} \tag{42}$$

The solutions are:

$$\begin{aligned}
\langle\langle c_{\mathbf{k},j}|c^{\dagger}_{\mathbf{k}',j'}\rangle\rangle_{i\Omega_n} &= \frac{\delta(\mathbf{k}-\mathbf{k}')\delta_{j,j'}(i\Omega_n-\lambda)}{(i\Omega_n-\lambda)(i\Omega_n-\varepsilon_{\mathbf{k}}) - \mathcal{J}^2J^2(J+1)^2|V|^2}\\
\langle\langle f_{\mathbf{k},j}|f^{\dagger}_{\mathbf{k}',j'}\rangle\rangle_{i\Omega_n} &= \frac{\delta(\mathbf{k}-\mathbf{k}')\delta_{j,j'}(i\Omega_n-\varepsilon_{\mathbf{k}})}{(i\Omega_n-\lambda)(i\Omega_n-\varepsilon_{\mathbf{k}}) - \mathcal{J}^2J^2(J+1)^2|V|^2}\\
\langle\langle c_{\mathbf{k},j}|f^{\dagger}_{\mathbf{k}',j'}\rangle\rangle_{i\Omega_n} &= -\frac{\delta(\mathbf{k}-\mathbf{k}')\delta_{j,j'}\mathcal{J}J(J+1)V^{\dagger}}{(i\Omega_n-\lambda)(i\Omega_n-\varepsilon_{\mathbf{k}}) - \mathcal{J}^2J^2(J+1)^2|V|^2}\\
\langle\langle f_{\mathbf{k},j}|c^{\dagger}_{\mathbf{k}',j'}\rangle\rangle_{i\Omega_n} &= -\frac{\delta(\mathbf{k}-\mathbf{k}')\delta_{j,j'}\mathcal{J}J(J+1)V}{(i\Omega_n-\lambda)(i\Omega_n-\varepsilon_{\mathbf{k}}) - \mathcal{J}^2J^2(J+1)^2|V|^2}.
\end{aligned} \tag{43}$$

The Green's functions will now be used to calculate occupation numbers for the conduction band and local moments. For the conduction band,

$$\begin{aligned} n^c &= \sum_j n_j^c = \frac{1}{N}\sum_{\mathbf{k},j}\langle c_{\mathbf{k},j}^\dagger c_{\mathbf{k},j}\rangle \\ &= \frac{1}{N}\sum_{\mathbf{k},j}\lim_{\tau\to 0^-}\langle\langle c_{\mathbf{k},j}(\tau)|c_{\mathbf{k}',j'}^\dagger(0)\rangle\rangle \\ &= \frac{1}{N}\sum_{\mathbf{k},j}\lim_{\tau\to 0^-}\frac{1}{\beta}\sum_n\langle\langle c_{\mathbf{k},j}|c_{\mathbf{k}',j'}^\dagger\rangle\rangle_{i\Omega_n} \\ &= \frac{2J+1}{N}\sum_{\mathbf{k}}\lim_{\tau\to 0^-}\frac{1}{\beta}\sum_n\frac{i\Omega_n-\lambda}{(i\Omega_n-\lambda)(i\Omega_n-\varepsilon_{\mathbf{k}})-\mathcal{J}^2J^2(J+1)^2|V|^2}\,. \end{aligned} \tag{44}$$

The summation over $n\in\mathbb{Z}$ can be carried out with an integral in the complex plane, with contributions coming from the poles (29). Using

$$\Delta(\mathbf{k}) = \sqrt{\left(\frac{\lambda-\varepsilon_{\mathbf{k}}}{2}\right)^2+\mathcal{J}^2J^2(J+1)^2|V|^2}\,, \tag{45}$$

the occupation number is

$$\begin{aligned} n^c &= \frac{2J+1}{N}\sum_{\mathbf{k}}\lim_{\tau\to 0^-}\frac{-1}{2\pi i}\oint dz\frac{e^{-i\Omega_n\tau}}{e^{\beta z}+1}\frac{z-\lambda}{(z-\lambda)(z-\varepsilon_{\mathbf{k}})-\mathcal{J}^2J^2(J+1)^2|V|^2} \\ &= \frac{2J+1}{N}\sum_{\mathbf{k}}\frac{\left[\frac{\varepsilon_{\mathbf{k}}-\lambda}{2}+\Delta(\mathbf{k})\right]f\left(\frac{\varepsilon_{\mathbf{k}}+\lambda}{2}+\Delta(\mathbf{k})\right)-\left[\frac{\varepsilon_{\mathbf{k}}-\lambda}{2}-\Delta(\mathbf{k})\right]f\left(\frac{\varepsilon_{\mathbf{k}}+\lambda}{2}-\Delta(\mathbf{k})\right)}{2\Delta(\mathbf{k})} \\ &= \frac{2J+1}{N}\sum_{\mathbf{k}}\frac{\left|\Delta(\mathbf{k})+\frac{\varepsilon_{\mathbf{k}}-\lambda}{2}\right|f\left(\frac{\varepsilon_{\mathbf{k}}+\lambda}{2}+\Delta(\mathbf{k})\right)+\left|\Delta(\mathbf{k})-\frac{\varepsilon_{\mathbf{k}}-\lambda}{2}\right|f\left(\frac{\varepsilon_{\mathbf{k}}+\lambda}{2}-\Delta(\mathbf{k})\right)}{2\Delta(\mathbf{k})}\,. \end{aligned} \tag{46}$$

Likewise, the local moment occupation number is

$$\begin{aligned}
n^f &= \frac{1}{N}\sum_{\mathbf{k},j}\langle f^\dagger_{\mathbf{k},j} f_{\mathbf{k},j}\rangle \\
&= \frac{2J+1}{N}\sum_{\mathbf{k}}\lim_{\tau\to 0^-}\frac{-1}{2\pi i}\oint dz \frac{\mathrm{e}^{-i\Omega_n\tau}}{\mathrm{e}^{\beta z}+1}\frac{z-\varepsilon_{\mathbf{k}}}{(z-\lambda)(z-\varepsilon_{\mathbf{k}})-\mathcal{J}^2J^2(J+1)^2|V|^2} \\
&= \frac{2J+1}{N}\sum_{\mathbf{k}}\frac{\left[\frac{\lambda-\varepsilon_{\mathbf{k}}}{2}+\Delta(\mathbf{k})\right]f\left(\frac{\varepsilon_{\mathbf{k}}+\lambda}{2}+\Delta(\mathbf{k})\right)-\left[\frac{\lambda-\varepsilon_{\mathbf{k}}}{2}-\Delta(\mathbf{k})\right]f\left(\frac{\varepsilon_{\mathbf{k}}+\lambda}{2}-\Delta(\mathbf{k})\right)}{2\Delta(\mathbf{k})} \\
&= \frac{2J+1}{N}\sum_{\mathbf{k}}\frac{\left[\frac{\varepsilon_{\mathbf{k}}-\lambda}{2}+\Delta(\mathbf{k})\right]f\left(\frac{\varepsilon_{\mathbf{k}}+\lambda}{2}-\Delta(\mathbf{k})\right)-\left[\frac{\varepsilon_{\mathbf{k}}-\lambda}{2}-\Delta(\mathbf{k})\right]f\left(\frac{\varepsilon_{\mathbf{k}}+\lambda}{2}+\Delta(\mathbf{k})\right)}{2\Delta(\mathbf{k})} \\
&= \frac{2J+1}{N}\sum_{\mathbf{k}}\frac{\left|\Delta(\mathbf{k})+\frac{\lambda-\varepsilon_{\mathbf{k}}}{2}\right|f\left(\frac{\varepsilon_{\mathbf{k}}+\lambda}{2}+\Delta(\mathbf{k})\right)+\left|\Delta(\mathbf{k})-\frac{\lambda-\varepsilon_{\mathbf{k}}}{2}\right|f\left(\frac{\varepsilon_{\mathbf{k}}+\lambda}{2}-\Delta(\mathbf{k})\right)}{2\Delta(\mathbf{k})}.
\end{aligned} \tag{47}$$

Combined with (16), the Lagrange-multiplier λ can be resolved:

$$\lambda\left(\sum_{\mathbf{k},j}\langle f^\dagger_{\mathbf{k},j} f_{\mathbf{k},j}\rangle - N\right) \quad\to\quad \lambda\left(\sum_{\mathbf{k}}\langle f^\dagger_{\mathbf{k},j} f_{\mathbf{k},j}\rangle - \frac{N}{2J+1}\right) \quad \forall j \tag{48}$$

or, per particle,

$$\lambda\left(\frac{1}{N}\sum_{\mathbf{k}}\langle f^\dagger_{\mathbf{k},j} f_{\mathbf{k},j}\rangle - \frac{1}{2J+1}\right) \quad \forall j\,. \tag{49}$$

The average for the f-operators appears in (47) and hence the equation for λ becomes

$$\frac{1}{2J+1} = \frac{1}{N}\sum_{\mathbf{k}}\frac{\left|\Delta(\mathbf{k})+\frac{\lambda-\varepsilon_{\mathbf{k}}}{2}\right|f\left(\frac{\varepsilon_{\mathbf{k}}+\lambda}{2}+\Delta(\mathbf{k})\right)+\left|\Delta(\mathbf{k})-\frac{\lambda-\varepsilon_{\mathbf{k}}}{2}\right|f\left(\frac{\varepsilon_{\mathbf{k}}+\lambda}{2}-\Delta(\mathbf{k})\right)}{2\Delta(\mathbf{k})}. \tag{50}$$

The final occupation number is the hybridization constant. Calculation of this leads to a self-consistency equation:

$$\begin{aligned} V &= \lim_{\tau\to 0^-} \frac{1}{N}\sum_{\mathbf{k}} \langle c^\dagger_{\mathbf{k},j} f_{\mathbf{k},j}\rangle \\ &= \lim_{\tau\to 0^-} \frac{1}{N}\sum_{\mathbf{k}} \langle\langle f_{\mathbf{k},j}(\tau) | c^\dagger_{\mathbf{k}',j'}(0)\rangle\rangle \\ &= \lim_{\tau\to 0^-} \frac{1}{N}\sum_{\mathbf{k}} \frac{1}{\beta}\sum_n e^{-i\Omega_n\tau}\langle\langle f_{\mathbf{k},j} | c^\dagger_{\mathbf{k}',j'}\rangle\rangle_{i\Omega_n} \\ &= \lim_{\tau\to 0^-} \frac{1}{N}\sum_{\mathbf{k}} \frac{-1}{2\pi i}\oint \frac{e^{-z\tau}}{e^{\beta z}+1}\frac{-\mathcal{J}J(J+1)V}{(z-\lambda)(z-\varepsilon_{\mathbf{k}}) - \mathcal{J}^2J^2(J+1)^2|V|^2}. \end{aligned} \tag{51}$$

Solution of this, using equation (29) and (45) is

$$\begin{aligned} V &= \frac{\mathcal{J}J(J+1)V}{2N}\sum_{\mathbf{k}} \frac{f\left(w^-_{\mathbf{k}}\right) - f\left(w^+_{\mathbf{k}}\right)}{\Delta(\mathbf{k})}, \quad \text{or,} \\ \frac{1}{\mathcal{J}} &= \frac{J(J+1)}{2N}\sum_{\mathbf{k}} \frac{f\left(w^-_{\mathbf{k}}\right) - f\left(w^+_{\mathbf{k}}\right)}{\Delta(\mathbf{k})}. \end{aligned} \tag{52}$$

This result is in agreement with (35).

There are, in this treatment of the Kondo phase, four non-operator quantities in the Hamiltonian of (23) and each is manifestly independent of J_z. They are N, $\varepsilon_{\mathbf{k}}$, $\mathcal{J}$, λ. The fifth quantity, V, has acquired an independence from J_z through the assumption of isotropy. It follows that, without an external field, the J_z states are degenerate and that no physical quantity that is calculated here can depend on a particular J_z. Moreover, the form of the calculated quantities does not change with J — only the values of the quantities change. As will be seen, this is not true of the magnetically ordered phase.

Kondo-PM Phase Boundary

In this work, the Kondo phase is defined by a nonzero hybridization. The energy scale, T_K, is defined as the $V = 0$ boundary of the Kondo phase. Then, at the $V = 0$ boundary, the Hamiltonian reduces to a noninteracting one and the system enters the paramagnetic (PM) phase. The dressed occupation numbers become the bare ones; this can be seen by setting $V = 0$ in (45) and inserting the result into (46) and (47). The occupation numbers become

$$\begin{aligned} n_j^f &= f(\lambda)\,, \text{and} \\ n_j^c &= \frac{1}{N}\sum_{\mathbf{k}} f(\varepsilon_{\mathbf{k}})\,. \end{aligned} \tag{53}$$

At the Kondo-PM boundary, the magnetization must be zero. However, this condition has already been satisfied by (16). With the bare occupation numbers, (50) becomes

$$\begin{aligned} \frac{1}{2J+1} &= f(\lambda)\,, \text{or} \\ \frac{1}{2J+1} &= \left(\mathrm{e}^{(\lambda-\mu)\beta}+1\right)^{-1} \text{ and therefore} \\ \lambda &= \mu + k_B T \,\mathrm{Ln}\, 2J \;=\; \mu + \frac{\mathrm{Ln}\, 2J}{\beta}\,. \end{aligned} \tag{54}$$

The self-consistency equation (35) becomes

$$\frac{1}{\mathcal{J}} = \frac{J(J+1)}{2}\sum_{\mathbf{k}} \frac{f(\lambda) - f(\varepsilon_{\mathbf{k}})}{\lambda - \varepsilon_{\mathbf{k}}}. \tag{55}$$

Finally, the free energy reduces to that of the PM phase, or

$$\begin{aligned}\mathcal{F} = (2J+1)\sum_{\mathbf{k}} \varepsilon_{\mathbf{k}} f(\varepsilon_{\mathbf{k}})) \\ + \frac{2J+1}{\beta}\sum_{\mathbf{k}} f(\varepsilon_{\mathbf{k}})\,\mathrm{Ln}\, f(\varepsilon_{\mathbf{k}}) \\ + \frac{2J+1}{\beta}\sum_{\mathbf{k}} [1-f(\varepsilon_{\mathbf{k}})]\,\mathrm{Ln}\,[1-f(\varepsilon_{\mathbf{k}})]\,. \end{aligned} \tag{56}$$

3.3 Zero Temperature

The double-time Green's functions can be reached from the Matsubara Green's functions by making the replacement $i\Omega_n \to \omega + i\eta$ with $\eta \in \mathbb{R}$ being an infinitesimal quantity with a sign determined by the energy ω: $\eta = sgn(\omega)$. The average indicated by angle brackets is then no longer a thermal one. Instead, it is,

$$\langle O \rangle = \frac{\langle \Psi_0 | O | \Psi_0 \rangle}{\langle \Psi_0 | \Psi_0 \rangle} \tag{57}$$

where Ψ_0 is the ground state in the Heisenberg representation. With this understanding, the equations from the previous, finite-temperature section will hold when the limit $T \to 0$ is taken.

The Green's function solutions (43) become, with η quantities omitted,

$$\begin{aligned}
\langle\langle c_{\mathbf{k},j} | c^{\dagger}_{\mathbf{k}',j'} \rangle\rangle_{\omega} &= \frac{\delta(\mathbf{k}-\mathbf{k}')\delta_{j,j'}(\omega-\lambda)}{(\omega-\lambda)(\omega-\varepsilon_{\mathbf{k}}) - \mathcal{J}^2 J^2 (J+1)^2 |V|^2} \\
\langle\langle f_{\mathbf{k},j} | f^{\dagger}_{\mathbf{k}',j'} \rangle\rangle_{\omega} &= \frac{\delta(\mathbf{k}-\mathbf{k}')\delta_{j,j'}(\omega-\varepsilon_{\mathbf{k}})}{(\omega-\lambda)(\omega-\varepsilon_{\mathbf{k}}) - \mathcal{J}^2 J^2 (J+1)^2 |V|^2} \\
\langle\langle c_{\mathbf{k},j} | f^{\dagger}_{\mathbf{k}',j'} \rangle\rangle_{\omega} &= -\frac{\delta(\mathbf{k}-\mathbf{k}')\delta_{j,j'}\mathcal{J}J(J+1)V^{\dagger}}{(\omega-\lambda)(\omega-\varepsilon_{\mathbf{k}}) - \mathcal{J}^2 J^2 (J+1)^2 |V|^2} \\
\langle\langle f_{\mathbf{k},j} | c^{\dagger}_{\mathbf{k}',j'} \rangle\rangle_{\omega} &= -\frac{\delta(\mathbf{k}-\mathbf{k}')\delta_{j,j'}\mathcal{J}J(J+1)V}{(\omega-\lambda)(\omega-\varepsilon_{\mathbf{k}}) - \mathcal{J}^2 J^2 (J+1)^2 |V|^2}.
\end{aligned} \tag{58}$$

The conduction band occupation number is reachable from either of two means:

$$\begin{aligned} n^c &= \lim_{T\to 0} \frac{1}{N}\sum_{\mathbf{k},j} \lim_{\tau\to 0^-} \langle\langle c_{\mathbf{k},j}(\tau)|c^\dagger_{\mathbf{k}',j'}(0)\rangle\rangle \text{, or,} \\ &= \lim_{T\to 0}\int_{-\infty}^{\infty} d\omega f(\omega)\left[-\frac{1}{\pi}\,\mathrm{Tr}\,\mathrm{Im}\,\langle\langle c_{\mathbf{k},j}|c^\dagger_{\mathbf{k}',j'}\rangle\rangle_\omega\right]. \end{aligned} \tag{59}$$

The $T\to 0$ limit is needed in the second line only because of the introduction of the Fermi-Dirac function. However, the limit can be taken immediately:

$$= \int_{-\infty}^{\mu} d\omega\left[-\frac{1}{\pi}\,\mathrm{Tr}\,\mathrm{Im}\,\langle\langle c_{\mathbf{k},j}|c^\dagger_{\mathbf{k}',j'}\rangle\rangle_\omega\right]. \tag{60}$$

Either method results in an occupation number of

$$n^c = \frac{2J+1}{N}\sum_{\mathbf{k}} \frac{\left|\Delta(\mathbf{k})+\frac{\varepsilon_\mathbf{k}-\lambda}{2}\right|\Theta\left(\mu-\frac{\varepsilon_\mathbf{k}+\lambda}{2}-\Delta(\mathbf{k})\right)+\left|\Delta(\mathbf{k})-\frac{\varepsilon_\mathbf{k}-\lambda}{2}\right|\Theta\left(\mu-\frac{\varepsilon_\mathbf{k}+\lambda}{2}+\Delta(\mathbf{k})\right)}{2\Delta(\mathbf{k})}. \tag{61}$$

The self-consistency equation (35) likewise becomes

$$\frac{1}{\mathcal{J}} = \frac{J(J+1)}{2N}\sum_{\mathbf{k}} \frac{\Theta\left(\mu-w^-_\mathbf{k}\right)-\Theta\left(\mu-w^+_\mathbf{k}\right)}{\Delta(\mathbf{k})}. \tag{62}$$

The local moment occupation number, however, requires extra care. At $T=0$, (47) becomes

$$n^f = \frac{2J+1}{N}\sum_{\mathbf{k}} \frac{\left|\Delta(\mathbf{k})+\frac{\lambda-\varepsilon_\mathbf{k}}{2}\right|\Theta\left(\mu-\frac{\varepsilon_\mathbf{k}+\lambda}{2}-\Delta(\mathbf{k})\right)+\left|\Delta(\mathbf{k})-\frac{\lambda-\varepsilon_\mathbf{k}}{2}\right|\Theta\left(\mu-\frac{\varepsilon_\mathbf{k}+\lambda}{2}+\Delta(\mathbf{k})\right)}{2\Delta(\mathbf{k})}. \tag{63}$$

The system must be in its ground state, and so only the lowest possible energy states may be filled. Hence, in each of (61) through (63), the only step function to survive is that with an argument involving the lowest energy level. With respect to μ, that would be $w_{\mathbf{k}}^{-}$. Because the summation variable is $\mathbf{k}$, the step function arguments might be rewritten for clarity in the form

$$\mu - \frac{\varepsilon_{\mathbf{k}} + \lambda}{2} \pm \Delta(\mathbf{k})) \rightarrow \mathbf{k} - K, \tag{64}$$

where one might then retain only the step function of lowest energies K. However, satisfying the argument leads to a transcendental equation due to the tight-binding form of $\varepsilon_{\mathbf{k}}$. In practice, the numerical computation of these expressions involves all step functions, and one of μ or λ must be fixed and the other computed after. For example, if μ is not fixed, then n^f cannot be solved through the satisfaction of the single-occupancy constraint for λ; both μ and λ are required for both n^c and n^f. In this treatment, moreover, $\mathcal{J}$ and V appear together in each physical quantity except for the left-hand side of (62). Therefore, $\mathcal{J}^2|V|^2$ (and hence $\mathcal{J}|V|$) may be fixed so that μ and λ can be computed from n^c and n^f, and then $|V|$ can be computed from $\mathcal{J}^{-1}$ in (62).

CHAPTER 4

THE MAGNETICALLY-ORDERED PHASE

Magnetic ordering will now be discussed. In the process of linearizing the Hamiltonian (10), hybridization constants will be considered zero. Net magnetizations will also be considered as zero. Only magnetism transverse to a possible external field will be considered; the z-component of the interaction term (6) will be dropped.

4.1 Dependence on J

Whereas expressions in the Kondo phase could be derived without specifying the total angular momentum, the same is not true of the magnetically-ordered (MO) phase. As can be seen in appendix B for $J = 3/2$, solving for the Green's functions and then dropping the J_z-dependence of the ordering constants, M and S, leads to inconsistencies. Rather, suitable definitions for the ordering constants must be used such that J_z-dependence is removed systematically. This, then, does not constitute an assumption in the same sense as that of isotropic hybridization.

Notwithstanding, for a $J = 1/2$ magnetically-ordered phase, the results for anisotropic ordering constants are identical to those for isotropic ordering constants. Thus, no assumption of isotropy is required.

4.2 Mean-Field Approximation

In the MO phase, the quantities of interest will be the ordering constants. These constants represent staggered changes in J_z, and in this work only changes of unity will be considered. Momentum transfer will be represented by an ordering vector $\mathbf{q}$. Whereas in the Kondo-phase mean-field Hamiltonian, $\mathbf{q}$ was a summation variable, here it is fixed. No restrictions are placed upon $\mathbf{q}$; it may be incommensurate.

If the ordering constants are defined in a manner similar to the hybridization constants, i.e.,

$$\begin{aligned} M^{+}_{\mathbf{q},j\to j+1} &= \frac{1}{N}\sum_{\mathbf{k}}\langle f^{\dagger}_{\mathbf{k}-\mathbf{q},j+1} f_{\mathbf{k},j}\rangle \;=\; \frac{1}{N}\sum_{\mathbf{k}}\langle f^{\dagger}_{\mathbf{k},j+1} f_{\mathbf{k}+\mathbf{q},j}\rangle, \\ S^{+}_{\mathbf{q},j\to j+1} &= \frac{1}{N}\sum_{\mathbf{k}}\langle c^{\dagger}_{\mathbf{k}-\mathbf{q},j+1} c_{\mathbf{k},j}\rangle \;=\; \frac{1}{N}\sum_{\mathbf{k}}\langle c^{\dagger}_{\mathbf{k},j+1} c_{\mathbf{k}+\mathbf{q},j}\rangle. \end{aligned} \tag{65}$$

then the mean-field MO-phase Hamiltonian becomes

$$\begin{aligned} H_{\mathbf{q}} = &\sum_{\mathbf{k},j}\varepsilon_{\mathbf{k}} c^{\dagger}_{\mathbf{k},j} c_{\mathbf{k},j} + \lambda\Big(\sum_{\mathbf{k},j} f^{\dagger}_{\mathbf{k},j} f_{\mathbf{k},j} - N\Big) \\ &- \mathcal{J} M^{+}_{\mathbf{q},j\to j+1}\sum_{\mathbf{k},j}\frac{J(J+1)-j(j+1)}{2} c^{\dagger}_{\mathbf{k}+\mathbf{q},j} c_{\mathbf{k},j+1} \\ &- \mathcal{J} S^{+}_{\mathbf{q},j\to j+1}\sum_{\mathbf{k},j}\frac{J(J+1)-j(j+1)}{2} f^{\dagger}_{\mathbf{k}+\mathbf{q},j} f_{\mathbf{k},j+1} \\ &+ N\mathcal{J}\sum_{j}\frac{J(J+1)-j(j+1)}{2} M^{+}_{\mathbf{q},j\to j+1} S^{-}_{\mathbf{q},j+1\to j} \\ &+ H.C.. \end{aligned} \tag{66}$$

As such, the J_z-dependence of the ordering constants cannot be dropped, and unlike in the Kondo phase, isotropic constants stemming from (65) cannot be used in a consistent way.

See appendix *B*. However, if the ordering constants are defined as

$$M^{+}_{\mathbf{q}} = \frac{1}{N}\sum_{\mathbf{k},j}\langle r_j f^{\dagger}_{\mathbf{k}-\mathbf{q},j+1} f_{\mathbf{k},j}\rangle = \frac{1}{N}\sum_{\mathbf{k},j}\langle r_j f^{\dagger}_{\mathbf{k},j+1} f_{\mathbf{k}+\mathbf{q},j}\rangle,$$
$$S^{+}_{\mathbf{q}} = \frac{1}{N}\sum_{\mathbf{k},j}\langle r_j c^{\dagger}_{\mathbf{k}-\mathbf{q},j+1} c_{\mathbf{k},j}\rangle = \frac{1}{N}\sum_{\mathbf{k},j}\langle r_j c^{\dagger}_{\mathbf{k},j+1} c_{\mathbf{k}+\mathbf{q},j}\rangle, \tag{67}$$

then the mean-field Hamiltonian takes the form,

$$\begin{aligned} H_{\mathbf{q}} = &\sum_{\mathbf{k},j}\varepsilon_{\mathbf{k}} c^{\dagger}_{\mathbf{k},j} c_{\mathbf{k},j} + \lambda\Big(\sum_{\mathbf{k},j} f^{\dagger}_{\mathbf{k},j} f_{\mathbf{k},j} - N\Big) \\ &- \frac{\mathcal{J} M^{+}_{\mathbf{q}}}{2}\sum_{\mathbf{k},j} r_j c^{\dagger}_{\mathbf{k}+\mathbf{q},j} c_{\mathbf{k},j+1} \\ &- \frac{\mathcal{J} S^{+}_{\mathbf{q}}}{2}\sum_{\mathbf{k},j} r_j f^{\dagger}_{\mathbf{k}+\mathbf{q},j} f_{\mathbf{k},j+1} \\ &+ \frac{N\mathcal{J}}{2} M^{+}_{\mathbf{q}} S^{-}_{\mathbf{q}} + \text{Comp. Conj.}. \end{aligned} \tag{68}$$

Equation (67) defines the ordering constants in a fundamentally different way than (13) defines the hybridization constant due to the summation over J_z values.

4.3 $J = \frac{3}{2}$: Finite Temperature

Variational Method

Apparent in (68), in the mean-field representation there are no c-f operator cross-terms. It is possible, therefore, to write a block-diagonal matrix for the Hamiltonian using two 4×4 matrices, one for the c terms and one for the f terms. For the c terms, the vector representation of

$$\Big[c^{\dagger}_{\mathbf{k},\frac{3}{2}} \quad c^{\dagger}_{\mathbf{k}+\mathbf{q},\frac{1}{2}} \quad c^{\dagger}_{\mathbf{k}+2\mathbf{q},-\frac{1}{2}} c^{\dagger}_{\mathbf{k}+3\mathbf{q},-\frac{3}{2}}\Big] \tag{69}$$

leads to the matrix,

$$\begin{pmatrix} \varepsilon_{\mathbf{k}} & -\frac{\sqrt{3}}{2}\mathcal{J}M^{-}_{-\mathbf{q}} & 0 & 0 \\ -\frac{\sqrt{3}}{2}\mathcal{J}M^{+}_{\mathbf{q}} & \varepsilon_{\mathbf{k}+\mathbf{q}} & -\mathcal{J}M^{-}_{-\mathbf{q}} & 0 \\ 0 & -\mathcal{J}M^{+}_{\mathbf{q}} & \varepsilon_{\mathbf{k}+2\mathbf{q}} & -\frac{\sqrt{3}}{2}\mathcal{J}M^{-}_{-\mathbf{q}} \\ 0 & 0 & -\frac{\sqrt{3}}{2}\mathcal{J}M^{+}_{\mathbf{q}} & \varepsilon_{\mathbf{k}+3\mathbf{q}}. \end{pmatrix} \tag{70}$$

For the f terms, a vector

$$\begin{bmatrix} f^{\dagger}_{\mathbf{k},\frac{3}{2}} & f^{\dagger}_{\mathbf{k}+\mathbf{q},\frac{1}{2}} & f^{\dagger}_{\mathbf{k}+2\mathbf{q},-\frac{1}{2}} f^{\dagger}_{\mathbf{k}+3\mathbf{q},-\frac{3}{2}} \end{bmatrix} \tag{71}$$

leads to the matrix,

$$\begin{pmatrix} \lambda & -\frac{\sqrt{3}}{2}\mathcal{J}S^{-}_{-\mathbf{q}} & 0 & 0 \\ -\frac{\sqrt{3}}{2}\mathcal{J}S^{+}_{\mathbf{q}} & \lambda & -\mathcal{J}S^{-}_{-\mathbf{q}} & 0 \\ 0 & -\mathcal{J}S^{+}_{\mathbf{q}} & \lambda & -\frac{\sqrt{3}}{2}\mathcal{J}S^{-}_{-\mathbf{q}} \\ 0 & 0 & -\frac{\sqrt{3}}{2}\mathcal{J}S^{+}_{\mathbf{q}} & \lambda. \end{pmatrix} \tag{72}$$

The aforementioned matrix for the Hamiltonian is formed with (70) and (72), and the corresponding state vector is produced by joining those of (69) and (71). Altogether the Hamiltonian can be expressed as

$$H_{\mathbf{q}} = E_0^{MO} - N\lambda + \sum_{\mathbf{k}} \psi^{\dagger}_{\mathbf{k},\mathbf{q}} \mathbf{H}_{\mathbf{k},\mathbf{q}} \psi_{\mathbf{k},\mathbf{q}} \tag{73}$$

where

$$E_0^{MO} = \frac{N\mathcal{J}}{2}\left(M^{+}_{\mathbf{q}} S^{-}_{-\mathbf{q}} + S^{+}_{\mathbf{q}} M^{-}_{-\mathbf{q}}\right). \tag{74}$$

While the eigenvalues of (72) corresponding to the interacting local moments are found to be

$$v_j(\mathbf{q}) = \lambda + j\mathcal{J}|S_{\mathbf{q}}|\,, \tag{75}$$

those from (70) for the conduction bands are comparatively much harder to find, as they involve the solution of a quartic equation in $\mathbf{q}$-dependent conduction electron energies. Their discussion will be postponed for the Green's function method.

Self-consistency equations may be written by minimizing the diagonalized Hamiltonian with respect to $S^{\pm}$ or $M^{\pm}$. For the local moments, $M^{\pm}$ is given by:

$$M^{\pm}_{\pm\mathbf{q}} = -\frac{S^{\pm}_{\pm\mathbf{q}}}{|S_{\mathbf{q}}|}\left[\frac{3}{2}\left\{f\left(\lambda - \frac{3}{2}\mathcal{J}|S_{\mathbf{q}}|\right) - f\left(\lambda + \frac{3}{2}\mathcal{J}|S_{\mathbf{q}}|\right)\right\} + \frac{1}{2}\left\{f\left(\lambda - \frac{1}{2}\mathcal{J}|S_{\mathbf{q}}|\right) - f\left(\lambda + \frac{1}{2}\mathcal{J}|S_{\mathbf{q}}|\right)\right\}\right]. \tag{76}$$

Green's Function Method

Just as in the Kondo phase, in the MO phase the equations of motion for the Green's functions produce a dependent set of equations which is then solved through the use of a

Fourier transform. The c-c Green's functions are as follows:

$$
\begin{aligned}
D(\mathbf{k},\mathbf{q})\,\langle\langle c_{\mathbf{k},\frac{3}{2}}|c^{\dagger}_{\mathbf{k}',j'}\rangle\rangle_{i\Omega_n} \quad = \\
\delta^{\frac{3}{2},j'}_{\mathbf{k},\mathbf{k}'}\Bigg(\quad & (i\Omega_n-\varepsilon_{\mathbf{k}+\mathbf{q}})\left[(i\Omega_n-\varepsilon_{\mathbf{k}+2\mathbf{q}})(i\Omega_n-\varepsilon_{\mathbf{k}+3\mathbf{q}})-\frac{3}{4}\mathcal{J}^2|M_{\mathbf{q}}|^2\right] \\
& -\mathcal{J}^2|M_{\mathbf{q}}|^2(i\Omega_n-\varepsilon_{\mathbf{k}+3\mathbf{q}})\Bigg) \\
-\delta^{\frac{1}{2},j'}_{\mathbf{k}+\mathbf{q},\mathbf{k}'}\,&\frac{\sqrt{3}}{2}\mathcal{J}M^{-}_{-\mathbf{q}}\left[(i\Omega_n-\varepsilon_{\mathbf{k}+2\mathbf{q}})(i\Omega_n-\varepsilon_{\mathbf{k}+3\mathbf{q}})-\frac{3}{4}\mathcal{J}^2|M_{\mathbf{q}}|^2\right] \\
+\delta^{-\frac{1}{2},j'}_{\mathbf{k}+2\mathbf{q},\mathbf{k}'}\,&\frac{\sqrt{3}}{2}\mathcal{J}^2\left(M^{-}_{-\mathbf{q}}\right)^2(i\Omega_n-\varepsilon_{\mathbf{k}+3\mathbf{q}}) \\
-\delta^{-\frac{3}{2},j'}_{\mathbf{k}+3\mathbf{q},\mathbf{k}'}\,&\frac{3}{4}\mathcal{J}^3\left(M^{-}_{-\mathbf{q}}\right)^3,
\end{aligned}
\tag{77}
$$

$$
\begin{aligned}
D(\mathbf{k}-\mathbf{q},\mathbf{q})\,\langle\langle c_{\mathbf{k},\frac{1}{2}}|c^{\dagger}_{\mathbf{k}',j'}\rangle\rangle_{i\Omega_n} \quad = \\
\delta^{\frac{1}{2},j'}_{\mathbf{k},\mathbf{k}'}\quad & (i\Omega_n-\varepsilon_{\mathbf{k}-\mathbf{q}})\left[(i\Omega_n-\varepsilon_{\mathbf{k}+\mathbf{q}})(i\Omega_n-\varepsilon_{\mathbf{k}+2\mathbf{q}})-\frac{3}{4}\mathcal{J}^2|M_{\mathbf{q}}|^2\right] \\
-\delta^{\frac{3}{2},j'}_{\mathbf{k}-\mathbf{q},\mathbf{k}'}\,&\frac{\sqrt{3}}{2}\mathcal{J}M^{+}_{\mathbf{q}}\left[(i\Omega_n-\varepsilon_{\mathbf{k}+\mathbf{q}})(i\Omega_n-\varepsilon_{\mathbf{k}+2\mathbf{q}})-\frac{3}{4}\mathcal{J}^2|M_{\mathbf{q}}|^2\right] \\
-\delta^{-\frac{1}{2},j'}_{\mathbf{k}+\mathbf{q},\mathbf{k}'}\,&\mathcal{J}M^{-}_{-\mathbf{q}}(i\Omega_n-\varepsilon_{\mathbf{k}+2\mathbf{q}})(i\Omega_n-\varepsilon_{\mathbf{k}-\mathbf{q}}) \\
+\delta^{-\frac{3}{2},j'}_{\mathbf{k}+2\mathbf{q},\mathbf{k}'}\,&\frac{\sqrt{3}}{2}\mathcal{J}^2\left(M^{-}_{-\mathbf{q}}\right)^2(i\Omega_n-\varepsilon_{\mathbf{k}-\mathbf{q}}),
\end{aligned}
\tag{78}
$$

$$
\begin{aligned}
D(\mathbf{k}+\mathbf{q},-\mathbf{q})\,\langle\langle c_{\mathbf{k},\frac{-1}{2}}|c^{\dagger}_{\mathbf{k}',j'}\rangle\rangle_{i\Omega_n} \quad = \\
\delta^{-\frac{1}{2},j'}_{\mathbf{k},\mathbf{k}'}\quad & (i\Omega_n-\varepsilon_{\mathbf{k}+\mathbf{q}})\left[(i\Omega_n-\varepsilon_{\mathbf{k}-\mathbf{q}})(i\Omega_n-\varepsilon_{\mathbf{k}-2\mathbf{q}})-\frac{3}{4}\mathcal{J}^2|M_{\mathbf{q}}|^2\right] \\
-\delta^{-\frac{3}{2},j'}_{\mathbf{k}+\mathbf{q},\mathbf{k}'}\,&\frac{\sqrt{3}}{2}\mathcal{J}M^{-}_{-\mathbf{q}}\left[(i\Omega_n-\varepsilon_{\mathbf{k}-\mathbf{q}})(i\Omega_n-\varepsilon_{\mathbf{k}-2\mathbf{q}})-\frac{3}{4}\mathcal{J}^2|M_{\mathbf{q}}|^2\right] \\
-\delta^{\frac{1}{2},j'}_{\mathbf{k}-\mathbf{q},\mathbf{k}'}\,&\mathcal{J}M^{+}_{\mathbf{q}}(i\Omega_n-\varepsilon_{\mathbf{k}-2\mathbf{q}})(i\Omega_n-\varepsilon_{\mathbf{k}+\mathbf{q}}) \\
+\delta^{\frac{3}{2},j'}_{\mathbf{k}-2\mathbf{q},\mathbf{k}'}\,&\frac{\sqrt{3}}{2}\mathcal{J}^2\left(M^{+}_{\mathbf{q}}\right)^2(i\Omega_n-\varepsilon_{\mathbf{k}+\mathbf{q}}),\ \text{and}
\end{aligned}
\tag{79}
$$

$$
\begin{aligned}
&D(\mathbf{k},-\mathbf{q})\,\langle\langle c_{\mathbf{k},\frac{-3}{2}}|c^{\dagger}_{\mathbf{k}',j'}\rangle\rangle_{i\Omega_n} \quad = \\
&\delta^{-\frac{3}{2},j'}_{\mathbf{k},\mathbf{k}'}\Bigg(\quad (i\Omega_n-\varepsilon_{\mathbf{k}-\mathbf{q}})\left[(i\Omega_n-\varepsilon_{\mathbf{k}-2\mathbf{q}})(i\Omega_n-\varepsilon_{\mathbf{k}-3\mathbf{q}})-\frac{3}{4}\mathcal{J}^2|M_{\mathbf{q}}|^2\right] \\
&\qquad\qquad -\mathcal{J}^2|M_{\mathbf{q}}|^2(i\Omega_n-\varepsilon_{\mathbf{k}-3\mathbf{q}})\Bigg) \\
&-\delta^{-\frac{1}{2},j'}_{\mathbf{k}-\mathbf{q},\mathbf{k}'}\frac{\sqrt{3}}{2}\mathcal{J}M^{+}_{\mathbf{q}}\left[(i\Omega_n-\varepsilon_{\mathbf{k}-2\mathbf{q}})(i\Omega_n-\varepsilon_{\mathbf{k}-3\mathbf{q}})-\frac{3}{4}\mathcal{J}^2|M_{\mathbf{q}}|^2\right] \\
&+\delta^{\frac{1}{2},j'}_{\mathbf{k}-2\mathbf{q},\mathbf{k}'}\frac{\sqrt{3}}{2}\mathcal{J}^2\left(M^{+}_{\mathbf{q}}\right)^2(i\Omega_n-\varepsilon_{\mathbf{k}-3\mathbf{q}}) \\
&-\delta^{\frac{3}{2},j'}_{\mathbf{k}-3\mathbf{q},\mathbf{k}'}\frac{3}{4}\mathcal{J}^3(M^{+}_{\mathbf{q}})^3\,;
\end{aligned}
\tag{80}
$$

where

$$
\begin{aligned}
D(\mathbf{k},\mathbf{q}) =&(i\Omega_n-\varepsilon_{\mathbf{k}})(i\Omega_n-\varepsilon_{\mathbf{k}+\mathbf{q}})(i\Omega_n-\varepsilon_{\mathbf{k}+2\mathbf{q}})(i\Omega_n-\varepsilon_{\mathbf{k}+3\mathbf{q}}) \\
&-\mathcal{J}^2|M_{\mathbf{q}}|^2\Bigg[\frac{3}{4}(i\Omega_n-\varepsilon_{\mathbf{k}})(i\Omega_n-\varepsilon_{\mathbf{k}+\mathbf{q}}) \\
&\qquad+\frac{3}{4}(i\Omega_n-\varepsilon_{\mathbf{k}+3\mathbf{q}})(i\Omega_n-\varepsilon_{\mathbf{k}+2\mathbf{q}}) \\
&\qquad+(i\Omega_n-\varepsilon_{\mathbf{k}+3\mathbf{q}})(i\Omega_n-\varepsilon_{\mathbf{k}})\Bigg] \\
&+\frac{9}{16}\mathcal{J}^4|M_{\mathbf{q}}|^4\,.
\end{aligned}
\tag{81}
$$

The f-f Green's functions have similar forms to those of c-c and can be obtained by making the following replacements, where $n\in Z$:

$$
\begin{aligned}
&M^{\pm}_{\pm\mathbf{q}}\rightarrow S^{\pm}_{\pm\mathbf{q}} \\
&\varepsilon_{\mathbf{k}+n\mathbf{q}}\rightarrow\lambda\,.
\end{aligned}
\tag{82}
$$

This permits a few simplifications, the most notable of which is in the denominators, all of which become

$$
d(\mathbf{q})=(i\Omega_n-\lambda)^4-\frac{5}{2}\mathcal{J}^2|S_{\mathbf{q}}|^2\left(i\Omega_n-\lambda\right)^2+\frac{9}{16}\mathcal{J}^4|S_{\mathbf{q}}|^4\,,
\tag{83}
$$

which is readily factorizable into

$$d(\mathbf{q}) = (i\Omega_n - \lambda + \frac{3}{2}\mathcal{J}|S_\mathbf{q}|)(i\Omega_n - \lambda - \frac{3}{2}\mathcal{J}|S_\mathbf{q}|) \times (i\Omega_n - \lambda + \frac{1}{2}\mathcal{J}|S_\mathbf{q}|)(i\Omega_n - \lambda - \frac{1}{2}\mathcal{J}|S_\mathbf{q}|). \tag{84}$$

Deriving an expression for $M^+_\mathbf{q}$,

$$\begin{aligned} M^+_\mathbf{q} &= \frac{1}{N}\sum_{\mathbf{k},j}\langle f^\dagger_{\mathbf{k}-\mathbf{q},j+1} f_{\mathbf{k},j}\rangle \\ &= \frac{1}{N}\sum_{\mathbf{k},j}\lim_{\tau\to 0^-}\langle\langle f_{\mathbf{k},j}(\tau)|f^\dagger_{\mathbf{k}-\mathbf{q},j+1}(0)\rangle\rangle \\ &= \frac{1}{N}\sum_{\mathbf{k},j}\lim_{\tau\to 0^-}\frac{1}{\beta}\sum_n e^{-i\Omega_n\tau}\langle\langle f_{\mathbf{k},j}|f^\dagger_{\mathbf{k}-\mathbf{q},j+1}\rangle\rangle_{i\Omega_n} \\ &= \lim_{\tau\to 0^-}\frac{1}{N\beta}\sum_{\mathbf{k},n} e^{-i\Omega_n\tau}\Big[\langle\langle f_{\mathbf{k},-\frac{3}{2}}|f^\dagger_{\mathbf{k}-\mathbf{q},-\frac{1}{2}}\rangle\rangle_{i\Omega_n} \\ &\qquad + \langle\langle f_{\mathbf{k},-\frac{1}{2}}|f^\dagger_{\mathbf{k}-\mathbf{q},\frac{1}{2}}\rangle\rangle_{i\Omega_n} + \langle\langle f_{\mathbf{k},\frac{1}{2}}|f^\dagger_{\mathbf{k}-\mathbf{q},\frac{3}{2}}\rangle\rangle_{i\Omega_n}\Big]. \end{aligned} \tag{85}$$

Performing the summation inside the square brackets of the final line gives

$$-\mathcal{J}S^+_\mathbf{q}\frac{5(i\Omega_n-\lambda)^2 - \frac{9}{4}\mathcal{J}^2|S_\mathbf{q}|^2}{(i\Omega_n-\lambda)^4 - \frac{5}{2}\mathcal{J}^2|S_\mathbf{q}|^2\big(i\Omega_n-\lambda\big)^2 + \frac{9}{16}\mathcal{J}^4|S_\mathbf{q}|^4}. \tag{86}$$

The summation over n may be replaced by an integral in the complex plane with a contour excluding the imaginary axis, and, lacking any $\mathbf{k}$-dependence, the summation over $\mathbf{k}$ produces a multiple of N. Making use of the factorization (84), performing the integral then leads to

$$M^+_\mathbf{q} = -\frac{S^+_\mathbf{q}}{|S_\mathbf{q}|}\Big(\frac{3}{2}f\big(\lambda+\frac{3}{2}\mathcal{J}|S_\mathbf{q}|\big) - \frac{3}{2}f\big(\lambda-\frac{3}{2}\mathcal{J}|S_\mathbf{q}|\big) + \frac{1}{2}f\big(\lambda+\frac{1}{2}\mathcal{J}|S_\mathbf{q}|\big) - \frac{1}{2}f\big(\lambda+\frac{1}{2}\mathcal{J}|S_\mathbf{q}|\big)\Big). \tag{87}$$

$M_{\mathbf{q}}^{-}$ is found similarly and, together with (87), the two expressions are in agreement with (76). Accordingly,

$$M_{\mathbf{q}}^{+}S_{-\mathbf{q}}^{-} = -|S_{\mathbf{q}}|\Big(\frac{3}{2}f\big(\lambda+\frac{3}{2}\mathcal{J}|S_{\mathbf{q}}|\big) - \frac{3}{2}f\big(\lambda-\frac{3}{2}\mathcal{J}|S_{\mathbf{q}}|\big) + \frac{1}{2}f\big(\lambda+\frac{1}{2}\mathcal{J}|S_{\mathbf{q}}|\big) - \frac{1}{2}f\big(\lambda+\frac{1}{2}\mathcal{J}|S_{\mathbf{q}}|\big)\Big). \tag{88}$$

Continuing with the local moments, the occupation number is given by

$$\begin{aligned} n_{\mathbf{q}}^{f} &= \frac{1}{N}\sum_{\mathbf{k},j}\langle f_{\mathbf{k},j}^{\dagger}f_{\mathbf{k},j}\rangle \\ &= f\big(\lambda+\frac{3}{2}\mathcal{J}|S_{\mathbf{q}}|\big)+f\big(\lambda-\frac{3}{2}\mathcal{J}|S_{\mathbf{q}}|\big)+f\big(\lambda+\frac{1}{2}\mathcal{J}|S_{\mathbf{q}}|\big)+f\big(\lambda-\frac{1}{2}\mathcal{J}|S_{\mathbf{q}}|\big). \end{aligned} \tag{89}$$

Moving on to the itinerant moments, the Green's functions will be expressed as Fourier transforms of their time-ordered formulations. The fourier-transformed time-ordered formulations can be reached from the Matsubara formulations by the replacement of $i\Omega_n \rightarrow \omega \pm i\eta$ in (77) through (81). In particular, because the Green's functions all have the form of ratios, each will be written as a numerator, $A(z)$, over a denominator, $B(z)$. Separating the arguments of the functions, z, into real and imaginary parts as $\omega + i\eta$, both ω and η are real numbers. Further, η will be infinitesimal and non-negative. Assuming that for an arbitrary such Green's function, G, a Taylor-expansion exists about $\eta = 0$, G can be written as

$$G(\omega - i\eta) = \frac{A(\omega - i\eta)}{B(\omega - i\eta)} \sim \frac{A(\omega) - i\eta\frac{\partial A}{\partial \omega}}{B(\omega) - i\eta\frac{\partial B}{\partial \omega}} = \eta\frac{A(\omega)\frac{\partial B}{\partial \omega} - B(\omega)\frac{\partial A}{\partial \omega}}{B^2(\omega) + \eta^2\big(\frac{\partial B}{\partial \omega}\big)^2} \tag{90}$$

To first order, the imaginary part is then

$$\mathrm{Im}\, G(\omega - i\eta) \sim \eta \frac{A(\omega)\frac{\partial B}{\partial \omega} - B(\omega)\frac{\partial A}{\partial \omega}}{B^2(\omega) + \eta^2 \left(\frac{\partial B}{\partial \omega}\right)^2} \tag{91}$$

Dropping higher order terms and rewriting, and using the Poisson kernel for the Dirac delta function,

$$= \pi\delta\left(\frac{B(\omega)}{\frac{\partial B}{\partial \omega}}\right) \frac{A(\omega)\frac{\partial B}{\partial \omega} - B(\omega)\frac{\partial A}{\partial \omega}}{\left(\frac{\partial B}{\partial \omega}\right)^2}. \tag{92}$$

Considering the zero of the delta function, the above leads to

$$\mathrm{Im}\, G(\omega - i\eta) \sim \pi\delta\left(\frac{B(\omega)}{\frac{\partial B}{\partial \omega}}\right) \frac{A(\omega)}{\frac{\partial B}{\partial \omega}}. \tag{93}$$

With this formulation, a self-consistency equation for the conduction electron magnetization can be obtained:

$$\begin{aligned} S^+_{\mathbf{q}} &= \frac{1}{N}\sum_j \int d\omega f(\omega) \frac{1}{\pi} \mathrm{Tr}\ \mathrm{Im}\ \langle\langle c_{\mathbf{k},j} | c^\dagger_{\mathbf{k}-\mathbf{q},j+1}\rangle\rangle_\omega \\ &= \frac{1}{N\pi}\sum_{\mathbf{k},j} \int d\omega f(\omega) \left[\pi\delta\left(\frac{B(\mathbf{k},\omega)}{\frac{\partial B}{\partial \omega}}\right) \frac{A(\mathbf{k},j,\omega)}{\frac{\partial B}{\partial \omega}}\right] \end{aligned} \tag{94}$$

To carry out the sum over j, the expressions of (78) through (80) must be shifted by various multiples of $\mathbf{q}$ so that the denominators become identical. Performing this shift, $B(\mathbf{k},\omega)$ is

given by (81), and

$$\begin{aligned}\sum_j A(\mathbf{k},j,\omega) &= -\mathcal{J}M_{\mathbf{q}}^{+}\left[\frac{3}{2}\left(\omega-\varepsilon_{\mathbf{k}+\mathbf{q}}\right)\left(\omega-\varepsilon_{\mathbf{k}}\right)+2\left(\omega-\varepsilon_{\mathbf{k}}\right)\left(\omega-\varepsilon_{\mathbf{k}+3\mathbf{q}}\right)\right.\\ &\qquad\left.+\frac{3}{2}\left(\omega-\varepsilon_{\mathbf{k}+2\mathbf{q}}\right)\left(\omega-\varepsilon_{\mathbf{k}+3\mathbf{q}}\right)-\frac{9}{4}\mathcal{J}^2|M_{\mathbf{q}}|^2\right],\\ \frac{\partial B}{\partial\omega} &= \left(2\omega-\varepsilon_{\mathbf{k}}-\varepsilon_{\mathbf{k}+3\mathbf{q}}\right)\left[\left(\omega-\varepsilon_{\mathbf{k}+\mathbf{q}}\right)\left(\omega-\varepsilon_{\mathbf{k}+2\mathbf{q}}\right)-\frac{7}{4}\mathcal{J}^2|M_{\mathbf{q}}|^2\right]\\ &\quad+\left(2\omega-\varepsilon_{\mathbf{k}+\mathbf{q}}-\varepsilon_{\mathbf{k}+2\mathbf{q}}\right)\left[\left(\omega-\varepsilon_{\mathbf{k}}\right)\left(\omega-\varepsilon_{\mathbf{k}+3\mathbf{q}}\right)-\frac{3}{4}\mathcal{J}^2|M_{\mathbf{q}}|^2\right]\end{aligned} \tag{95}$$

For the numerical computation of the delta function in (94), the heat kernel formulation has been used:

$$\delta\left(\frac{B(\mathbf{k},\omega)}{\dfrac{\partial B}{\partial\omega}}\right) = \frac{1}{\eta\sqrt{2\pi}}\exp\left[-\frac{\left(B(\mathbf{k},\omega)\right)^2}{2\eta^2\left(\dfrac{\partial B}{\partial\omega}\right)^2}\right] \tag{96}$$

The self-consistency equation implied by (94) can be explicated as well as readied for numerical computation by multiplying both sides of (94) by $S_{-\mathbf{q}}^{-}$, then by substituting the resulting $M_{\mathbf{q}}^{+}S_{-\mathbf{q}}^{-}$ on the right-hand side with (88) and simplifying from both sides a factor of $|S_{\mathbf{q}}|$. The self-consistency equation is then in terms of $|S_{\mathbf{q}}|$.

For the itinerant moment occupation number,

$$n_{\mathbf{q}}^{c} = \frac{1}{N}\sum_j\int d\omega f(\omega)\frac{1}{\pi}\mathrm{Tr\ Im}\ \langle\langle c_{\mathbf{k},j}|c_{\mathbf{k},j}^{\dagger}\rangle\rangle_{\omega}. \tag{97}$$

Upon making the replacement in (97) with (93), $B(\omega)$ is given by (81) and the derivative of $B(\omega)$ is given by (95). However, in this case $A(\omega)$ equals $B(\omega)$. Hence,

$$n_{\mathbf{q}}^{c} = \frac{1}{N}\sum_{\mathbf{k}}\int d\omega f(\omega)\delta\left(\frac{B(\mathbf{k},\omega)}{\frac{\partial B}{\partial \omega}}\right). \tag{98}$$

Free Energy

Combination of the results for the variational and Green's function methods provides a means for numerically calculating the canonical free energy without having explicit expressions for the eigenvalues of the interacting system. Beginning with the diagonalized Hamiltonian,

$$\begin{aligned} H'_{\mathbf{q}} &= E_0^{MO} - N\lambda \\ &\quad + \sum_{\mathbf{k},j} u_j(\mathbf{k},\mathbf{q}) U_j^{\dagger}(\mathbf{k},\mathbf{q}) U_j(\mathbf{k},\mathbf{q}) \\ &\quad + \sum_{\mathbf{k},j} v_j(\mathbf{q}) V_j^{\dagger}(\mathbf{k},\mathbf{q}) V_j(\mathbf{k},\mathbf{q}), \end{aligned} \tag{99}$$

where the v eigenvalues are given by (75), the capital letters indicate operators, and the u eigenvalues describe the interacting conduction electron eigenvalues. E_0^{MO} can be examined more closely by rewriting it and substituting $M_{\mathbf{q}}^{\pm}$ with (76):

$$\begin{aligned} \frac{2E_0^{MO}}{N\mathcal{J}} &= M_{\mathbf{q}}^{+}S_{\mathbf{q}}^{-} + S_{\mathbf{q}}^{+}M_{\mathbf{q}}^{-} \\ &= \left[\frac{S_{\mathbf{q}}^{+}}{|S_{\mathbf{q}}|}S_{\mathbf{q}}^{-} + S_{\mathbf{q}}^{+}\frac{S_{\mathbf{q}}^{-}}{|S_{\mathbf{q}}|}\right] \\ &\quad \times \left[\frac{3}{2}\left\{f\left(\lambda - \frac{3}{2}\mathcal{J}|S_{\mathbf{q}}|\right) - f\left(\lambda + \frac{3}{2}\mathcal{J}|S_{\mathbf{q}}|\right)\right\}\right. \\ &\qquad \left. + \frac{1}{2}\left\{f\left(\lambda - \frac{1}{2}\mathcal{J}|S_{\mathbf{q}}|\right) - f\left(\lambda + \frac{1}{2}\mathcal{J}|S_{\mathbf{q}}|\right)\right\}\right] \end{aligned} \tag{100}$$

Calling the quantity in the second set of square brackets, having Fermi functions, as χ_f,

$$\frac{2E_0^{MO}}{N\mathcal{J}} = 2|S_{\mathbf{q}}|\chi_f(\mathbf{q})\,. \tag{101}$$

Hence, E_0^{MO} is a real number. The free energy can be expressed, in general, as

$$\begin{aligned}\mathcal{F} &= -\beta^{-1}\,\mathrm{Ln}\,\mathrm{Tr}\,\mathrm{e}^{-H'_{\mathbf{q}}\beta}\,, \text{ or}\\ &= \langle E\rangle - TS\,.\end{aligned} \tag{102}$$

Examining the second line of (99) with respect to the average, $\langle E\rangle$, and using (75),

$$\begin{aligned}\sum_{\mathbf{k},j}\langle v_j(\mathbf{q})V_j^{\dagger}(\mathbf{k},\mathbf{q})V_j(\mathbf{k},\mathbf{q})\rangle =& \sum_{\mathbf{k},j} v_j(\mathbf{q})f\big(v_j(\mathbf{q})\big)\\ =& N\sum_j\big[\lambda + j\mathcal{J}|S_{\mathbf{q}}|\big]f\big(\lambda + j\mathcal{J}|S_{\mathbf{q}}|\big)\end{aligned} \tag{103}$$

The free energy is

$$\begin{aligned}\mathcal{F} = E_0^{MO} - N\lambda + N\sum_j v_j(\mathbf{q})f\big(v_j(\mathbf{q})\big) + \sum_{\mathbf{k},j} u_j(\mathbf{q})f\left(u_j(\mathbf{q})\right)\\ + \beta^{-1}\sum_{\mathbf{k},j} f\left(u_j(\mathbf{k},\mathbf{q})\right)\,\mathrm{Ln}\,f\left(u_j(\mathbf{k},\mathbf{q})\right)\\ + \beta^{-1}\sum_{\mathbf{k},j} f\left(v_j(\mathbf{q})\right)\,\mathrm{Ln}\,f\left(v_j(\mathbf{q})\right)\\ + \beta^{-1}\sum_{\mathbf{k},j}\left[1-f\left(u_j(\mathbf{k},\mathbf{q})\right)\right]\,\mathrm{Ln}\,\left[1-f\left(u_j(\mathbf{k},\mathbf{q})\right)\right]\\ + \beta^{-1}\sum_{\mathbf{k},j}\left[1-f\left(v_j(\mathbf{q})\right)\right]\,\mathrm{Ln}\,\left[1-f\left(v_j(\mathbf{q})\right)\right]\end{aligned} \tag{104}$$

In a numerical calculation, any sum found above which involves a u-value may be calculated like so: the term is rewritten as an integral with the delta function defined by

(96), (81), and (95), for example

$$\sum_{\mathbf{k},j} f\left(u_j(\mathbf{k},\mathbf{q})\right) \mathrm{Ln}\, f\left(u_j(\mathbf{k},\mathbf{q})\right) = \sum_{\mathbf{k}} \int d\omega f(\omega)\, \mathrm{Ln}\, f(\omega)\, \delta\left(\frac{B(\mathbf{k},\omega)}{\frac{\partial B}{\partial \omega}}\right) \text{ and}$$

$$\sum_{\mathbf{k},j} u_j(\mathbf{k},\mathbf{q})\, f\left(u_j(\mathbf{k},\mathbf{q})\right) = \sum_{\mathbf{k},j} \int d\omega\, \omega f(\omega)\, \delta\left(\frac{B(\mathbf{k},\omega)}{\frac{\partial B}{\partial \omega}}\right). \tag{105}$$

MO-PM Phase Boundary

The boundary between the ordered and paramagnetic (PM) phases can be found by approaching it from within the ordered phase, that is, by taking the limit of vanishing ordering constants. Just as with the Kondo-PM boundary, the Hamiltonian in this limit is a noninteracting one. Therefore, one arrives at the same expression for λ, namely,

$$\lambda = \mu + k_B T \mathrm{Ln}3 = \mu + \frac{\mathrm{Ln}3}{\beta}. \tag{106}$$

Examining $M^{\pm}_{\pm\mathbf{q}}$, the Fermi functions are expanded about $|S_{\mathbf{q}}|$ to first order and (106) is applied:

$$\begin{aligned} M^{\pm}_{\pm\mathbf{q}} &= \frac{S^{\pm}_{\pm\mathbf{q}}}{|S_{\mathbf{q}}|}\left[\frac{3}{2}\left\{f\left(\lambda - \frac{3}{2}\mathcal{J}|S_{\mathbf{q}}|\right) - f\left(\lambda + \frac{3}{2}\mathcal{J}|S_{\mathbf{q}}|\right)\right\}\right. \\ &\qquad \left. + \frac{1}{2}\left\{f\left(\lambda - \frac{1}{2}\mathcal{J}|S_{\mathbf{q}}|\right) - f\left(\lambda + \frac{1}{2}\mathcal{J}|S_{\mathbf{q}}|\right)\right\}\right] \\ &= \frac{S^{\pm}_{\pm\mathbf{q}}}{|S_{\mathbf{q}}|}\left[\frac{3}{2}\left\{3\frac{\mathcal{J}|S_{\mathbf{q}}|\beta}{4\cosh^2\frac{(\lambda-\mu)\beta}{2}}\right\} + \frac{1}{2}\left\{\frac{\mathcal{J}|S_{\mathbf{q}}|\beta}{4\cosh^2\frac{(\lambda-\mu)\beta}{2}}\right\}\right] \\ &= S^{\pm}_{\pm\mathbf{q}}\left[\frac{15}{16}\mathcal{J}\beta\right] \end{aligned} \tag{107}$$

For the conduction-band ordering constant, a first-order approximation results in

$$\begin{aligned} S^{\pm}_{\pm\mathbf{q}} &= \mathcal{J} M^{\pm}_{\pm\mathbf{q}} \frac{1}{N} \sum_{\mathbf{k}} \left[\frac{3}{2} \frac{f\left(\varepsilon_{\mathbf{k}+2\mathbf{q}}\right) - f\left(\varepsilon_{\mathbf{k}+3\mathbf{q}}\right)}{\varepsilon_{\mathbf{k}+3\mathbf{q}} - \varepsilon_{\mathbf{k}+2\mathbf{q}}} \right. \\ &\qquad \left. + 2 \frac{f\left(\varepsilon_{\mathbf{k}+\mathbf{q}}\right) - f\left(\varepsilon_{\mathbf{k}+2\mathbf{q}}\right)}{\varepsilon_{\mathbf{k}+2\mathbf{q}} - \varepsilon_{\mathbf{k}+\mathbf{q}}} + \frac{3}{2} \frac{f\left(\varepsilon_{\mathbf{k}}\right) - f\left(\varepsilon_{\mathbf{k}+\mathbf{q}}\right)}{\varepsilon_{\mathbf{k}+\mathbf{q}} - \varepsilon_{\mathbf{k}}} \right] \\ &= \mathcal{J} M^{\pm}_{\pm\mathbf{q}} \chi^{0}_{c}(\mathbf{q}) , \end{aligned} \tag{108}$$

which is then substituted into (107) to arrive at the MO-PM boundary self-consistency equation,

$$1 = \frac{15}{16} \mathcal{J}^2 \beta \chi^{0}_{c}(\mathbf{q}) \tag{109}$$

The conduction band occupation number becomes

$$n^{0c}_{\mathbf{q}} = \frac{1}{N} \sum_{\mathbf{k}} \left[f\left(\varepsilon_{\mathbf{k}}\right) + f\left(\varepsilon_{\mathbf{k}+\mathbf{q}}\right) + f\left(\varepsilon_{\mathbf{k}+2\mathbf{q}}\right) + f\left(\varepsilon_{\mathbf{k}+3\mathbf{q}}\right) \right] \tag{110}$$

4.4 $J = \frac{3}{2}$: Zero Temperature

Replacement of Fermi functions by step functions leads to the following. The conduction band occupation (98) becomes

$$n^{c}_{\mathbf{q}} = \frac{1}{N} \sum_{\mathbf{k}} \int_{-\infty}^{\mu} d\omega \delta \left(\frac{B(\mathbf{k}, \omega)}{\dfrac{\partial B}{\partial \omega}} \right) ; \tag{111}$$

the local moment occupation (89) becomes, by filling only the lowest-lying state,

$$n^{f}_{\mathbf{q}} = \Theta\left(\mu - \lambda + \frac{3}{2} \mathcal{J} |S_{\mathbf{q}}|\right) = 1 ; \tag{112}$$

the magnitude of the local-moment ordering constant (87) may be resolved, again by filling only the lowest-lying state, to be

$$M^{\pm}_{\pm\mathbf{q}} = \frac{S^{\pm}_{\pm\mathbf{q}}}{|S_{\mathbf{q}}|}\frac{3}{2}\Theta\left(\lambda - \frac{3}{2}\mathcal{J}|S_{\mathbf{q}}|\right), \text{ hence}$$
$$|M_{\mathbf{q}}| = \frac{3}{2}; \tag{113}$$

and the equation (94) for $S^{+}_{\mathbf{q}}$ becomes

$$S^{+}_{\mathbf{q}} = \frac{1}{N\pi}\sum_{\mathbf{k},j}\int_{-\infty}^{\mu} d\omega \left[\pi\delta\left(\frac{B(\mathbf{k},\omega)}{\frac{\partial B}{\partial\omega}}\right)\frac{A(\mathbf{k},j,\omega)}{\frac{\partial B}{\partial\omega}}\right], \tag{114}$$

which then leads to the self-consistency equation for $|S_{\mathbf{q}}|$ by multiplying both sides by $S^{-}_{-\mathbf{q}}$ and substituting for $M^{+}_{\mathbf{q}}S^{-}_{-\mathbf{q}}$. Knowing, at zero temperature, the value of $|M_{\mathbf{q}}|$ from (113), satisfying the self-consistency equation becomes much simpler than at finite temperatures.

The free energy reduces to the energy, or, the first line of (104), where Fermi functions are replaced with step functions. In the limit $T \to 0$, (103) cancels exactly with $E_0^{MO} - N\lambda$, and therefore the zero temperature energy $\langle E\rangle$ reduces to the conduction band energies.

4.5 $S = \frac{1}{2}$: Finite Temperature

With the rotation matrix for $S = \frac{1}{2}$ as given by (12), the definition of the ordering constants in (67) now reduces to, for example,

$$M^{+}_{\mathbf{q}} = \frac{1}{N}\sum_{\mathbf{k}}\langle r_{-\frac{1}{2}} f^{\dagger}_{\mathbf{k}-\mathbf{q},\frac{1}{2}} f_{\mathbf{k},-\frac{1}{2}}\rangle = \frac{1}{N}\sum_{\mathbf{k}}\langle f^{\dagger}_{\mathbf{k}-\mathbf{q},\frac{1}{2}} f_{\mathbf{k},-\frac{1}{2}}\rangle. \tag{115}$$

Therefore, the ordering constants become

$$\begin{aligned} M_{\mathbf{q}}^{+} &= \frac{1}{N}\sum_{\mathbf{k}}\langle f_{\mathbf{k},\frac{1}{2}}^{\dagger} f_{\mathbf{k}+\mathbf{q},-\frac{1}{2}}\rangle = \frac{1}{N}\sum_{\mathbf{k}}\langle f_{\mathbf{k}-\mathbf{q},\frac{1}{2}}^{\dagger} f_{\mathbf{k},-\frac{1}{2}}\rangle, \\ S_{\mathbf{q}}^{+} &= \frac{1}{N}\sum_{\mathbf{k}}\langle c_{\mathbf{k},\frac{1}{2}}^{\dagger} c_{\mathbf{k}+\mathbf{q},-\frac{1}{2}}\rangle = \frac{1}{N}\sum_{\mathbf{k}}\langle c_{\mathbf{k}-\mathbf{q},\frac{1}{2}}^{\dagger} c_{\mathbf{k},-\frac{1}{2}}\rangle, \text{ and} \\ M_{-\mathbf{q}}^{-} &= \left(M_{\mathbf{q}}^{+}\right)^{\dagger}, \quad S_{-\mathbf{q}}^{-} = \left(S_{\mathbf{q}}^{+}\right)^{\dagger}. \end{aligned} \tag{116}$$

Variational Method

Just as in the mean-field representation of the $J = \frac{3}{2}$ system, there no c-f operator cross-terms. In the $S = \frac{1}{2}$ system, the column vector of operators and matrix for the Hamiltonian are written

$$\left[c_{\mathbf{k},\frac{1}{2}}^{\dagger} \quad c_{\mathbf{k}+\mathbf{q},-\frac{1}{2}}^{\dagger} \quad f_{\mathbf{k},\frac{1}{2}}^{\dagger} \quad f_{\mathbf{k}+\mathbf{q},-\frac{1}{2}}^{\dagger}\right], \text{ and} \tag{117}$$

$$\begin{pmatrix} \varepsilon_{\mathbf{k}} & -\frac{1}{2}\mathcal{J}M_{-\mathbf{q}}^{-} & 0 & 0 \\ -\frac{1}{2}\mathcal{J}M_{\mathbf{q}}^{+} & \varepsilon_{\mathbf{k}+\mathbf{q}} & 0 & 0 \\ 0 & 0 & \lambda & -\frac{1}{2}\mathcal{J}S_{-\mathbf{q}}^{-} \\ 0 & 0 & -\frac{1}{2}\mathcal{J}S_{\mathbf{q}}^{+} & \lambda \end{pmatrix}. \tag{118}$$

Equivalently, the momenta of the c, f, and ε terms in (117) and (118) can be shifted by subtracting a $\mathbf{q}$.

The Hamiltonian can thusly be written as

$$H_{\mathbf{q}} = E_0^{MO} - N\lambda + \sum_{\mathbf{k}} \psi_{\mathbf{k},\mathbf{q}}^{\dagger} \mathbf{H}_{\mathbf{k},\mathbf{q}} \psi_{\mathbf{k},\mathbf{q}} \tag{119}$$

where

$$E_0^{MO} = \frac{N\mathcal{J}}{2}\left(M_{\mathbf{q}}^{+}S_{-\mathbf{q}}^{-} + S_{\mathbf{q}}^{+}M_{-\mathbf{q}}^{-}\right). \tag{120}$$

Because of the form of the matrix in (118) as compared to that of the $J = \frac{3}{2}$ system, the eigenvalues are found in a straightforward manner. For the interacting local moments, they are found to be

$$v_j(\mathbf{q}) = \lambda + j\mathcal{J}|S_{\mathbf{q}}|\,, \tag{121}$$

and for the conduction band,

$$\begin{aligned} u_{\mathbf{k},\mathbf{q}}^{\pm} &= \frac{\varepsilon_{\mathbf{k}} + \varepsilon_{\mathbf{k}+\mathbf{q}}}{2} \pm \sqrt{\left(\frac{\varepsilon_{\mathbf{k}} - \varepsilon_{\mathbf{k}+\mathbf{q}}}{2}\right)^2 + \frac{\mathcal{J}^2|M_{\mathbf{q}}|^2}{4}} \\ &= \frac{\varepsilon_{\mathbf{k}-\mathbf{q}} + \varepsilon_{\mathbf{k}}}{2} \pm \sqrt{\left(\frac{\varepsilon_{\mathbf{k}-\mathbf{q}} - \varepsilon_{\mathbf{k}}}{2}\right)^2 + \frac{\mathcal{J}^2|M_{\mathbf{q}}|^2}{4}} \end{aligned} \tag{122}$$

Hereafter, the interchangeability of the $(\mathbf{k},\mathbf{k}+\mathbf{q})$ and $(\mathbf{k}-\mathbf{q},\mathbf{k})$ differences will be implicitly assumed.

The free energy takes the same form as (104), with the caveat that the symbols, such as E_0^{MO}, refer to the $S = \frac{1}{2}$ definitions given in this section. Extremization of the free energy leads to the expressions for the ordering constants:

$$M_{\pm\mathbf{q}}^{\pm} = -\frac{1}{2}\frac{S_{\pm\mathbf{q}}^{\pm}}{|S_{\mathbf{q}}|}\left[f\left(\lambda - \frac{\mathcal{J}|S_{\mathbf{q}}|}{2}\right) - f\left(\lambda + \frac{\mathcal{J}|S_{\mathbf{q}}|}{2}\right)\right], \text{ and} \tag{123}$$

$$S_{\pm\mathbf{q}}^{\pm} = -\frac{\mathcal{J}M_{\pm\mathbf{q}}^{\pm}}{4N}\sum_{\mathbf{k}}\frac{f\left(\frac{\varepsilon_{\mathbf{k}}+\varepsilon_{\mathbf{k}-\mathbf{q}}}{2} - \Delta_{\mathbf{k}}\right) - f\left(\frac{\varepsilon_{\mathbf{k}}+\varepsilon_{\mathbf{k}-\mathbf{q}}}{2} + \Delta_{\mathbf{k}}\right)}{\Delta_{\mathbf{k}}}, \tag{124}$$

where

$$\Delta_{\mathbf{k}} = \sqrt{\left(\frac{\varepsilon_{\mathbf{k}-\mathbf{q}} - \varepsilon_{\mathbf{k}}}{2}\right)^2 + \frac{\mathcal{J}^2|M_{\mathbf{q}}|^2}{4}}. \tag{125}$$

Green's Function Method

The Matsubara-type Green's functions for the $S = \frac{1}{2}$ are:

$$\begin{aligned}
\langle\langle c_{\mathbf{k},\uparrow} | c^{\dagger}_{\mathbf{k}',j'} \rangle\rangle_{i\Omega_n} &= \frac{\delta_{\uparrow,j'}\delta(\mathbf{k}-\mathbf{k}')(i\Omega - \varepsilon_{\mathbf{k}+\mathbf{q}}) - \delta_{\downarrow,j'}\delta(\mathbf{k}+\mathbf{q}-\mathbf{k}')\frac{\mathcal{J}M^{-}_{-\mathbf{q}}}{2}}{(i\Omega - \varepsilon_{\mathbf{k}})(i\Omega - \varepsilon_{\mathbf{k}+\mathbf{q}}) - \frac{\mathcal{J}^2|M_{\mathbf{q}}|^2}{4}}, \\
\langle\langle c_{\mathbf{k},\downarrow} | c^{\dagger}_{\mathbf{k}',j'} \rangle\rangle_{i\Omega_n} &= \frac{\delta_{\downarrow,j'}\delta(\mathbf{k}-\mathbf{k}')(i\Omega - \varepsilon_{\mathbf{k}-\mathbf{q}}) - \delta_{\uparrow,j'}\delta(\mathbf{k}-\mathbf{q}-\mathbf{k}')\frac{\mathcal{J}M^{+}_{\mathbf{q}}}{2}}{(i\Omega - \varepsilon_{\mathbf{k}})(i\Omega - \varepsilon_{\mathbf{k}-\mathbf{q}}) - \frac{\mathcal{J}^2|M_{\mathbf{q}}|^2}{4}}, \\
\langle\langle f_{\mathbf{k},\uparrow} | f^{\dagger}_{\mathbf{k}',j'} \rangle\rangle_{i\Omega_n} &= \frac{\delta_{\uparrow,j'}\delta(\mathbf{k}-\mathbf{k}')(i\Omega - \lambda) - \delta_{\downarrow,j'}\delta(\mathbf{k}+\mathbf{q}-\mathbf{k}')\frac{\mathcal{J}S^{-}_{-\mathbf{q}}}{2}}{(i\Omega - \lambda)^2 - \frac{\mathcal{J}^2|S_{\mathbf{q}}|^2}{4}}, \text{ and} \\
\langle\langle f_{\mathbf{k},\downarrow} | f^{\dagger}_{\mathbf{k}',j'} \rangle\rangle_{i\Omega_n} &= \frac{\delta_{\downarrow,j'}\delta(\mathbf{k}-\mathbf{k}')(i\Omega - \lambda) - \delta_{\uparrow,j'}\delta(\mathbf{k}-\mathbf{q}-\mathbf{k}')\frac{\mathcal{J}S^{+}_{\mathbf{q}}}{2}}{(i\Omega - \lambda)^2 - \frac{\mathcal{J}^2|S_{\mathbf{q}}|^2}{4}}.
\end{aligned} \tag{126}$$

The occupation numbers are

$$n^f = f(\lambda - \frac{1}{2}\mathcal{J}|S_{\mathbf{q}}|) + f(\lambda + \frac{1}{2}\mathcal{J}|S_{\mathbf{q}}|), \text{ and} \tag{127}$$

$$\begin{aligned}
n^c = \frac{1}{N}\sum_{\mathbf{k}}\frac{1}{\Delta_{\mathbf{k}}}\Bigg(& \left[\frac{\varepsilon_{\mathbf{k}-\mathbf{q}} - \varepsilon_{\mathbf{k}}}{2} + \Delta_{\mathbf{k}}\right] f\big(\frac{\varepsilon_{\mathbf{k}} + \varepsilon_{\mathbf{k}-\mathbf{q}}}{2} - \Delta_{\mathbf{k}}\big) \\
& - \left[\frac{\varepsilon_{\mathbf{k}-\mathbf{q}} - \varepsilon_{\mathbf{k}}}{2} - \Delta_{\mathbf{k}}\right] f\big(\frac{\varepsilon_{\mathbf{k}} + \varepsilon_{\mathbf{k}-\mathbf{q}}}{2} + \Delta_{\mathbf{k}}\big) \quad \Bigg).
\end{aligned} \tag{128}$$

The ordering constants found from the above Green's functions are equivalent to those of (123) and (124).

4.6 $S = \frac{1}{2}$: MO-PM Phase Boundary

As in all other cases thus far discussed, the $S = \frac{1}{2}$ ordered Hamiltonian reduces to a non-interacting one at the boundary with the PM phase due to the vanishing of the ordering constants. The dressed occupation numbers reduce to their bare counterparts. The Lagrange multiplier λ is resolved from (54) as

$$\lambda = \mu + k_B T \mathrm{Ln} 2J = \mu. \tag{129}$$

In a manner similar to the $J = \frac{3}{2}$ case, the self-consistency equation for $|S_{\mathbf{q}}|$ becomes

$$1 = \frac{1}{32} \mathcal{J} \beta \frac{1}{N} \sum_{\mathbf{k}} \frac{f(\varepsilon_{\mathbf{k}}) - f\left(\varepsilon_{\mathbf{k}-\mathbf{q}}\right)}{\varepsilon_{\mathbf{k}-\mathbf{q}} - \varepsilon_{\mathbf{k}}}. \tag{130}$$

4.7 $S = \frac{1}{2}$: Zero Temperature

In the limit $T \to 0$ only the lowest-lying energy levels are occupied. For the local-moment occupation number, this is expressible as

$$n^f = \Theta(\mu - \lambda + \frac{1}{2} \mathcal{J} |S_{\mathbf{q}}|), \tag{131}$$

which mimicks what appears in the $J = \frac{3}{2}$ zero-temperature section, above. Unlike the said $J = \frac{3}{2}$ derivation, in $S = \frac{1}{2}$, the explicit representation of the eigenvalues related to the interacting conduction band allows a further point to be made. With the presence of the

ordering vector $\mathbf{q}$, an interacting itinerant moment may occupy a higher energy state even at zero temperature. This can be seen by comparing $\varepsilon_{\mathbf{k}}$ and $\varepsilon_{\mathbf{k}\pm\mathbf{q}}$: the presence of $\mathbf{q}$ may place $u^{+}(\mathbf{k},\mathbf{q})$ above the band gap. Hence, the conduction-band occupation number retains both $u^{-}(\mathbf{k},\mathbf{q})$ and $u^{+}(\mathbf{k},\mathbf{q})$ terms.

$$n^{c} = \frac{1}{N}\sum_{\mathbf{k}}\frac{1}{\Delta_{\mathbf{k}}}\Bigg(\quad \left[\frac{\varepsilon_{\mathbf{k}-\mathbf{q}}-\varepsilon_{\mathbf{k}}}{2}+\Delta_{\mathbf{k}}\right]\Theta\big(\mu-\frac{\varepsilon_{\mathbf{k}}+\varepsilon_{\mathbf{k}-\mathbf{q}}}{2}+\Delta_{\mathbf{k}}\big) \\ -\left[\frac{\varepsilon_{\mathbf{k}-\mathbf{q}}-\varepsilon_{\mathbf{k}}}{2}-\Delta_{\mathbf{k}}\right]\Theta\big(\mu-\frac{\varepsilon_{\mathbf{k}}+\varepsilon_{\mathbf{k}-\mathbf{q}}}{2}-\Delta_{\mathbf{k}}\big) \quad \Bigg). \tag{132}$$

This is ultimately true for the $J=\frac{3}{2}$ case as well, but the argument has less clarity due to the delta-function expressions used to circumvent solutions of either the determinant of the matrix (70) or the denominators of the Green's functions.

The f-f ordering constant at zero temperature becomes

$$M^{\pm}_{\pm\mathbf{q}} = -\frac{1}{2}\frac{S^{\pm}_{\pm\mathbf{q}}}{|S_{\mathbf{q}}|}\Theta\big(\mu-\lambda+\frac{\mathcal{J}|S_{\mathbf{q}}|}{2}\big). \tag{133}$$

With the above, the constant is resolved to be

$$|M_{\mathbf{q}}| = \frac{1}{2}. \tag{134}$$

Likewise, for the purposes of resolving $|S_{\mathbf{q}}|$ numerically,

$$M^{+}_{\mathbf{q}}S^{-}_{-\mathbf{q}} = -\frac{1}{2}|S_{\mathbf{q}}|\,\Theta\big(\mu-\lambda+\frac{\mathcal{J}|S_{\mathbf{q}}|}{2}\big). \tag{135}$$

The c-c ordering constant then becomes

$$S^{\pm}_{\pm\mathbf{q}} = -\frac{\mathcal{J}M^{\pm}_{\pm\mathbf{q}}}{4N}\sum_{\mathbf{k}}\frac{\Theta\big(\mu-\frac{\varepsilon_{\mathbf{k}}+\varepsilon_{\mathbf{k}-\mathbf{q}}}{2}+\Delta_{\mathbf{k}}\big)-\Theta\big(\mu-\frac{\varepsilon_{\mathbf{k}}+\varepsilon_{\mathbf{k}-\mathbf{q}}}{2}-\Delta_{\mathbf{k}}\big)}{\Delta_{\mathbf{k}}}, \tag{136}$$

or, multiplying both sides by $S_{\mathbf{q}}^{-}$ and using (135),

$$|S_{\mathbf{q}}| = \frac{\mathcal{J}}{8N}\sum_{\mathbf{k}}\frac{\Theta\left(\mu - \frac{\varepsilon_{\mathbf{k}}+\varepsilon_{\mathbf{k}-\mathbf{q}}}{2} + \Delta_{\mathbf{k}}\right) - \Theta\left(\mu - \frac{\varepsilon_{\mathbf{k}}+\varepsilon_{\mathbf{k}-\mathbf{q}}}{2} - \Delta_{\mathbf{k}}\right)}{\Delta_{\mathbf{k}}}. \tag{137}$$

The free energy reduces to the energy, and just as with the $J = \frac{3}{2}$ case,

$$\lim_{T\to 0}\left[v_{-\frac{1}{2}}(\mathbf{q})f\left(v_{-\frac{1}{2}}(\mathbf{q})\right) + v_{\frac{1}{2}}(\mathbf{q})f\left(v_{\frac{1}{2}}(\mathbf{q})\right)\right] = \left(\lambda - \frac{1}{2}\mathcal{J}|S_{\mathbf{q}}|\right), \tag{138}$$

$$E_0^{MO} = \frac{1}{2}N\mathcal{J}|S_{\mathbf{q}}|, \tag{139}$$

so that

$$\lim_{T\to 0}\left[\sum_j v_j(\mathbf{q})f\left(v_j(\mathbf{q})\right) + E_0^{MO} - N\lambda\right] = 0. \tag{140}$$

Thusly the energy reduces to that of the conduction band energies.

CHAPTER 5

DISCUSSION AND RESULTS

In this chapter, the application and results of the methodology laid out in chapters 2 through 4 will be detailed. This involves, first, a discussion of numerics: the computer code, algorithms, indeterminacies, and shortcuts will be reviewed below in section 5.1. Results for the spin-half system will appear in section 5.2, and for the spin-three-halves system in 5.3. Discussion of the results will follow in 5.4.

Hereafter, the Lagrange multiplier, λ, found in (10) and appearing throughout this work, will be interpreted as the energy level of the local moments, E_f. The bandwidth, which can be found from (4) to be $12t$, will be designated as W for convenience.

5.1 Implementation

With respect to computational algorithms, each portion of the phase diagram for each total angular momentum is taken as a separate case. For instance, in $S = \frac{1}{2}$, datapoints for the finite-temperature PM-MO boundary are calculated separately from zero-temperature energies. Each portion of the phase diagram, having its own constraints, self-consistency equations, and appropriate constants, therefore has its own algorithm. Ideally, an algorithm begins with the fewest necessary values that must be chosen as independent variables, and then proceeds to calculate values from those, until the self-consistency condition may be

computed and free energies tabulated, where appropriate. The $S = \frac{3}{2}$ Kondo phase will be used as an illustration. At the Kondo-PM boundary, the algorithm is as follows:

1. A temperature T and chemical potential μ are chosen. The hybridization is set: $|V| = 0$.
2. The local-moment energy level is set: $E_f = \mu + k_B T \log 3$.
3. The conduction band occupation n_c is calculated through the bare density of states.
4. $\mathcal{J}$ is calculated from the self-consistency condition (55).
5. Steps 1 through 4 are repeated for various values of T and μ to produce a dataset which is then filtered for a desired $\mathcal{J}$ and binned by n_c.
6. Each n_c bin is filtered for the greatest T. This maximal T is T_K.
7. The resulting histogram displays an estimate of the Kondo-PM boundary in the n_c-T plane.

Away from the boundary with the PM phase, the amount of computation increases. At $T = 0$, where the target result is not T_K but the free energy F, the algorithm becomes:

1. Values for the product $\mathcal{J}|V|$ and E_f are chosen.
2. μ is calculated such that the local-moment occupation satisfies $n_f = 1$.
3. With μ, E_f, and $\mathcal{J}|V|$, n_c is calculated.
4. n_f is recalculated as a "sanity" check.
5. $\mathcal{J}$ is calculated from (62), and $|V|$ is then calculated having knowledge of $\mathcal{J}$.
6. F is calculated.

7. Steps 1 through 6 are repeated for various values of $\mathcal{J}|V|$ and E_f to produce a dataset which is then filtered for a desired $\mathcal{J}$ and binned by n_c.

8. Each n_c is filtered for the least F. This minimal F can be compared to a minimal F calculated in the MO phase at $T = 0$.

9. The resulting histogram displays an estimate of the $T = 0$ energy with repect to n_c.

While the above two algorithms do not depend upon each other, the latter must be used before finite-temperature points lying away from the PM boundary can be calculated. This is because the parameter space (T,μ,E_f,$\mathcal{J}$,$|V|$) must be searched for self-consistent tuples of parameters, and having guesses that are likely to be near self-consistency greatly improves the chances of reaching said tuples. This, in a practical sense, means that solution requires an educated guess at $|V|$. However, at the Kondo-PM boundary, a vanishing $|V|$ implies a lack of information from which an educated guess can be drawn. At $T = 0$, however, a $|V| > 0$ is produced. Furthermore, even having an educated guess from which the process of solution can begin, the algorithm used below is not guaranteed to reach definite success or failure. It is as follows:

1. A pre-calculated set of values is used from the $T = 0$ algorithm: n_c,μ,E_f,$\mathcal{J}$, and $|V|$.

2. A temperature T is chosen.

3. T, and the input-guesses of step 1 are used to calculate a new value for μ, μ', such that n_c retains its step-1 value to within a specified uncertainty.

4. With μ', $\mathcal{J}$ is recalculated using (35). This will be $\mathcal{J}'$.

5. With μ' and $\mathcal{J}'$, an E_f' is calculated.

6. $\mathcal{J}'$ and E_f' are compared against $\mathcal{J}$ and E_f, and if the values do not match to within a specified uncertainty, $|V|'$ is calculated. If, however, a match is found, then the process may end with a calculation of F.

7. The process returns to step 3 using μ', $\mathcal{J}'$, E_f', and $|V|'$ as its starting guesses.

Without any further refinement of this algorithm, the process will not terminate until success is reached, that being defined by guess values matching calculated (or primed) values. Success is reached, therefore, by discovery of a fixed point in parameter space. If parameter space were made finite by physical considerations, and the search through it were ergodic, then the speed of success ought to be inversely related to the size of the basin (or basins) of attraction in parameter space. To frame this discussion in terms of dynamics, the algorithm above defines a map h:(μ,E_f,$\mathcal{J}$,$|V|$)$\rightarrow$(μ',E_f',$\mathcal{J}'$,$|V|'$). For simplicity, the parameter tuplet will be denoted ξ. Success is possible if the map is eventually periodic, i.e., if in the orbit of h, $h^{n+i}(\xi) = h^n$ for some $n \in \mathcal{Z}$ and for $i = 1$. The map must have a fixed point of period 1. However, in practice, h is often found to be eventually periodic with $i > 1$, which implies that self-consistency is not reached, and that the algorithm will not terminate. Hence, fixed points of period 2 or more cause the computation to loop without end. Refinement of the algorithm is prudent: under certain conditions, such as the detection of a fixed point of period greater than unity, the values in ξ' are randomized before the algorithm returns to step (3). Ergodicity of the parameter-space search is now dependent on the pseudorandom number generator used. Even so, resources for computation are limited and the algorithm cannot be allowed to iterate until it indefinitely reaches success. A further refinement is therefore required, that being of forced cessation when a specified number of iterations have been performed without the achievement of self-consistency. After refining the above algorithm, its results can be said to be indeterminate: one does not know prior to execution whether the algorithm will find a self-consistent data tuplet or self-terminate in failure.

Altogether, the greatest implementational difficulties for the Kondo phase lie in computing finite-temperature, finite-hybridization datapoints. Moreover, many of the relationships derived in chapter 3 contain sums over momentum vectors, $\mathbf{k}$, which can be converted into integrals over energy via

$$\sum_{\mathbf{k}} = \int_{-\infty}^{\infty} dE \rho(E), \tag{141}$$

where $\rho(x)$ is the density of states. However, for uniformity of code between algorithms, vector summations are used in the calculations for this work with the exception of the density of states plots found in Figure 5.4. In the MO phase, however, such replacement is complicated by the presence of the ordering vector $\mathbf{q}$. Because of this complication, no replacements of summations by integrals are performed for MO-phase calculations.

The algorithms for the MO phase necessarily differ from those of the Kondo phase in two major ways. For the first, magnetic ordering is expressed via the vector $\mathbf{q}$. In the algorithms used in this work, $\mathbf{q}$ becomes an independent variable and is thus chosen in the first step. Datapoints are computed at various $\mathbf{q}$ values. These test-$\mathbf{q}$'s are gotten by sampling at regular intervals each directional component on $[-\pi, \pi)$. When the resulting datapoints are processed for highest temperature (T_{MO}) or for least free energy, $\mathbf{q}$ must be considered. In other words, at a given n_c, T_{MO} corresponds to the highest T that any tested $\mathbf{q}$ could produce. For the second way in which the algorithms of the MO and Kondo phases differ, the MO phase contains two constants which must be self-consistently determined, $|M|$ and $|S|$, and not just one, $|V|$. At zero-temperature, $|M|$ is fixed by (113), and the equations for $|S|$ require a value for $\mathcal{J}$ (or else vice versa). In practice, this means that the zero-temperature is complicated only by the many floating-point computations needed to evaluate its quantities. The finite-temperature, non-PM-boundary algorithm is also simpler than its Kondo-phase counterpart. The following is for $S = \frac{3}{2}$:

1. A pre-calculated set of values is used from the $T = 0$ algorithm: n_c,μ,E_f, and $|S|$. $\mathcal{J}$ has been fixed by the $T = 0$ calculation, and $|M|$ is initially fixed by (113).

2. T and $\mathbf{q}$ are chosen.

3. T, $\mathbf{q}$, and the input-guesses of step 1 are used to calculate a new value for μ, μ', such that n_c retains its step-1 value to within a specified uncertainty.

4. With μ', $|S|'$ is calculated from using (94) and the alterations found below it in the text.

5. With μ' and $|S|'$, an E_f' is calculated.

6. From these values, $|M|'$ is calculated. If, to within a specified uncertainty, $|M| = |M|'$, F may be computed and the algorithm terminated.

7. If not, the algorithm returns to step 3 using the primed values as its guesses.

At first glance, this algorithm has all of the difficulties that the Kondo-version has. In practice, however, this algorithm generally terminates successfully in just a few iterations, with exceptions becoming more prevalent as the temperature increases. Whereas the Kondo-version algorithm consumes resources by its iterations and randomization, the MO-version consumes resources with the monumentous task of computing n_c, which is itself interdependent with computations of μ and E_f.

Specifically, the aforementioned difficulties of the finite-temperature, non-PM-boundary algorithms have impacted the results of this work. To produce the first-order Kondo-MO phase boundary, free energies must be examined at datapoints sufficiently close to each other in a ($\mathcal{J}$,n_c,T) parameter space so as to allow reasonable comparison. Because the MO-phase datapoints are more reliably computed, they are computed first. However, the use of integrals over $\mathbf{k}$-summations of heat-kernel expressions for Dirac delta functions,

such as in (98), demands lower precisions in order to reach completion inside of realistic constraints on resources. If a datapoint can be computed in the MO phase, then a nearby, if not identical, datapoint must be computed in the Kondo phase. However, some such datapoints have yet to be obtained. At best, extrapolation along the Kondo free energy curve might be used from the nearest possible datapoints to obtain an intersection with the MO free energy curve. Extrapolation is not done here. It is with these considerations in mind that the Kondo-MO phase boundary be regarded as an estimate even within the realm of mean-field approximations.

The algorithms for free energies and critical temperatures (T_K and T_{MO}), above, have been implemented in the C programming language with the GNU C compiler. All computations have been made on 64-bit architectures, in 64-bit X-based operating system environments and with 64-bit code libraries. Floating-point numerical operations are carried out in double precision (8-byte representation). Methods for adaptive numerical integration and for interpolation of the bare density of states (see below) were provided by the GNU Scientific Library (GSL). Pseudorandom number generation was provided by the Mersenne twister dSFMT library, written by M. Saito and M. Matsumoto. When executed on Temple University's Owl's Nest 2, the underlying architecture was Intel technology, and hence propietary Intel libraries provided the underpinnings for GSL and transcendental function calls. Data, once produced, have been processed with scripts in PERL or Python, for example to filter for a target $\mathcal{J}$ or to identify maximal critical temperatures.

Summations over $\mathbf{k}$ have been implemented with custom code, using either a trapezoidal method or a Simpson's rule method. With n divisions of an interval of length L, the trapezoidal rule produces for a cube $(L/n)^3 = I^3$ calculations. As an example, this work uses a domain of $\mathbf{k} \in [-\pi, \pi)$, so that an interval size of 0.001 produces, in three dimensions, about 2.5×10^{11} calculations of a summand. Interval sizes from 1×10^{-3} down to

1×10^{-6} have been used in this work variously with trapezoidal and Simpson's rules, where resources are balanced against precision.

As mentioned earlier in this section, for a small subset of calculations, summations over $\mathbf{k}$ are replaced by integrals over energy. This replacement is made to achieve reduced resource load in a manner that will now be demonstrated.

For the bare density of states the following expression provides a starting point:

$$\rho_0(E) = \sum_{\mathbf{k}} \delta\big(E - \varepsilon_{\mathbf{k}}\big), \tag{142}$$

where $\varepsilon_{\mathbf{k}}$ is given by equation (4). The Dirac delta is then replaced by its Fourier transformation:

$$\begin{aligned}
\rho_0(E) &= \sum_{\mathbf{k}} \int_{-\infty}^{\infty} d\omega \, \mathrm{e}^{i\omega\left(E-\varepsilon_{\mathbf{k}}\right)} \\
&= \int_{-\infty}^{\infty} \frac{d\omega}{2\pi} \, \mathrm{e}^{i\omega E} \sum_{\mathbf{k}} \mathrm{e}^{-i\omega\varepsilon_{\mathbf{k}}} \\
&= \int_{-\infty}^{\infty} \frac{d\omega}{2\pi} \, \mathrm{e}^{i\omega E} \left[\sum_{k_x} \mathrm{e}^{i2t\omega\cos k_x a}\right] \left[\sum_{k_y} \mathrm{e}^{i2t\omega\cos k_y a}\right] \left[\sum_{k_z} \mathrm{e}^{i2t\omega\cos k_z a}\right],
\end{aligned} \tag{143}$$

or, due to the invariance of $\varepsilon_{\mathbf{k}}$ under interchange of axes,

$$= \int_{-\infty}^{\infty} \frac{d\omega}{2\pi} \, \mathrm{e}^{i\omega E} \left[\sum_{k} \mathrm{e}^{i2t\omega\cos ka}\right]^3, \tag{144}$$

where the axis index has been dropped. Making a change of variables, $a\mathbf{k} \to \mathbf{k}'$, with the summation of $\mathbf{k}'$ running from $-\pi$ to π:

$$\begin{aligned} &= \int_{-\infty}^{\infty} \frac{d\omega}{2\pi} e^{i\omega E} \left[\sum_{k' \in [-\pi,\pi]} e^{i2t\omega\cos k'} \right]^3. \\ &= \int_{-\infty}^{\infty} \frac{d\omega}{2\pi} e^{i\omega E} \left[\int_{-\pi}^{\pi} \frac{dk'}{2\pi} e^{i2t\omega\cos k'} \right]^3 \\ &= \int_{-\infty}^{\infty} \frac{d\omega}{2\pi} e^{i\omega E} \left[\int_{0}^{\pi} \frac{dk'}{\pi} e^{i2t\omega\cos k'} \right]^3, \end{aligned} \tag{145}$$

where the summation over k' has been treated in the continuous limit as an integral. In the final line of (145), the evenness of the integrand with respect to k' has been taken into account. Using the following identity for the Bessel function,

$$J_n(x) = \frac{i^{-n}}{\pi} \int_0^{\pi} d\theta e^{ix\cos\theta} \cos n\theta, \tag{146}$$

a choice of $n = 0$, an identification of k' with θ, and an identification of $2\omega t$ with x, produces the bracketed term in (145). Rewritten with the Bessel function, the density of states becomes

$$\begin{aligned} \rho_0(\omega) &= \int_{-\infty}^{\infty} \frac{d\omega}{2\pi} e^{i\omega E} J_0^3(2\omega t) \\ &= \int_0^{\infty} \frac{d\omega}{\pi} J_0^3(2\omega t) \cos\omega E. \end{aligned} \tag{147}$$

Despite that GSL provides an implementation for the Bessel function, the above expression is not evaluated at runtime. Rather, the expression is evaluated beforehand and its values are tabulated. Then, at runtime, an interpolation of tabulated values is used. In this way, evaluation can proceed at much improved speeds.

Lastly, the components of $\mathbf{q}$-vectors are scanned at steps of $\frac{\pi}{4}$ for $S = \frac{3}{2}$ and $\frac{\pi}{6}$ for $S = \frac{1}{2}$ on the interval $[-\pi, \pi)$. However, because certain values of $\mathbf{q}$, such as $\mathbf{q} = (0,0,0)$, lead to

division by zero (for example, a vanishing denominator in (108)), from the components of $\mathbf{q}$ are subtracted a small amount equal to the minimum predetermined resolution for determining a value such as μ, n_c, or T in a bissecting search, and equal also to the maximum relative uncertainty for GSL numerical integration. This value, chosen before code compilation, ranges from 1×10^{-3} to 1×10^{-6}, so as to balance resources against precision. Calling this value ν, the effective interval for a component of $\mathbf{q}$ is $[-\pi - \nu, \pi - \nu)$, and the zero-vector becomes $\mathbf{q} = (-\nu, -\nu, -\nu)$.

5.2 Results for $S = \frac{1}{2}$

For a coupling strength 1/12 of the bandwidth, Figure 5.1 illustrates the magnetic behavior of a material at all conduction band occupations. Ferromagnetic (FM) ordering, represented by $\mathbf{q} \to (0,0,0)$, occurs when the bands are nearly empty and nearly filled. As n_c approaches 2, FM ordering is lost in a small, finite-T region where SDW ordering remains. As seen in Table 5.1, as n_c approaches complete filling, the ordering vector at $T = 0$ approaches $(0,0,0)$ to the highest calculated fillings. However, in Table 5.2, which displays data for $T > 0$, the ordering vector reaches $(0,0,0)$, but at $n_c \geq 1.96$ assumes an incommensurate (and hence non-zero) value. It is not clear whether the non-zero value of $\mathbf{q}$ at finite temperature and near-full occupation is an artifact of numerical computation.

The datapoints nearest to empty and complete filling were calculated at n_c's of .001 and 1.999, respectively, as can be seen in Table 5.2. It is therefore a conjecture, based on the trends seen in Figure 5.1, that T_{MO} should decrease to 0 as n_c approaches 0 or 2. In support of this, the $T = 0$ values of $\mathbf{q}$, as compared with the $T = 0$ values of magnitudes of the S ordering constant, as seen in Figure 5.2, suggest that a magnetic instability cannot exist when no there are no states available for spin-flip processes.

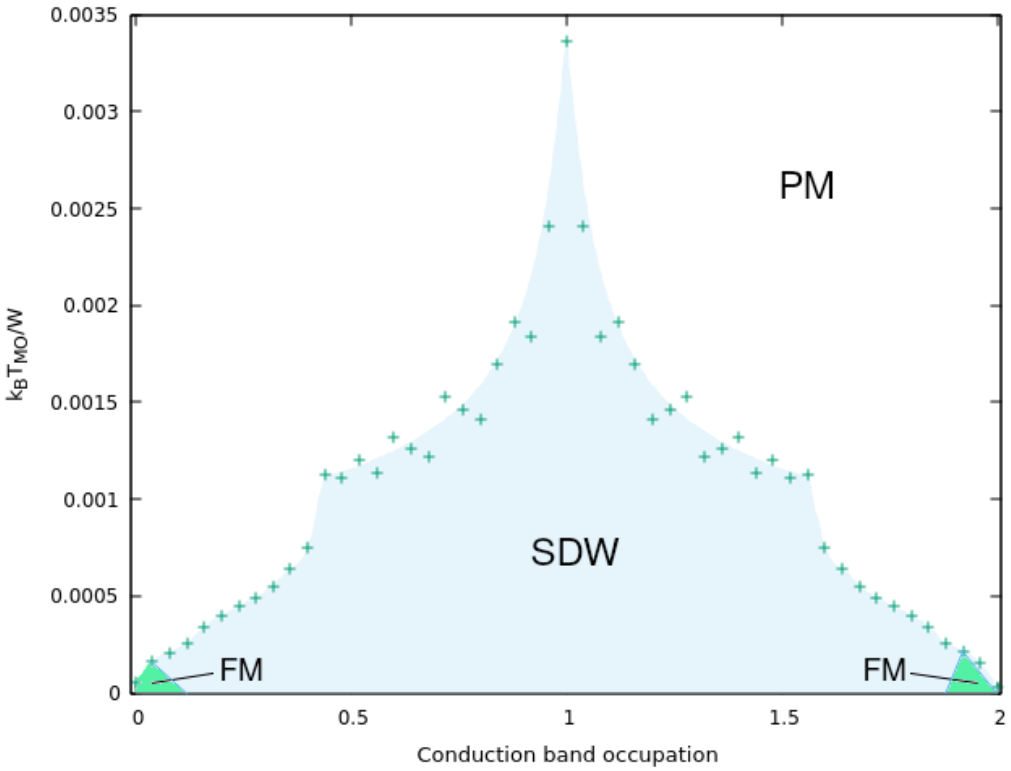

Figure 5.1: Phase diagram for S=1/2. $\mathcal{J}/W$=1/12. Colored regions are guides for the eye. See text for regions $n_c \to 0$ and $n_c \to 2$.

Figure 5.1 roughly displays a particle-hole symmetry in its ordering temperatures, the small asymmetries of which are attributed to both the binning of the data and to computational uncertainty. Assuming henceforth that this symmetry exists, then as the occupation of the conduction band moves towards half-filling ($n_c = 1$), one might expect that as the number of available states increases, the instability of the system towards magnetism should increase as well. Indeed, the ordering vector varies from $(0,0,0)$ (or nearly that, as mentioned above) to (π,π,π), and a spike in T_{MO} forms. The system can therefore be described by spin-density wave (SDW) magnetism away from empty and filled bands.

At higher ratios of $\mathcal{J}/W$, the Kondo phase is stabilized against magnetic ordering. Figure 5.3 demonstrates that at half-filling, increasing the coupling strength leads to a crossover whereby the local moments are screened. The crossover occurs at approximately

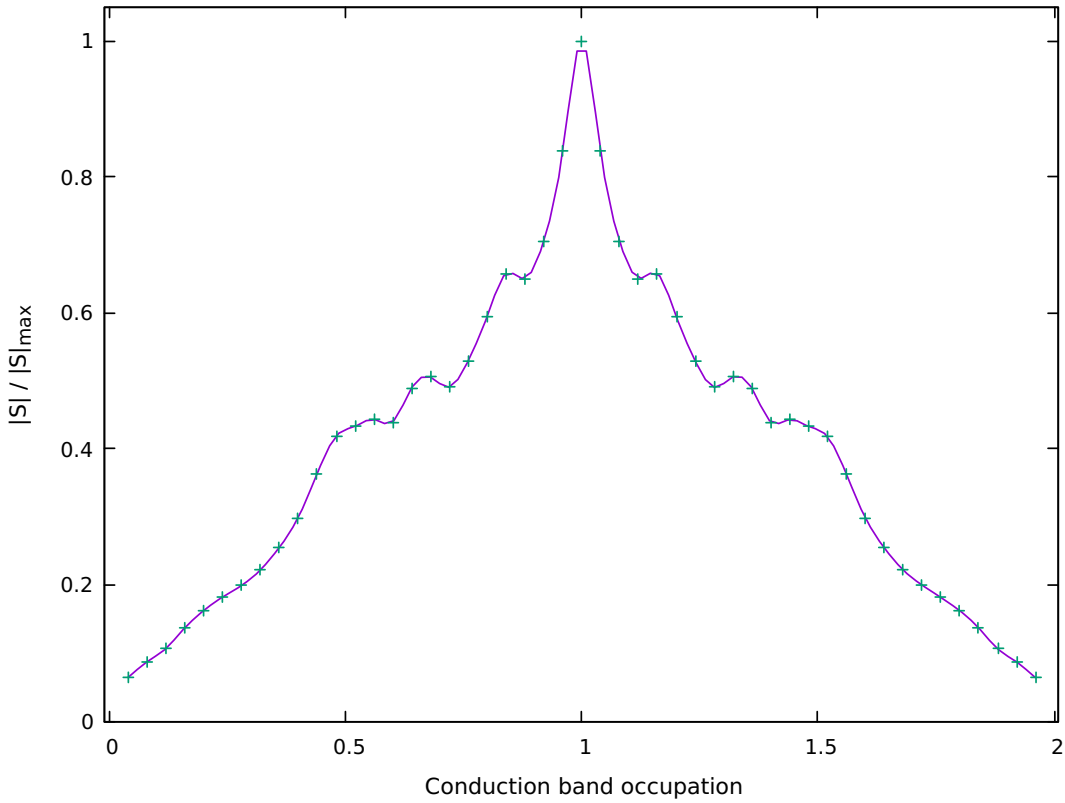

Figure 5.2: Dependency of the ordering constant $|S|$ on occupation, for a $S = 1/2$ system at $T = 0$. Interpolating spline is a guide for the eye.

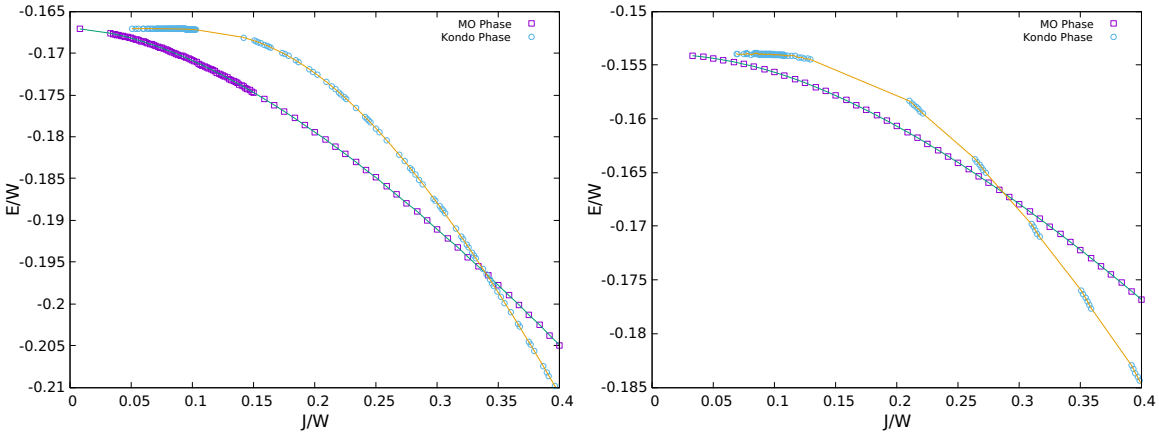

Figure 5.3: The MO-Kondo crossover for $S = 1/2$. The crossover occurs for (a) $n_c = 1$ or half-filling at $J/W \sim .34$ and for (b) $n_c = 0.7$, at $J/W \sim .29$. Lines are guides to the eye.

$\mathcal{J}/W = 0.34$, but considering the peak in critical temperatures exhibited by a magnetically-ordered system near half-filling, one might expect that crossovers occur at weaker couplings when n_c is away from half-filling. Two such possible crossovers are examined: for $n_c = 0.4$ and 0.7. At the former, the crossover occurs in the vicinity of $\mathcal{J}/W = 0.5$, but for the latter it occurs at about 0.29. The $\mathcal{J}/W$ curves for $n_c = 0.7$ are also displayed in Figure 5.3. Particle-hole symmetry dictates that a stabilization of the Kondo phase likewise occurs at $n_c = 1.3$, but it should be noted that a study has not been done, here, to identify the lowest $\mathcal{J}/W$ at which a crossover at any n_c can occur.

n_c	$\mathbf{q}$		n_c	$\mathbf{q}$
0.001	(0,0,0)		1.04	(1,1,1)
0.04	(0,0,0)		1.14	(1,1,$\frac{3}{4}$)
0.14	(1,0,0)		1.24	(1,1,$\frac{3}{4}$)
0.24	(1,$\frac{1}{4}$,0)		1.34	(1,1,$\frac{1}{2}$)
0.34	(1,$\frac{3}{4}$,0)		1.44	(1,1,$\frac{1}{4}$)
0.44	(1,1,0)		1.54	(1,1,0)
0.54	(1,1,$\frac{1}{4}$)		1.64	(1,$\frac{3}{4}$,0)
0.64	(1,1,$\frac{1}{2}$)		1.74	(1,$\frac{1}{4}$,0)
0.74	(1,1,$\frac{3}{4}$)		1.84	(1,0,0)
0.84	(1,1,$\frac{3}{4}$)		1.94	(0,0,0)
0.94	(1,1,1)		1.999	(0,0,0)

Table 5.1: $T = 0$ Ordering vectors by conduction band occupation. Components are given in units of π.

n_c	$\mathbf{q}$		n_c	$\mathbf{q}$		n_c	$\mathbf{q}$
0.001	(0,0,0)		0.68	(1,1,$\frac{1}{2}$)		1.36	(1,1,$\frac{1}{2}$)
0.04	(0,0,0)		0.72	(1,1,$\frac{2}{3}$)		1.40	(1,1,$\frac{1}{2}$)
0.08	($\frac{1}{6}$,0,0)		0.76	(1,1,$\frac{2}{3}$)		1.44	(1,1,$\frac{1}{3}$)
0.12	($\frac{1}{6}$,0,0)		0.80	(1,1,$\frac{2}{3}$)		1.48	(1,1,$\frac{1}{3}$)
0.16	(1,0,0)		0.84	(1,1,$\frac{5}{6}$)		1.52	(1,1,$\frac{1}{6}$)
0.20	(1,0,0)		0.88	(1,1,$\frac{5}{6}$)		1.56	(1,1,0)
0.24	(1,0,0)		0.92	(1,1,$\frac{5}{6}$)		1.60	(1,$\frac{5}{6}$,0)
0.28	(1,$\frac{1}{2}$,0)		0.96	(1,1,1)		1.64	(1,$\frac{5}{6}$,0)
0.32	(1,$\frac{2}{3}$,0)		1.00	(1,1,1)		1.68	(1,$\frac{2}{3}$,0)
0.36	(1,$\frac{5}{6}$,0)		1.04	(1,1,1)		1.72	(1,$\frac{1}{2}$,0)
0.40	(1,$\frac{5}{6}$,0)		1.08	(1,1,$\frac{5}{6}$)		1.76	(1,0,0)
0.44	(1,1,0)		1.12	(1,1,$\frac{5}{6}$)		1.80	(1,0,0)
0.48	(1,1,$\frac{1}{6}$)		1.16	(1,1,$\frac{5}{6}$)		1.84	(1,0,0)
0.52	(1,1,$\frac{1}{3}$)		1.20	(1,1,$\frac{2}{3}$)		1.88	($\frac{1}{6}$,0,0)
0.56	(1,1,$\frac{1}{3}$)		1.24	(1,1,$\frac{2}{3}$)		1.92	(0,0,0)
0.60	(1,1,$\frac{1}{2}$)		1.28	(1,1,$\frac{2}{3}$)		1.96	($\frac{1}{6}$,0,0)
0.64	(1,1,$\frac{1}{2}$)		1.32	(1,1,$\frac{1}{2}$)		1.999	($\frac{1}{6}$,0,0)

Table 5.2: $T > 0$ Ordering vectors by conduction band occupation. Components are given in units of π.

5.3 Results for $J = \frac{3}{2}$

Beginning with the Kondo phase and a coupling strength of $\mathcal{J}/W = 1/12$, densities of states for the itinerant moments are shown in Figure 5.4. They illustrate that a small gap exists at the local-moment energy level. The functions for the densities depends on $\mathcal{J}$, E_f, and μ, which must be solved together. Hence, each of these figures is plotted for a different set of self-consistent values, yet in each the same basic form is seen, altered only by the position of the gap. Half-filling in the $S = 3/2$ system occurs when $n_f = 1$ and $n_c = 3$.

From the densities of states, one is led to the band structure. Figure 5.5 illustrates the band structure for the itinerant moments. Horizontal lines have been placed to indicate the local-moment level as well as the chemical potential, and the gapping of the bands due to interaction between local and itinerant moments is evident.

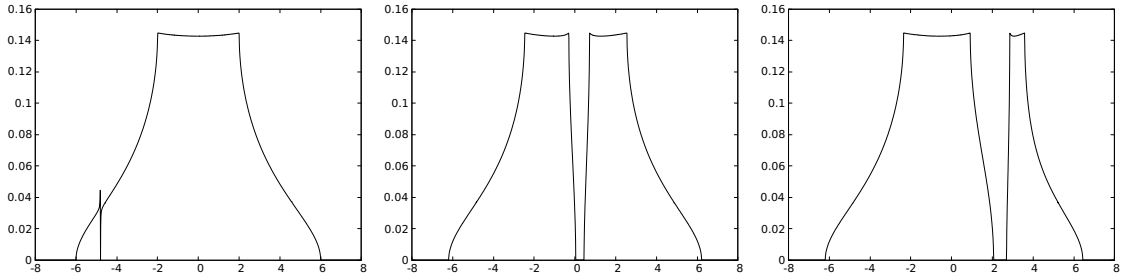

(a) $n_c = 0.2, E_f = -4.8$ **(b)** $n_c = 1.0, E_f = 0.25$ **(c)** $n_c = 1.5, E_f = 2.5$

Figure 5.4: Illustration of the gap at the local moment energy level in three exemplary densities of state in the Kondo phase. $J/W \sim 1/12$. $|V|$ varies between each plot due to self-consistency requirement. Axes are density (electrons/eV) versus energy (eV). Plots are normalized to unity.

In the $T = 0$ MO phase, the density of states evinces changes by selection of $\mathbf{q}$, and not by selection of n_c, due to the dependence of the density upon $|M|$ and not $|S|$. For this reason, the only occupation shown is that of $n_c = 0.68$, with concomitant values of $|S| = 0.64$, $|M| = 1.5$, $E_f = -2.0$, and $\mu = -3.0$. At this occupation, when $\mathbf{q}$-space is divided into increments of quarter-π, the ordering vector found to minimize the total energy is $(\frac{\pi}{4}, \frac{\pi}{4}, \frac{\pi}{4})$.

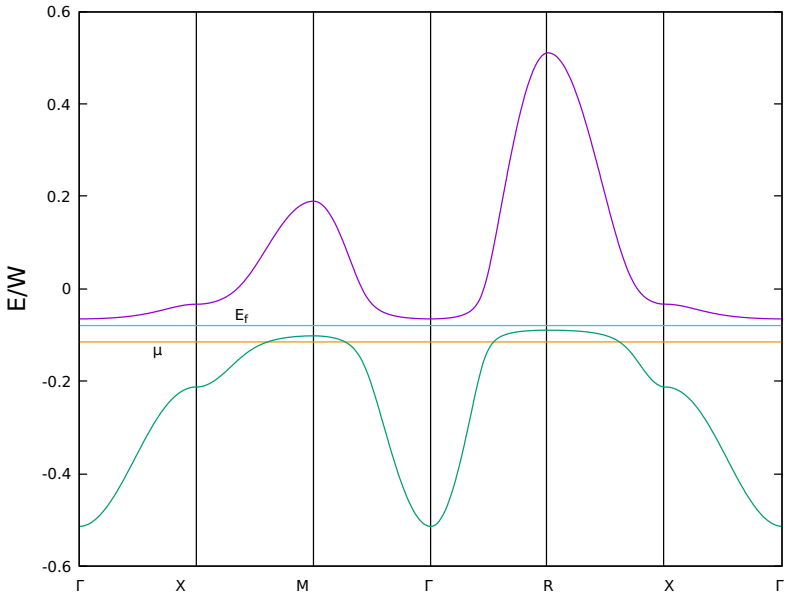

Figure 5.5: Band structure in the Kondo phase at $T = 0$. Upper and lower bands, given by plus and minus terms of (29), are separated at E_f. Values are $\mathcal{J}/W = 1/12$, $|V| = 0.25$, $E_f = -0.95$, $\mu = -1.4$, $n_c = 1.4$.

This vector indicates a SDW that is, in this work, considered to be incommensurate with the lattice. Three commensurate vectors are also chosen for the density plots. For (π,π,π), spikes are evident in the density of states at roughly ± 0.7 and ± 2.2 eV from zero energy, and may correspond to Van Hove singularities.

Similar to the $S = 1/2$ case, the length and direction of the ordering vectors changes with respect to n_c, and, moreover, tends to (0,0,0) as $n_c \to 0$ and to (π,π,π) as $n_c \to 2$. In further similarity, the ordering constant $|S|$ decreases towards zero as n_c approaches 0 and 4, as seen in Figure 5.10. The oddity found for $S = 1/2$, namely that near complete filling the system attained to ferromagnetism before again developing SDW magnetic order, is not seen in $S = 3/2$. Tables 5.3 and 5.4 list the energetically-favorable $\mathbf{q}$'s and their corresponding n_c's. As seen in these tables, the lowest and highest tested occupation numbers are 0.01 and 3.99, respectively. Hereafter, the trend $|S| \to 0$ as $n_c \to 0$ or 4 is assumed to be true.

While for $S = 1/2$ it was found that the MO phase is always favorable against the Kondo phase, in $S = 3/2$ this is not so. The plot of Figure 5.11 demonstrates that even at

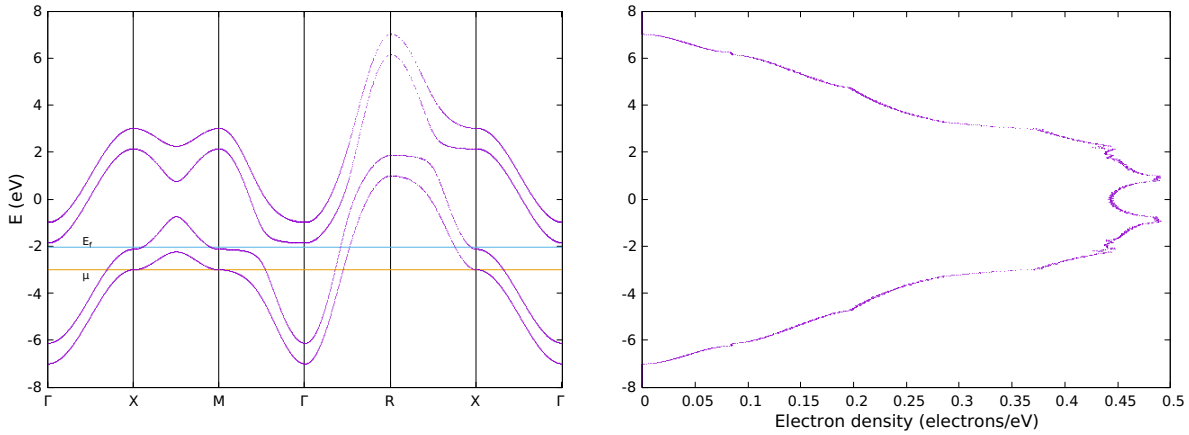

(a) **(b)**

Figure 5.6: Band structure (a) and density of states (b) for an SDW state with **q**=(π,0,0).

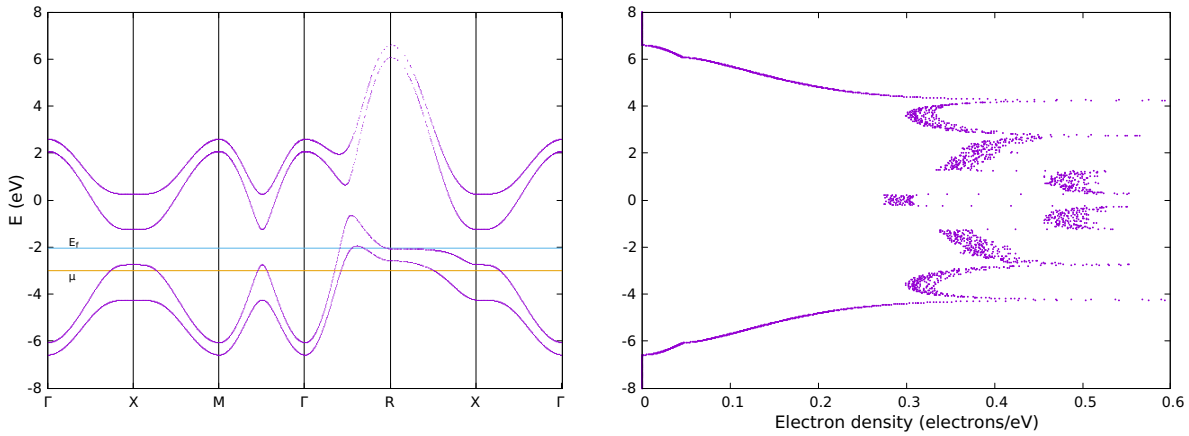

(a) **(b)**

Figure 5.7: Band structure (a) and density of states (b) for an SDW state with **q**=(π,π,0).

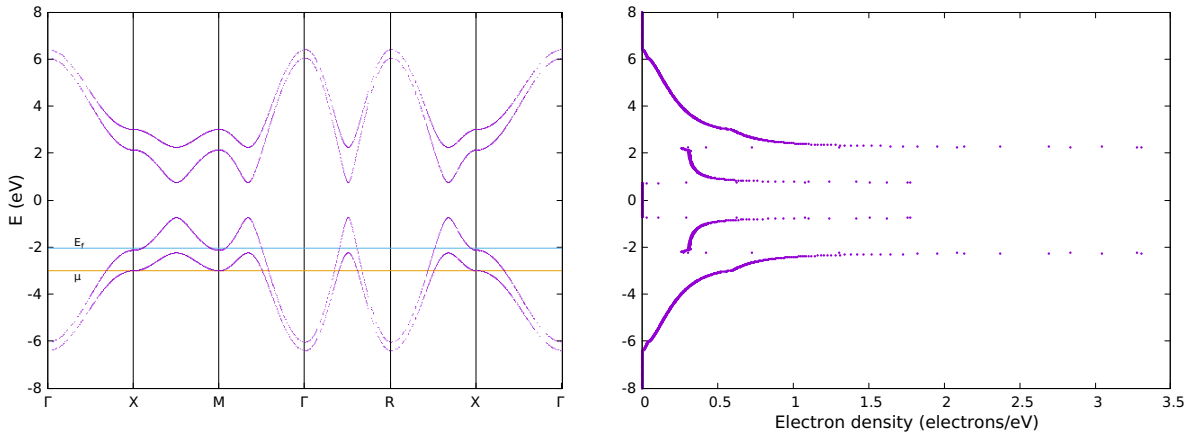

(a) **(b)**

Figure 5.8: Band structure (a) and density of states (b) for an SDW state (antiferromagnetic) with **q**=(π,π,π).

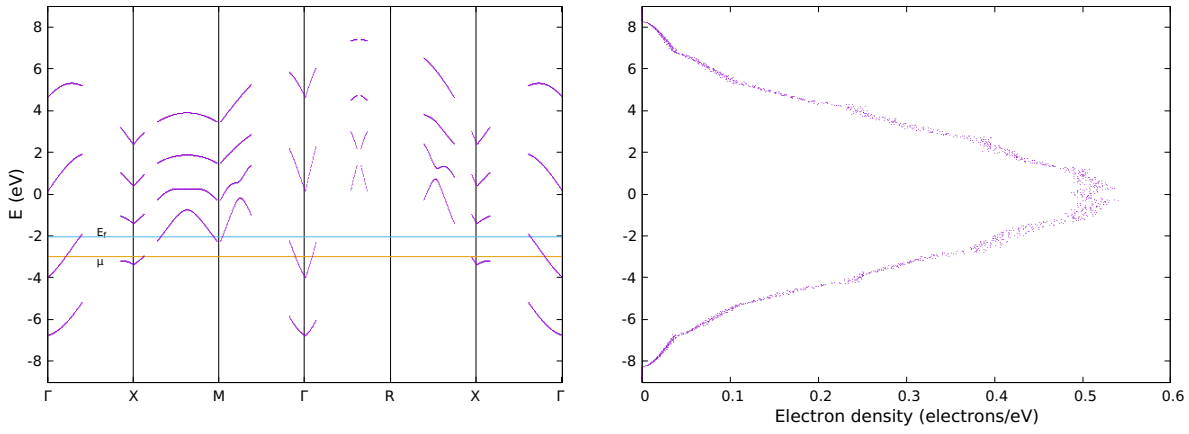

(a) **(b)**

Figure 5.9: Band structure (a) and density of states (b) for an SDW state with **q**=$(\frac{\pi}{4},\frac{\pi}{4},\frac{\pi}{4})$.

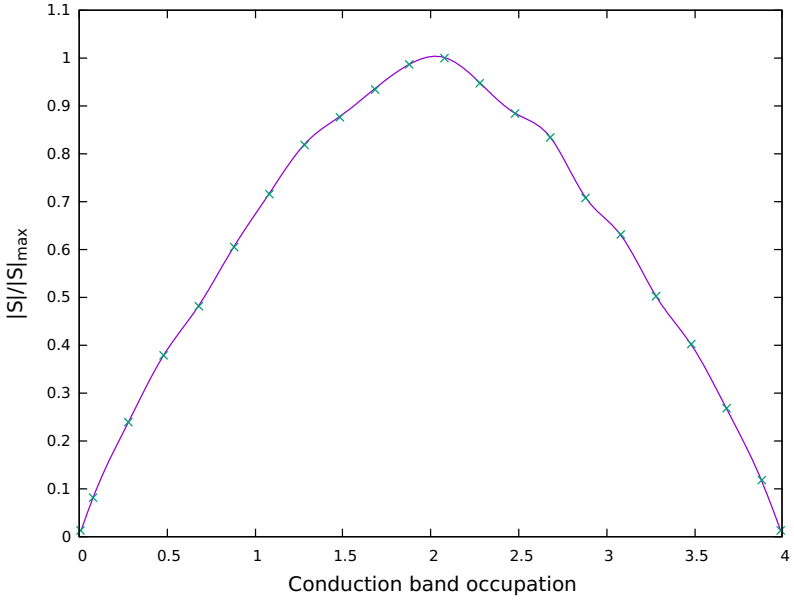

Figure 5.10: Dependency of the ordering constant $|S|$ on occupation, for a $S = 3/2$ system at $T = 0$. $\mathcal{J}/W = 1/12$. Data are not sampled symmetrically about $n_c = 2$. Interpolating spline is a guide for the eye.

Table 5.3: $T = 0$ Ordering vectors by conduction band occupation. $\mathcal{J}/W = 1/12$. Components are given in units of π.

n_c	$\mathbf{q}$		n_c	$\mathbf{q}$
0.01	(0,0,0)		2.08	(1,1,1)
0.08	(0,0,0)		2.28	$(1,1,\frac{3}{4})$
0.28	(0,0,0)		2.48	$(1,\frac{3}{4},\frac{3}{4})$
0.48	(0,0,0)		2.68	$(\frac{3}{4},\frac{3}{4},\frac{3}{4})$
0.68	$(\frac{1}{4},\frac{1}{4},\frac{1}{4})$		2.88	$(\frac{3}{4},\frac{3}{4},\frac{1}{2})$
0.88	$(\frac{1}{2},\frac{1}{2},\frac{1}{2})$		3.08	$(\frac{1}{2},\frac{1}{2},\frac{1}{2})$
1.08	$(\frac{3}{4},\frac{1}{2},\frac{1}{2})$		3.28	$(\frac{1}{4},\frac{1}{4},\frac{1}{4})$
1.28	$(\frac{3}{4},\frac{3}{4},\frac{3}{4})$		3.48	(0,0,0)
1.48	$(\frac{3}{4},\frac{3}{4},\frac{3}{4})$		3.68	(0,0,0)
1.68	$(1,1,\frac{3}{4})$		3.88	(0,0,0)
1.88	(1,1,1)		3.99	(0,0,0)

Table 5.4: $T > 0$ Ordering vectors by conduction band occupation. $\mathcal{J}/W = 1/12$. Components are given in units of π.

n_c	$\mathbf{q}$		n_c	$\mathbf{q}$
0.01	(0,0,0)		2.08	(1,1,1)
0.08	(0,0,0)		2.28	(1,1,1)
0.28	(0,0,0)		2.48	(1,1,1)
0.48	(1,0,0)		2.68	(1,1,1)
0.68	$(1,\frac{1}{2},0)$		2.88	$(1,1,\frac{1}{4})$
0.88	(1,1,0)		3.08	(1,1,0)
1.08	$(1,1,\frac{1}{4})$		3.28	$(1,\frac{3}{4},0)$
1.28	$(1,1,\frac{3}{4})$		3.48	(1,0,0)
1.48	(1,1,1)		3.68	(1,0,0)
1.68	(1,1,1)		3.88	(0,0,0)
1.88	(1,1,1)		3.99	(0,0,0)

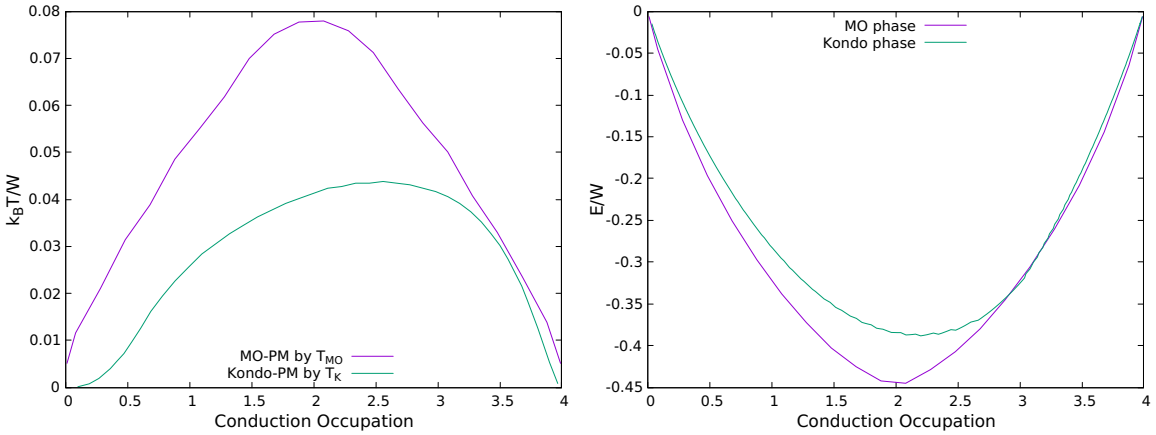

Figure 5.11: Comparison of MO and Kondo phase quantities at $\mathcal{J}/W = 1/12$: (a) at finite-temperature, possible boundaries with the PM phase are indicated by critical temperatures T_K/W and T_{MO}/W vs occupation; (b) at zero-temperature, total energy favors MO phase except near $n_c = 3.1$.

this coupling strength ($\mathcal{J}/W = 1/12$), the Kondo temperatures very nearly reach the same values as the magnetic ordering temperatures. Since they do not, there is no Kondo-PM phase transition at $T > 0$. Also in Figure 5.11, the $T = 0$ energy curves illustrate that for a small region of n_c, the Kondo phase is favorable. Notably, the Kondo phase does not possess particle-hole symmetry for $S = 3/2$. T_K is highest in a region away from $n_c = 2$ but not quite $n_c = 3$. This is also true, but to a lesser extent, of its least total energy. To draw a phase diagram from $S = 3/2$ all that remains is to investigate the free energies of points near $n_c = 3.1$ as the temperature of the system is raised. In this way, a Kondo-MO boundary can be approximated, where the transition will be of first order.

Figure 5.12 displays such a phase diagram. In this diagram, datapoints appearing as circles and squares indicate the following: at this coordinate in the n_c-T plane, calculations of free energy for the Kondo and MO phase were near enough to permit comparison, so that a circle indicates energy-favorability for the Kondo phase and a square indicates energy-favorability for the MO phase. Lack of a datapoint indicates only that a comparison could not be made at that coordinate (see section 5.1 above for challenges surrounding these

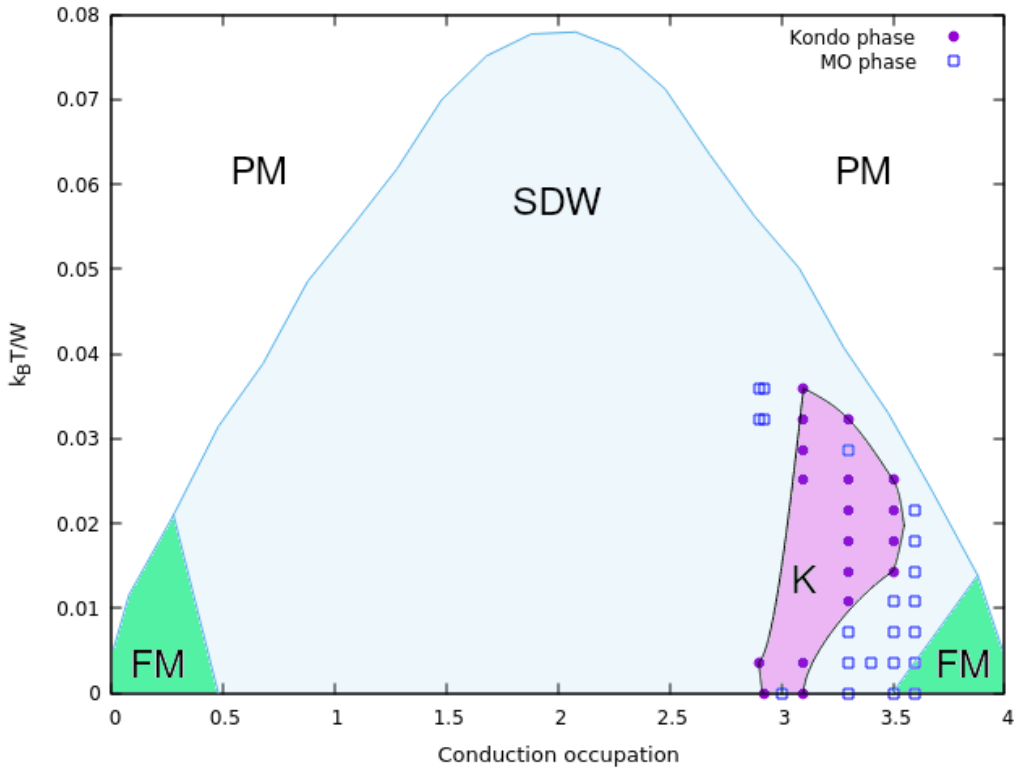

Figure 5.12: Phase diagram for the S=3/2 system at coupling $\mathcal{J}/W = 1/12$. Points at which a comparison between Kondo and MO free energies could be made are indicated by circles and squares. For these and the Kondo phase boundary, see text. Boundaries demarcating ordering within the MO phase are linear estimates connecting $T = 0$ and T_{MO} values.

points). The curved boundary of the Kondo phase is thusly educated guesswork based on the circles and squares appearing in the diagram. As the region is drawn, it wholly contains two MO-phase points. The point closest to $k_BT/W = 0$ is likely attributable to numerical uncertainty. As for the point near $k_BT/W = 0.3$, statements of neither numerical uncertainty nor of boundary shapes can be made with confidence. Nevertheless, the general appearance of the Kondo phase is that of a reentrant phase, in that a magnetically-ordered system at low temperatures can experience a transition to a non-magnetic state, then to a magnetic state, and finally to a paramagnetic state as the temperature is raised. Moving on to the MO phase, diagonal lines separate the SDW and FM phases in the lower left- and right-hand regions, but these also represent educated guesswork. Systematic free energy calculations were not done to delineate regions of FM or from other types of SDW ordering. Rather, data in Tables 5.3 and 5.4 were used to draw connecting lines from the MO-PM boundary to the $T = 0$ data. However, of note are three free-energy datapoints found in the vicinity of $n_c = 3.5$. These points confirm FM ordering.

With the proximity of the T_K-curve so close to the T_{MO} curve in Figure 5.11, one might expect that upon increasing the coupling strength, the Kondo phase will obtain a boundary with the PM phase. Indeed, at $n_c = 3.4$, $T_K = T_{MO}$ when $\mathcal{J}/W$ reaches approximately 0.10. As in the $S = 1/2$ case, a systematic search for the lowest possible $\mathcal{J}/W$ has not been done, so the value 0.10 may not be the lowest at which the Kondo-PM boundary can be expected to exist. The same can be said of the zero-temperature crossover, where at $n_c = 3.0$ the Kondo-phase energy reaches the MO-phase energy at $\mathcal{J}/W = 0.076$.

At higher coupling strength, $\mathcal{J}/W = 1/6$, the reentrant nature of the Kondo phase is lost. As seen in Figure 5.13, the Kondo-PM phase boundary alters the shape of the right-hand portion of the plot, and the FM phase has vanished at the nearly-filled limit. MO order only remains, in this area, in a small pocket at low temperatures. While this diagram is constructed in the same manner as for that of the weaker coupling strength, three issues are

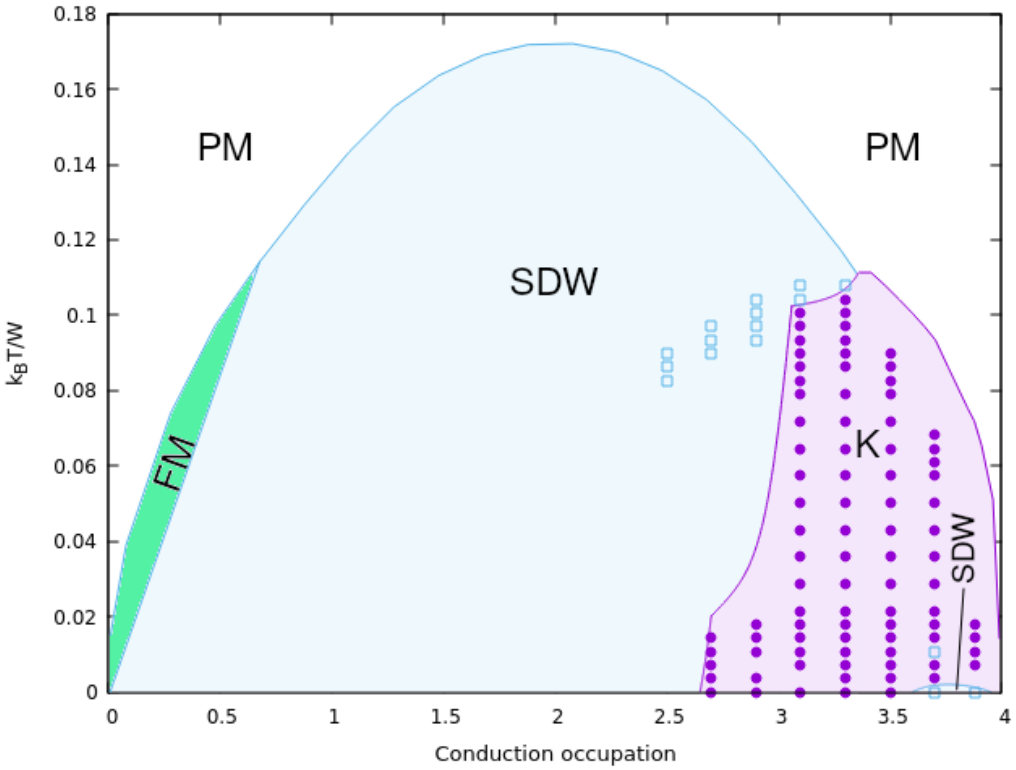

Figure 5.13: Phase diagram for the S=3/2 system at coupling $\mathcal{J}/W = 1/6$. Points at which a comparison between Kondo and MO free energies could be made are indicated by circles and squares. For the Kondo-PM phase boundary, see text. Boundaries demarcating SDW from FM ordering are linear estimates connecting FM-orderings at $T = 0$ and T_{MO}.

Table 5.5: $T = 0$ Ordering vectors by conduction band occupation. $\mathcal{J}/W = 1/6$. Components are given in units of π.

n_c	$\mathbf{q}$		n_c	$\mathbf{q}$
0.01	(0,0,0)		2.08	(1,1,1)
0.08	($\frac{1}{4}$,0,0)		2.28	(1,1,$\frac{3}{4}$)
0.28	($\frac{1}{4}$,0,0)		2.48	($\frac{3}{4}$,$\frac{3}{4}$,$\frac{3}{4}$)
0.48	($\frac{1}{4}$,0,0)		2.68	($\frac{3}{4}$,$\frac{3}{4}$,$\frac{3}{4}$)
0.68	($\frac{1}{4}$,$\frac{1}{4}$,$\frac{1}{4}$)		2.88	($\frac{3}{4}$,$\frac{1}{2}$,$\frac{1}{2}$)
0.88	($\frac{1}{2}$,$\frac{1}{2}$,$\frac{1}{2}$)		3.08	($\frac{1}{2}$,$\frac{1}{2}$,$\frac{1}{2}$)
1.08	($\frac{1}{2}$,$\frac{1}{2}$,$\frac{1}{2}$)		3.28	($\frac{1}{2}$,$\frac{1}{2}$,$\frac{1}{4}$)
1.28	($\frac{3}{4}$,$\frac{3}{4}$,$\frac{3}{4}$)		3.48	($\frac{1}{4}$,$\frac{1}{4}$,$\frac{1}{4}$)
1.48	($\frac{3}{4}$,$\frac{3}{4}$,$\frac{3}{4}$)		3.68	($\frac{1}{4}$,$\frac{1}{4}$,0)
1.68	(1,1,$\frac{3}{4}$)		3.88	(0,0,0)
1.88	(1,1,1)		3.99	(0,0,0)

Table 5.6: $T > 0$ Ordering vectors by conduction band occupation. $\mathcal{J}/W = 1/6$. Components are given in units of π.

n_c	$\mathbf{q}$		n_c	$\mathbf{q}$
0.01	(0,0,0)		2.08	(1,1,1)
0.08	(0,0,0)		2.28	(1,1,1)
0.28	(0,0,0)		2.48	(1,1,1)
0.48	(0,0,0)		2.68	(1,1,1)
0.68	(0,0,0)		2.88	(1,1,1)
0.88	(1,1,0)		3.08	(1,1,0)
1.08	(1,1,1)		3.28	(1,0,0)
1.28	(1,1,1)		3.48	(0,0,0)
1.48	(1,1,1)		3.68	(0,0,0)
1.68	(1,1,1)		3.88	(0,0,0)
1.88	(1,1,1)		3.99	(0,0,0)

of note. The first is the presence of a MO-phase point inside the Kondo phase at $n_c \sim 3.7$, which is attributed to numerical uncertainty. The second is that the T_K curve which forms the Kondo-PM boundary ends at $n_c = 3.96$. However, given the downward trend of T_K, given the energetic favorability of the Kondo phase over the MO phase at $n_c = 3.99$, and proceeding under the assumption that $T_K \to 0$ as $T \to 0$, the T_K curve has been artificially extended from the point (3.96,0.0051) down towards the lower right-hand corner. Finally, of note is the FM phase on the left-hand side of the diagram. As before, a diagonal line connects the largest-n_c point with $\mathbf{q}$=(0,0,0) from $T > 0$ to the largest-n_c point of same $\mathbf{q}$ at $T = 0$. Whereas for $\mathcal{J}/W = 1/12$ a system tends to reach FM ordering at larger n_c for $T = 0$ than for $T > 0$, for $\mathcal{J}/W = 1/6$, the opposite occurs. Ordering vectors for various occupation numbers appear in Tables 5.5 and 5.6.

5.4 Discussion of Results

In both $S = 1/2$ and $3/2$, the order constant $|S|$ tends to zero as the conduction bands approach zero and complete filling. An explanation for this has already been mentioned in brief in section 5.2. When considering the Ruderman-Kittel-Kasuya-Yosida (RKKY) interaction for impurities in a lattice, magnetic order is achieved through the interaction of local moments via the itinerant ones. In this respect it is necessary that spin-flip interactions take place. From the perspective of scattering, there must be a non-zero cross-section for spin-flip processes. In the framework of $J > 1/2$ and the Coqblin-Schrieffer interaction [42], j-values may change by more than unity, but the idea is the same: there must be states available for j-exchange to take place between itinerant and local moments. At $T = 0$, such states occur in greatest number nearest to the Fermi surface, and in Figures 5.2 and 5.10 this is when $n_c = 1.0$ and 2.0, respectively. On the other hand, when the conduction bands are nearly empty or nearly filled, there are few states available for j-exchange, and Figures 5.2 and 5.10 accordingly show small $|S|$ values. By extension, when no states are available, that is, when the bands are completely empty or filled, a magnetic instability cannot exist, and only an external magnetic field can order the system. Hence, at these boundaries the system must be paramagnetic. The same must therefore be true of the Kondo phase and the hybridization constant: when no states are available, conduction electrons cannot interact with – and thus cannot screen – the local moments. Again, the same conclusion is reached: at the empty- and filled-band boundary cases, the system must be paramagnetic.

So it is that as these two boundary cases are approached, the Kondo and MO phases are suppressed and the system heads toward the PM phase. However, until a boundary is reached, the PM phase does not occur without a finite temperature: competition persists between the Kondo and MO phases up until the bands are either empty or filled. In general, however, from the MO phase it can be seen that $|S| - |M| \neq 0$, and even as the conduction band becomes emptied or filled, equality is not achieved. This is what one expects for a

magnetic system below its Neel temperature; the system exhibits ordering until there is no means by which ordering may be achieved.

With respect to the exhaustion problem, more information than the quantity $|S| - |M|$ is required. When the problem was initially formulated, exhaustion was related to the weak-coupling, small-occupation case where T^*/T_K was dependent on coupling strength. However, under the formulation by Burdin *et al* [16], T^*/T_K is dependent only on occupation number (and hence there is only one characteristic temperature for the system). Indeed, in Nozieres' 2005 work [43], he frames the question of exhaustion in terms of precession, and when he takes Burdin's work into consideration, he concludes that exhaustion does not occur. Only the strongly hybridized conduction electrons contribute to local moment compensation. In this work, the coherent Fermi liquid state is not addressed, and so statements about T^*/T_K cannot be made. However, if in this work the coexistence of Kondo and magnetic behaviors were allowed, then $|V|$ could be studied in relation to the quantity $|S| - |M|$. In other words, the hybridized moments might be studied with respect to screening. These statements aside, this work indicates that a sample may be fabricated with an arbitrary occupation number, and that it may be pushed into a desired phase by tuning of the coupling strength.

Comparing $S = 1/2$ results from this work with that of other analytical results, among the most notable of phase diagrams for three-dimensional systems is that of Lacroix and Cyrot [1]. In their paper, Lacroix and Cyrot include RKKY terms in their Hamiltonian, and in doing so, they combine the longitudinal portion of their Kondo interaction (i.e., $\hat{S}^z \cdot \hat{M}^z$) with their RKKY interaction and treat the sum under a meanfield approximation, while the transverse portion is treated with a functional integral approach. By contrast, in this work the longitudinal interaction terms are made zero. Lacroix and Cyrot also assign a constant

density of states to the conduction electrons, specifically

$$\rho_0(\varepsilon) = \begin{cases} \frac{1}{2D} & -D < \varepsilon < D \\ 0 & \text{otherwise.} \end{cases} \tag{148}$$

Using a Green's function approach, they derive densities of states for conduction and impurity electrons in which both, once conditions on allowed energies are satisfied, have gaps. This work also finds gapped densities of states. They represent an antiferromagnetically-ordered system via two sublattices, but such is representable in this work with, for example, a $\mathbf{q} = (\pi, \pi, \pi)$ ordering vector. With these similarites and differences in mind, the phase diagram of 5.1 differs from that published by Lacroix and Cyrot. Figure 5.14 shows that, for $J/D = 2\mathcal{J}/W$, at half filling the system goes from the AFM phase to the Kondo phase between $\mathcal{J}/W$ between 0.25 and 0.30, while near $n_c = 0.6$ the crossover occurs at $\mathcal{J}/W \sim 0.2$. In this work, the half-filling transition occurs at $\mathcal{J}/W \sim 0.34$, while at $n_c = 0.7$ a transition was found at $\mathcal{J}/W \sim 0.29$. While at first glance it seems appropriate to say that the use of a tighting-binding approximation has raised the crossover value for the coupling strength, attention must be paid to two other points: first, that this work does not explicitly add RKKY terms to its Hamiltonian; and second, that n_c between 0.6 and 0.7 does not, in this work, have an ordering vector which

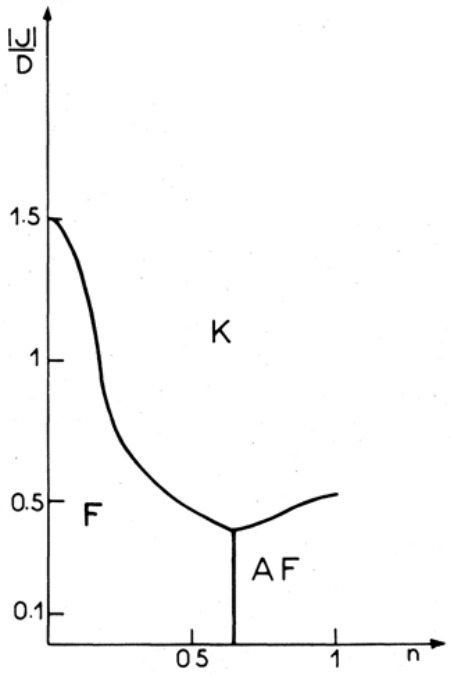

Figure 5.14: Phase diagram by Lacroix and Cyrot using a flat density of states and RKKY terms. Reprinted with permission from [1], copyright 1979 by the American Physical Society.

describes a two-sublattice system. Finally, at $\mathcal{J}/W = 1/12$, ferromagnetic ordering occurs at $n_c = 0.04$ in this work, while for Lacroix and Cyrot it occurs near $n_c = 0.6$.

On the matter of the changing values of the ordering vector, Ohashi *et al* [38] have applied an extended dynamical mean-field theory (DMFT) approach to a system with RKKY terms and external magnetic field. They use a three-dimensional cubic lattice under a tight-binding approximation. While their work does not focus on phase diagrams, they do present spectral-function and dynamical susceptibility results for various ordering vectors. In particular, at half-filling, zero external magnetic field, finite temperature $T = 0.05$, and with Kondo coupling $J_K = 0.5$, they examine the effects of increasing the RKKY coupling J: the dynamical spin susceptibility shows a peak which is greatest at $\mathbf{q} = (\pi, \pi, \pi)$. This peak, as J increases from zero towards the value of J_K, gains in height and occurs at lower and lower frequencies, indicating a growing instability towards antiferromagnetism (AFM). Here, it is argued that this work is most comparable to that of Ohashi *et al* when $J = J_K$, and that in such a case, their results are consistent with those of this work. Because Ohashi *et al* test only diagonal $\mathbf{q}$-vectors, i.e. having components (x, x, x) for some $x \in [-\pi, \pi]$, the instability found in this work at $n_c = 0.7$, which does not have a diagonal $\mathbf{q}$, is not applicable. However, the spike in the phase diagram of Figure 5.1 occurs at $\mathbf{q} = (\pi, \pi, \pi)$, and for this vector, it is most certainly the case that the antiferromagnetic instability is at its greatest.

A square-lattice $S = 1/2$ system was the subject of Li *et al* [2] in their self-consistent mean-field treatment of phases. Their goal was to shed light on a quantum critical point – something which is not done here – and to this end they allow hybridization and magnetization constants to have non-vanishing values simultaneously. There are still areas where comparison is possible, however. They use a tight-binding approximation for the conduction electron dispersion relation, both with and without next-nearest-neighbor hopping, and explore magnetism through an ordering vector. They do not, in contrast with this work, set the longitudinal component of the spin interaction to zero. Moreover, they investigate the

AFM phase in a heavy-fermion setting which this work does not. With said similarities and differences, they produce a Doniach-like T/t-vs-J/t diagram, seen in Figure 5.15.

Where $J/t = 12\mathcal{J}/W$, and where T/t is dimensionless in Figure 5.15 and equaling $12k_BT/W$ in this work, the diagram of Figure 5.1 can be interpreted as follows, with interest in the half-filling the spike in Figure 5.1: as J/t is raised from 0, the system is expected to be in a PM state; and as J/t is increased, the spike increases in height, and the magnetic crossover occurs at $T/t = 0.04$ and $J/t = 1$. In Figure 5.15, the crossover from PM to AFM behavior occurs nearby this point. Returning to $J/t = 0$ but at $T/t = 0$, Figure 5.3 can be interpreted as showing that as J/t is raised, the system is expected to experience a crossover from magnetic behavior to Kondo behavior at 4.0. In Figure 5.15, the zero-temperature crossover to Kondo behavior occurs, considering heavy-fermion behavior, at approximately 3.4. Complete agreement is not expected, however, due to the comparison between two- and three-dimensional lattices.

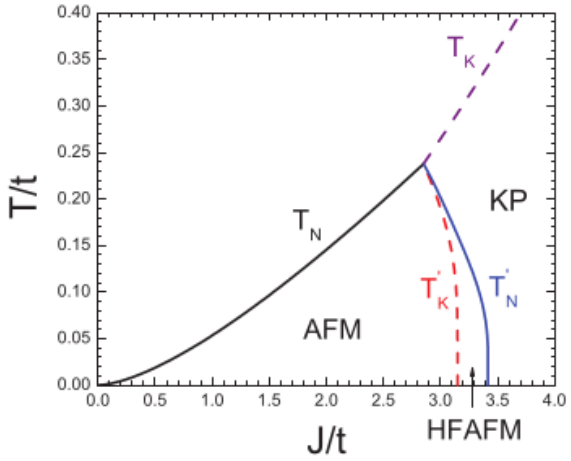

Figure 5.15: Phase diagram from Li *et al* [2] at half-filling with a nearest-neighbor tight-binding approximation. T_N and T_N' indicate Néel temperatures. KP indicates Kondo paramagnetism. © IOP Publishing. Reproduced with permission. All rights reserved

As recently as 2017, Costa *et al* [3] published an analysis of phases for an $S = 1/2$, square-lattice system under a mean-field treatment. In that analysis, the authors chose to use classical spin and hybridization averages of the form

$$\langle O_i \rangle = a^0 \left[\cos \mathbf{Q}\cdot\mathbf{R}_i, \sin \mathbf{Q}\cdot\mathbf{R}_i, 0 \right] \tag{149}$$

for an operator O and a constant a^0. They specifically use the above form to investigate spiral magnetism (which is, in the terminology of this work, SDW magnetism), but it is, by restricting the average to be in-plane, a classical version of the ordering constants used in this paper. Moreover, they use a tight-binding approximation and do not explicitly add an RKKY term to their Hamiltonian.

There is, therefore, an expectation for some degree of agreement between the results of Costa *et al* and of this work. However, that agreement is limited by the simultaneous non-zero values of hybridization and magnetization used by Costa *et al*.

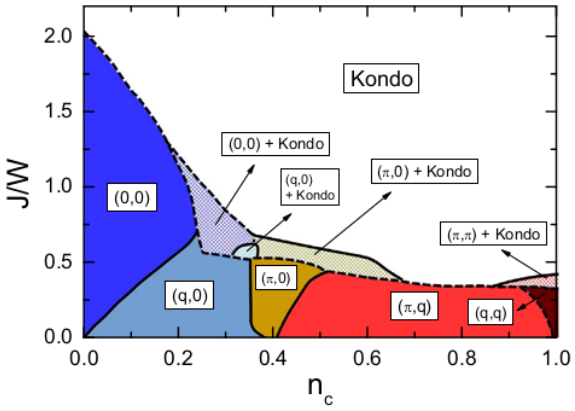

Figure 5.16: Phase diagram from Costa *et al* [3] at $T = 0$ using classical spin averages.

In the phase diagram of Figure 5.16, one sees that the ordering vectors are permitted to assume a continuous range of values, as indicated by components such as (π,q) which have only the first component fixed. The continuous range for components is an advantage over the use of intervals in this work. After all, the use of intervals is neither dictated by the model nor meant to suggest a restriction on **q**. Instead, the use of intervals is for resource conservation. That said, and considering also the square-versus-cubic lattices, the only comparison that can be made for **q** is between the continuous vector components of a given region in Figure 5.16 and the commensurateness or incommensurateness of vectors in Table 5.1. With this in mind, at $\mathcal{J}/W = 1/12$, Figures 5.16 and 5.1 agree until n_c approaches unity. There, Figure 5.16 indicates spiral magnetism while this work finds bipartite antiferromagnetism. When $\mathcal{J}/W = 0.34$, half-filling places the system, in Figure 5.16, approximately at the boundary of (q,q)-magnetism and (π,π)-magnetism

with Kondo behavior. This would be consistent with the present work, if one were to disregard that in this work Kondo and magnetic behavior are mutually exclusive of each other.

Before relating the results of this work to materials and experimentation, one might wish to reason through the consequences of increasing the spin degeneracy of a system (rather, the degeneracy of states due to higher total angular momentum when little to no external field is present) from that of $S = 1/2$ to that of $S = 3/2$ and then to compare those consequences with the results presented above, in section 5.3. First, particle-hole symmetry is lost in the Kondo phase due to both the coupling of c- and f-operators and the $n_f = 1$ constraint imposed through the Lagrange multiplier $\lambda = E_f$. Therefore, one might expect at higher degeneracies that the MO-phase curves resemble their lower-degeneracy selves, but one would not expect the same of the Kondo-phase curves. Indeed, in Figure 5.11, the T_K and E curves are skewed rightward from the center of the graph, $n_c = 2$. In a more practical sense, this rightward loss of symmetry, so to speak, means that materials in which there are more electrons than holes are more likely to show the Kondo effect. Even at coupling strength $\mathcal{J}/W = 1/12$, when a Kondo-PM boundary is not expected, the system still is expected to display Kondo behavior at low temperatures when n_c is near 3.1, but not when n_c is near 0.9.

Next, the question of how degeneracy impacts the competition between the RKKY and Kondo interactions arises. The binding energy for a Kondo singlet and an RKKY state can be written [14], where ρ is the density of states at the Fermi surface, as

$$\begin{aligned} \Phi_K &\propto \frac{e^{-\frac{1}{\rho\mathcal{J}}}}{\rho}, \\ \Phi_{RKKY} &\propto b\rho\mathcal{J}^2, \end{aligned} \tag{150}$$

where the constant b is included in the right-hand expression to indicate dependence on band structure, despite the statement of proportionality. Taking the simple view that if the

degeneracy increases so does the number of available states, then, neglecting changes in band structure and holding b constant, increasing the degeneracy permits the progression seen in Figure 5.17. Because this figure is of binding energies, intersection between the curves of a particular pair implies a crossover to Kondo behavior from magnetism. Inspection then reveals that as degeneracy increases, pairs come nearer and nearer to intersection, that the point of nearest approach occurs at weaker and weaker couplings, and that said nearest approach drops lower and lower in binding energy. Hence, at a lower degeneracy the Kondo effect may not appear, but at a higher degeneracy it may. This reasoning is consistent with the phase diagrams of Figures 5.1 and 5.12, in that the Kondo phase is not expected for $S = 1/2$, but is for $S = 3/2$.

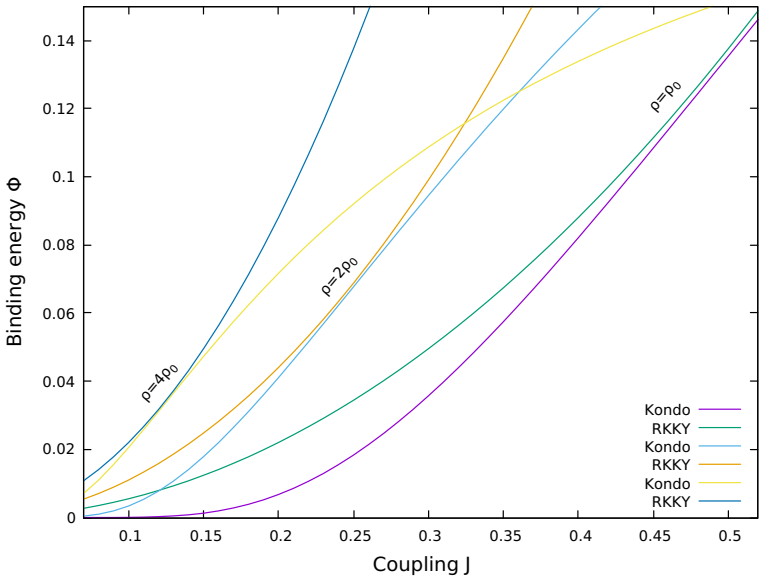

Figure 5.17: Doniach diagram illustrating the effects of increased degeneracy. ρ_0 is the density of states at the Fermi surface for some lowest-degeneracy system.

One may raise two important issues in the discussion of the Kondo-MO crossover: that the crossover for the $S = 1/2$ system occurs at a coupling strength not physically realizable, and that such a coupling strength corresponds to the small-U regime of the Anderson lattice, wherein localization of impurity moments is dubious. In short, one may question the usefulness of investigating the Kondo-MO crossover beyond the realm of theoretical exploits. These issues are addressed by laboratory dense-alloy materials, which are typically representable by $J = 5/2$ and 7/2 total angular momenta. Some of these materials are treated

as $S = 1/2$ through considerations of the crystalline electric field (CEF), and so the former issue will be addressed below. The latter issue is addressed by the degeneracy of angular momentum states. Both Coleman [36] and Read and Newns [37] argued that increased degeneracy leads to a drop in the critical coupling strength for the Kondo-MO crossover. In particular, Coleman used a $1/N$ expansion to deduce two energy scales for the Kondo Lattice, T_K and T_K/N, and to show that above T_K/N, although electron correlations are lost, the lattice can be approximated by the dilute alloy case. This dilute-case approximation was also the conclusion of Read and Newns. Taken together, these arguments indicate that the stability of the Kondo phase against ordering is increased, since, as N grows large, T_K remains near its single-impurity value, but the critical $\mathcal{J}$ decreases as order $(2J+1)^{-1}$. Indeed, in this work, the approximate zero-temperature ratio of coupling strengths for the crossover is $0.34/.076 \sim 4.5$, which is by order of magnitude consistent with Coleman's determination. In this way, the latter of the issues, that the coupling strength corresponds to the small-U Anderson lattice, is circumvented by systems with larger total angular momenta.

To consider the issue of physically realizable coupling strengths for $S = 1/2$, one must look to real materials. For some time, efforts had been made to use lighter elements so as to form concentrated alloys through $3d$ orbitals. However, at the time, it was found that such alloys could not be obtained: the d-orbitals are too large and form quasiparticle states through interaction with each other before Kondo-related behavior can be observed [44]. This led to the exploration of $4f$ and $5f$ shells, including rare-earth materials. Recently, there has been some work identifying transition-metal dense alloys, but as will now be seen through these and rare-earth materials, applying the results of this work to laboratory samples is far from straightforward.

A rare-earth material that has been the subject of several decades of work is $CeCu_6$. This material shows no signs of magnetic ordering until the milliKelvin range (< 2 mK)

[45, 19], but shows Kondo-like behavior in its resistivity [46]. It has integer valence [44] ($n_f \in \mathcal{Z}^+$) but through application of pressure can be pushed into an intermediate valence regime [46], although there have been calculations based on experiment that suggest it has non-integer valence [47]. Altogether, Cerium commonly has either 3+ or 4+ valence, but if in this compound it has 3+ valence, then this allows for an uncompensated $4f^1$ moment which may then hybridize with the conduction band. This situation might immediately suggest that a $J = 5/2$ Kondo model should be applied, and that, given the arguments above, with a degeneracy of $N = 6$, a Kondo phase should certainly be seen. However, experiment has elucidated several properties which make such a large-J model unnecessary at low temperatures. The resistivity of $CeCu_6$ displays a peak at 15 K [46], and its T_K has been determined to be around 35 K [48], with coherence setting in below 10 K for a T^* of about 3 K [49]. $CeCu_6$ has an orthorhombic structure [50], and by inelastic neutron scattering it has been found that the CEF splits a groundstate doublet into levels at 0, 7.0, and 13.8 meV [51]. In other words, T_K lies below the first excited CEF state of 82 K, and so in the Kondo phase, only two spin states will interact with the conduction band. One has good reason, at such temperatures, to treat the material with a $S = 1/2$ Kondo model. Doing so, and using the results of section 5.2, however, it becomes apparent that a lower limit of $\mathcal{J}$ must be determined through $\mathcal{J}/W = 0.29$, and to do this, an estimate of the bandwidth is required. Through electronic structure found in Murin *et al* [52] and Harima and Yanase [53], the bandwidth is estimated at 5 eV, which leads to a coupling of $\mathcal{J} = 1.45$ eV. Considering that $T_K \sim 35$ K (or $k_B T_K/W = 06.0 \times 10^{-4}$) and that $T_{MO} < 2$ mK (or $k_B T_{MO}/W = 3.4 \times 10^{-8}$), $\mathcal{J}$ must be considerably larger. This alone leads to the conclusion that a phase diagram for $CeCu_6$ cannot be described by the $S = 1/2$-case of the model used here.

Doping of $CeCu_6$ with gold has allowed researchers to raise the Néel temperature and to study, among other things, antiferromagnetic correlations in prepared samples. These doped Kondo alloys, $CeCu_{6-x}Au_x$, are notable for their heavy fermion properties, and for

their small magnetic moments [21]. Although at low temperatures $S = 1/2$ Kondo physics may be used to describe them because of CEF considerations, as in the undoped case, they may not have integer valences. This limits what can be said about them here. Nevertheless, a critical doping has been identified for $CeCu_{6-x}Au_x$ of $x \sim 0.1$ at which a magnetic moment appears and increases to its maximum at $x = 1$ of, at most, 1.15 μ_B [21]. This value is noticeably lower than the moment of the free Ce^{3+} ion of 2.56 μ_B, and is just one example of dense alloys which exhibit Kondo behavior and small magnetic moments. It is a limitation of this work that a statement cannot be made with regards to the Kondo interaction partially screening or suppressing magnetic order. The treatment used here precludes such an examination because hybridization and ordering constants are never considered non-zero simultaneously. That being said, the decreases in $|S|$-values seen in Figures 5.2 and 5.10 suggest a means by which small magnetic moments may exist in dense alloys without the coexistence of hybridization and ordering terms. However, it should be remembered that $|S|$ describes an itinerant-moment quantity; $|M|$ describes the local moments and at $T = 0$ has values given by (113) and (134).

For $J = 7/2$ materials, several Ytterbium compounds have been doped and studied as dense alloys. Notably, in Yb-based compounds, application of hydrostatic pressure lowers T_K, which is a trend opposite to that seen in Ce-based compounds [28]. For instance, YbCuAl is an intermediate valence material with a T_K of 66 K, and when doped with Yttrium, has been treated with a Coqblin-Schrieffer model [28]. For $YbCu_5$, integer valence and a Néel temperature of about 2 K is found when it is doped to $x = 2$ in $YbCu_{5-x}Al_x$ [27]. From electrical resistivity measurements, Kondo-like behavior is observed as the doped material approaches $x = 2$ [54]. As with $CeCu_6$, the CEF-splitting of $YbCu_3Al_2$ leads to a ground-state doublet and a first-excited state at 100 K [55]. The magnetic transition near 2 K has been found to be second-order, and the Kondo temperature is near 3 K [55]. To apply this work to $YbCu_3Al_2$, the Néel transition requires $T_{MO} > T_K$. It is not, and hence

the findings in this work, that is, that the transition should be first-order, disagree with experiment. Setting this discrepancy aside momentarily, the large CEF excitation temperature relative to T_K suggests the material may be treated as $S = 1/2$ at low temperatures. Unfortunately, estimates of electronic bandwidth were unable to be made, so a lower limit cannot be estimated for $\mathcal{J}$.

With either Cerium or Ytterbium, application of this work is questionable. A first attempt might lead one to apply, for example, an $S = 1/2$ treatment at low temperatures and then to apply $S = 5/2$ or $S = 7/2$ as the temperature is increased. This would constitute a phenomenological approach, and would likely produce sharp features in physical quantities such as occupation numbers. The forced introduction of higher degeneracy may even precipitate a first-order phase transition. Alternatively, one might begin with the Coqblin-Schrieffer interaction and apply the work of Cornut and Coqblin [56] which specifically treats the case of crystalline electric fields, although it must be extended from the single impurity to the lattice case. Measurements, such as of resistivity, can be complicated by the activation, so to speak, of additional J_z-states as the system is excited to higher crystal field states, and Cornut and Coqblin have examined such complications.

Repeated searches have failed to uncover any dense alloys for $J = 3/2$, which, unfortunately for this work, precludes any comparison between the results of section 5.3 and measurements on a laboratory material. Most likely, such materials would involve $3d$ orbitals and, thus, transition metals. It would be interesting to see whether a $3d$-derived dense alloy exhibited a reentrant Kondo phase, such as that seen in Figure 5.12. It may be the case that in the lee, so to speak, of the said figure's Kondo region, there is coexistence of Kondo and magnetic behaviors. Treatment of this falls under the domain of future work. Recently, there has been interest in the family of Iron pnictides, AFe_2As_2 (with 'A' being K, Rb, or Cs), as possible Kondo systems. The Kondo behavior in these systems is believed to result from $3d$ electrons. Large effective masses have been estimated from dHvA and ARPES

measurements for these superconductors, placing them in the heavy fermion category [57]. These hole-doped systems, if localization is strong enough for a Kondo model to be used, would fall under a $J = 5/2$ treatment.

5.5 Conclusion

An Hartree-Fock method has been applied to the lattice Kondo model using $S = 1/2$ and $J = 3/2$ pseudofermion representations of local and itinerant moments. While comparison between the diagrams presented here and realizable dense magnetic alloys is complicated by CEF considerations, there are still several theoretical results of note. It has been confirmed that without explicitly adding to the Kondo Hamiltonian terms for the RKKY interaction, a dense alloy may exhibit magnetic ordering, and that, by applying an ordering vector, several types of magnetic ordering can occur, including ferromagnetism, antiferromagnetism, and incommensurate spin density waves. This work confirms Coleman's argument through the 1/N expansion [36] that increased degeneracy bolsters the stability of the Kondo phase against magnetic ordering. This is seen by comparing the phase behavior of $S = 1/2$ and $J = 3/2$ systems at the same coupling strength, where the $S = 1/2$ system does not exhibit a Kondo effect but the $J = 3/2$ system does.

In $S = 1/2$, the Kondo phase is found to be unstable against magnetic ordering below coupling strength $\mathcal{J}/W = 0.29$. Rather, below this coupling strength, dense alloys describable by $S = 1/2$ physics will exhibit magnetic and paramagnetic phases only. At this spin degeneracy, particle-hole symmetry is apparent in the phase diagrams after accounting for numerical certainties. The MO phase exhibits a large spike in its ordering temperature at half-filling. At half-filling, the ordering is found to be of antiferromagnetic type.

In $J = 3/2$, a reentrant Kondo phase is reported for $\mathcal{J}/W = 1/12$, with first-order transitions to SDW magnetic order everywhere along its boundaries. The Kondo phase first

becomes energetically favorable at zero-temperature when the coupling strength is approximately 1/13 the bandwidth. For stronger coupling, $\mathcal{J}/W = 1/6$, the reentrant quality of the Kondo phase is no longer present. The particle-hole symmetry evident for $S = 1/2$ is lost for the $J = 3/2$ Kondo phase. This is apparent in the Kondo phase at lower coupling strength, but at higher coupling strength, even ferromagnetic ordering does not occur symmetrically with respect to occupation number.

Systems with $\mathcal{J}/W = 1/12$ show similarities between $S = 1/2$ and $J = 3/2$ in that ferromagnetism exists both at nearly-empty and at nearly-filled band occupations. The highest critical temperatures for magnetic ordering occur at $n_c = 1.0$ for the former and $n_c = 2.0$ for the latter. Behavior of both degeneracies at near-empty and near-filled occupations indicates that that the systems will be paramagnetic in the limiting cases of completely empty and filled bands.

Two areas in which further work would be most efficacious are: first, to produce results for higher-degeneracy systems, specifically $J = 5/2$ and $7/2$, so that integer-valence Cerium and Ytterbium systems may be reexamined; and second, to allow for the coexistence of hybridization and ordering constants, so as to further the understanding of small-moment Kondo lattice systems. Comparison with the phase diagram of Costa *et al* leads to a third area for further work: to shrink or altogether remove the interval size which is used to search **q**-space. All three of these forward-looking improvements would require greater computational resources. A final extension of this work, and perhaps the most interesting, would be to drop the assumption of isotropy in the hybridization and ordering constants.

REFERENCES CITED

[1] C. Lacroix and M. Cyrot, "Phase diagram of the Kondo lattice," *Phys. Rev. B*, vol. 20, no. 5, p. 1969, 1979.

[2] H. Li, Y. Liu, G.-M. Zhang, and L. Yu, "Phase evolution of the two-dimensional Kondo lattice model near half-filling," *J. Phys. Cond. Matt.*, vol. 15, p. 425601, 2015.

[3] N. Costa, J. Lima, and R. dos Santos, "Spiral magnetic phases on the Kondo Lattice Model: A Hartree–Fock approach," *J. Mag. Mag. Mat.*, vol. 423, p. 74, 2017.

[4] W. De Haas, J. De Boer, and G. Van den Berg, "The Electrical Resistance of Gold, Copper and Lead at Low Temperatures," *Physica*, vol. 1, no. 7, p. 1115, 1934.

[5] G. Van den Berg and J. D. Nobel, "Les propriétés à basses températures des alliages des métaux " normaux " avec des solutés de transition," *J. Phys. Radium*, vol. 23, no. 10, p. 665, 1962.

[6] J. Schrieffer and P. Wolff, "Relation between the Anderson and Kondo Hamiltonians," *Phys. Rev.*, vol. 149, no. 2, p. 149(491), 1966.

[7] M. Chan and M. Gulácsi, "The exact Schrieffer–Wolff transformation," *Phil. Mag.*, vol. 84, no. 12, p. 1265, 2004.

[8] C. Thomas, S. Simões, J. Iglesias, C. Lacroix, N. Perkins, and B. B. Coqblin, "Co-existence of Kondo effect and ferromagnetism in the Underscreened Kondo Lattice model," *AIP Conf. Proc.*, vol. 1419, p. 266, 2011.

[9] B. Schuh, "Kondo-Lattice: Kondo-Effect?," *Z. Physik B*, vol. 34, p. 37, 1979.

[10] R. Dong, J. Otsuki, and Y. Savrasov, "Scaling between periodic anderson and kondo lattice models," *Phys. Rev. B*, vol. 87, no. 15, p. 155106, 2013.

[11] K. Wilson, "The renormalization group: Critical phenomena and the Kondo problem," *Rev. Mod. Phys.*, vol. 47, no. 4, p. 773, 1975.

[12] N. Andrei, "Diagonalization of the Kondo Hamiltonian," *Phys. Rev. Lett.*, vol. 45, no. 5, p. 379, 1980.

[13] P. Wigman, "Exact solution of the s-d exchange model at T=0," *JETP Lett.*, vol. 31, no. 7, p. 364, 1980.

[14] S. Doniach, "The Kondo lattice and weak antiferromagnetism," *Physics*, 1977.

[15] N. Bickers, "Review of techniques in the large-N expansion for dilute magnetic alloys," *Rev. Mod. Phys.*, vol. 59, no. 4, p. 845, 1987.

[16] S. Burdin, A. Georges, and D. Grempel, "Coherence Scale of the Kondo Lattice," *Phys. Rev. Lett.*, vol. 85, no. 5, p. 1048, 2000.

[17] F. Steglich and S. Wirth, "Foundations of heavy-fermion superconductivity: lattice Kondo effect and Mott physics," *Rep. Prog. Phys.*, vol. 79, p. 084502, 2016.

[18] M. Dzero, J. Xia, V. Galitski, and P. Coleman, "Topological Kondo Insulators," *Ann. Rev. Cond. Matt. Phys.*, vol. 7, p. 249, 2016.

[19] H. Tsujii, E. Tanaka, Y. Ode, T. Katoh, and T. Mamiya, "Magnetic Order in the Heavy Fermion Compound $CeCu_6$ at mK Temperatures," *Phys. Rev. Lett.*, vol. 84, no. 23, p. 5407, 2000.

[20] T. Omuta, K. Fujiwara, J. Takeuchi, and Y. Kohori, "Nuclear magnetic relaxation of $CeCu_{6-x}Au_x$ for $0 \leq x \leq 1$," *Physica B*, vol. 259, p. 378, 1999.

[21] H. Löhneysen, H. Bartolf, S. Drotziger, C. Pfleiderer, O. Stockert, D. Souptel, W. Löser, and G. Behr, "Rare-earth intermetallic compounds at a magnetic instability," *J. Alloys and Compounds*, vol. 408, p. 9, 2006.

[22] K. Fujiwara, Y. Yamanashi, and K. Kumagai, "^{27}Al nuclear relaxation behavior of $CePd_2Al_3$," *Physica B*, vol. 199, p. 107, 1994.

[23] S. Mentink, G. Nieuwenhuys, A. Menovsky, J. Mydosh, A. Drost, E. Frikkee, Y. Bando, T. Takabatake, P. BSni, P. Fischer, A. Furrer, A. Amato, and A. Schenck, "Crystal symmetry and electronic properties of heavy-fermion MPd_2Al_3 (M = Ce, U)," *Physica B*, vol. 199, p. 143, 1994.

[24] C. Broholm, J. Kjems, W. Buyers, P. Matthews, T. Palstra, A. Menovsky, and J. Mydosh, "Magnetic Excitations and Ordering in the Heavy-Electron Superconductor URu_2Si_2," *Phys. Rev. Lett.*, vol. 58, no. 14, p. 1467, 1987.

[25] H. Amitsuka, K. Matsuda, I. Kawasaki, K. Tenya, M. Yokoyama, C. Sekine, N. Tateiwa, T. Kobayashi, S. Kawarazaki, and H. Yoshizawa, "Pressure–temperature phase diagram of the heavy-electron superconductor URu_2Si_2," *J. Mag. Mag. Mat.*, vol. 310, p. 214, 2007.

[26] E. Hassinger, G. Knebel, K. Izawa, P. Lejay, B. Salce, and J. Flouquet, "Temperature-pressure phase diagram of URu_2Si_2 from resistivity measurements and ac calorimetry: Hidden order and Fermi-surface nesting," *Phys. Rev. B*, vol. 77, no. 11, p. 115117, 2008.

[27] E. Bauer, R. Hauser, L. Keller, P. Fischer, O. Trovarelli, J. Sereni, J. Rieger, and G. Stewart, "Onset of magnetic order in $YbCu_{5-x}Al_x$," *Phys. Rev. B*, vol. 56, no. 2, p. 56(711), 1997.

[28] D. Rojas, F. Gandra, A. Medina, L. Fernández Barquín, and J. Gómez Sal, "Kondo temperature and Heavy Fermion behavior in $Yb_{1-x}Y_xCuAl$ series of alloys," *Physica B*, vol. 536, p. 176, 2018.

[29] S. Paschen, T. Lühmann, S. Wirth, P. Gegenwart, O. Trovarelli, C. Geibel, F. Steglich, P. Coleman, and Q. Si, "Hall-effect evolution across a heavy-fermion quantum critical point," *Nature*, vol. 432, no. 7019, p. 881, 2004.

[30] S. Friedemann, T. Westerkamp, M. Brando, N. Oeschler, S. Wirth, P. Gegenwart, C. Krellner, C. Geibel, and F. Steglich, "Detaching the antiferromagnetic quantum critical point from the Fermi-surface reconstruction in $YbRh_2Si_2$," *Nature Phys.*, vol. 5, no. 7, p. 465, 2009.

[31] P. Anderson and G. Yuval, "Exact results in the Kondo problem: equivalence to a classical one-dimensional Coulomb gas," *Phys. Rev. Lett.*, vol. 23, no. 2, p. 89, 1969.

[32] K. Ueda, H. Tsunetsugu, and M. Sigrist, "Phase diagram of the Kondo lattice model," *Physica B*, vol. 186, p. 358, 1993.

[33] P. Fazekas and E. Müller-Hartmann, "Magnetic and non-magnetic ground states of the Kondo lattice," *Z. Phys. B*, vol. 85, p. 285, 1991.

[34] P. Nozières, "Impuretés magnétiques et effet Kondo," *Ann. Phys. Fr.*, vol. 10, p. 19, 1985.

[35] P. Anderson in *Valence Fluctuations in Solids* (L. Falicov, W. Hanke, and M. Maple, eds.), p. 451, North-Holland, New York, 1981.

[36] P. Coleman, "1/N expansion for the Kondo lattice," *Phys. Rev. B*, vol. 28, no. 9, p. 28(5255), 1983.

[37] N. Read, D. Newns, and S. Doniach, "Stability of the Kondo lattice in the large-N limit," *Phys. Rev. B*, vol. 30, no. 7, p. 30(3841), 1984.

[38] T. Ohashi, S.-I. Suga, and N. Kawakami, "Magnetic properties of a Kondo insulator with RKKY interaction: Extended dynamical mean field study," *J. Phys. Cond. Matt.*, vol. 17, no. 28, p. 4547, 2005.

[39] A. Fetter and J. Walecka, *Quantum Theory of Many-Particle Systems*. Minneola, NY: Dover Publications, 2003.

[40] P. Anderson, "Localized magnetic states in metals," *Phys. Rev.*, vol. 124, no. 1, p. 41, 1961.

[41] L. Roth, "New method for linearizing many-body equations of motion in statistical mechanics," *Phys. Rev. Lett.*, vol. 20, no. 25, p. 1431, 1968.

[42] B. Coqblin and J. Schrieffer, "Exchange Interaction in Alloys with Cerium Impurities," *Phys. Rev.*, vol. 185, no. 2, p. 847, 1969.

[43] P. Nozières, "Kondo Lattices and the Mott Metal–Insulator Transition," *J. Phys. Soc. Jpn.*, vol. 74, no. 1, p. 4, 2005.

[44] V. Moshchalkov and N. Brandt, "Nonmagnetic Kondo lattices," *Sov. Phys. Usp.*, vol. 29, no. 8, p. 725, 1986.

[45] E. Schuberth, J. Schupp, R. Freese, and K. Andres, "More evidence for magnetic ordering in $CeCu_6$ at mK temperatures," *Phys. Rev. B*, vol. 51, no. 18, p. 12892, 1995.

[46] J. Thompson and Z. Fisk, "Kondo-lattice–mixed-valence resistance scaling in heavy fermion $CeCu_6$ under pressure," *Phys. Rev. B*, vol. 31, no. 1, p. 389, 1985.

[47] F. Marabelli and P. Wachter, "Temperature dependence of the optical conductivity of the heavy-fermion system $CeCu_6$," *Phys. Rev. B*, vol. 42, no. 6, p. 3307, 1990.

[48] Y.-f. Yang, Z. Fisk, H.-O. Lee, J. Thompson, and D. Pines, "Scaling the Kondo lattice," *Nature*, vol. 454, no. 31, p. 611, 2008.

[49] K. Satoh, T. Fujita, Y. Maeno, Y. Onuki, and T. Komatsubara, "Low-temperature specific heat of $Ce_xLa_{1-x}Cu_6$ in magnetic field," *J. Mag. Mag. Mat.*, vol. 76-77, p. 128, 1988.

[50] D. Cromer, A. Larson, and R. J. Roof, "The crystal structure of $CeCu_6$," *Acta Cryst.*, vol. 13, p. 913, 1960.

[51] E. Goremychkin and R. Osborn, "Neutron-spectroscopy study of the heavy-fermion compound $CeCu_6$," *Phys. Rev. B*, vol. 47, no. 21, p. 14580, 1993.

[52] A. Murin, I. Shabanova, and V. Trapeznikov, "Features of the Electronic Structure of Cerium-Based Systems," *Bull. Russ. Acad. Sci. Phys*, vol. 75, no. 2, p. 207, 2011.

[53] H. Harima and A. Yanase, "Fermi surfaces of $CeCu_6$ and $CeCu_2Si_2$," *J. Mag. Mag. Mat.*, vol. 108, p. 145, 1992.

[54] E. Bauer, K. Payer, R. Hauser, E. Gratz, D. Gignoux, D. Schmitt, N. Pillmayr, and G. Schaudy, "A crossover from intermediate valence to integer valence in $Yb(Cu,Al)_5$ compounds," *J. Mag. Mag. Mat.*, vol. 104-107, p. 651, 1992.

[55] P. Bonville and E. Bauer, "A ^{170}Yb Mössbauer spectroscopy and L_{III}-edge study of the Kondo lattice $YbCu_3Al_2$," *J. Phys. Cond. Matt.*, vol. 8, p. 7797, 1996.

[56] B. Cornut and B. Coqblin, "Influence of the Crystalline Field on the Kondo Effect of Alloys and Compounds with Cerium Impurities," *Phys. Rev. B*, vol. 5, no. 11, p. 4541, 1972.

[57] T. Terashima, N. Kurita, M. Kimata, M. Tomita, S. Tsuchiya, M. Imai, A. Sato, K. Kihou, C.-H. Lee, H. Kito, H. Eisaki, A. Iyo, T. Saito, H. Fukazawa, Y. Kohori, H. Harima, and S. Uji, "Fermi surface in KFe_2As_2 determined via de Haas–van Alphen oscillation measurements," *Phys. Rev. B*, vol. 87, p. 224512, 2013.

[58] H. Glyde, "Lecture Notes," in *PHYS 813 Statistical Mechanics and Thermodynamics*, http://www.physics.udel.edu/˜glyde/PHYS813/Lectures/.

APPENDIX A

CANONICAL FREE ENERGY

In both the Kondo and AFM phases appear diagonalized Hamiltonians of the form

$$\begin{aligned} H' = & E_0 \\ & + \sum_{k,\xi} x^{+}_{\mathbf{k}}(\xi) X^{\dagger}_{\mathbf{k},+}(\xi) X_{\mathbf{k},+}(\xi) \\ & + \sum_{k,\xi} x^{-}_{\mathbf{k}}(\xi) X^{\dagger}_{\mathbf{k},-}(\xi) X_{\mathbf{k},-}(\xi)\,. \end{aligned} \tag{151}$$

The X-operators represent the eigen-operators gotten by diagonalizing a Hamiltonian H, and are in this work formed from pairs of c and f operators. ξ represents the set of all quantum numbers appropriate to the Hamiltonian in question. When $\mathbf{k}$ is explicitly written, it is to be considered separate from ξ. Accordingly, the x-values are the eigenvalues for their corresponding operators. While H' has only X operators appearing in (151), one might imagine as many operators and associated eigenvalues as are appropriate, such as Y operators with y energies. In the following discussion [58], particles will be assumed to fermionic, as is appropiate to the pseudofermion approach used elsewhere in this work.

The free energy may be written

$$\mathcal{F} = -\beta^{-1} \operatorname{Ln} Z(T,V,N),$$

(152)

such that the partition function is a function of temperature, volume, and fixed total particle number. The partition function can be written for a quantum system as a sum over all possible energy states of the system,

$$Z(T,V,N) = \sum_{\text{energy states } \sigma} \mathrm{e}^{-\beta E_\sigma} = \operatorname{Tr} \mathrm{e}^{-\beta H'}. \tag{153}$$

Writing down the particle states contributing to a single system state using the eigenstates $x(\xi)$ and their occupations n_i,

$$E_{\sigma(r)} = E_0 + n_1 x^+(\xi_1) + n_2 x^+(\xi_2) + ... + n_r x^-(\xi_r).$$

(154)

Since every system state σ has a different distribution of particles in the r states, the sum over system states amounts to summing over each possible n_i such that the requirement

$$\sum_{i=1}^{r} n_i = N \tag{155}$$

is fulfilled. Replacing the sum over σ,

$$\operatorname{Tr} \mathrm{e}^{-\beta H'} = \sum_{n_1} \sum_{n_2} \cdots \sum_{n_r} \mathrm{e}^{-\beta \left(E_0 + n_1 x^+(\xi_1) + n_2 x^+(\xi_2) + ... + n_r x^-(\xi_r) \right)}.$$

(156)

Now, a digression will be made with the grand canonical partition function. For a moment, the restriction that the total number of particles, N, is fixed will be relaxed. To this end, Z is altered like so:

$$\mathcal{Z}(T,V,\mu) = \sum_N \mathrm{e}^{\mu\beta N} Z(T,V,N) = \mathrm{Tr}\,\mathrm{e}^{-\beta(H'-\mu N)}. \tag{157}$$

The advantage in making this change is that if N is not fixed, then the sums over possible n_i in (156) are no longer related through (155). Rather, each sum over n_i becomes independent of every other. (156) becomes

$$\mathrm{Tr}\,\mathrm{e}^{-\beta(H'-\mu N)} = \sum_{n_1} \mathrm{e}^{-\beta\left(E_0+n_1x^+(\xi_1)-\mu n_1\right)} \sum_{n_2} \mathrm{e}^{-\beta\left(E_0+n_2x^-(\xi_2)-\mu n_2\right)} \ldots \sum_{n_r} \mathrm{e}^{-\beta\left(E_0+n_rx^-(\xi_r)-\mu n_r\right)}. \tag{158}$$

Because the particles under discussion are fermions, each particle state is restricted to an occupation of 0 or 1. The summations of n_i can be written as

$$\left[\mathrm{e}^{-\beta E_0} + \mathrm{e}^{-\beta\left(E_0+x^+(\xi_1)-\mu\right)}\right] \left[\mathrm{e}^{-\beta E_0} + \mathrm{e}^{-\beta\left(E_0+x^-(\xi_2)-\mu\right)}\right] \ldots \left[\left[\mathrm{e}^{-\beta E_0} + \mathrm{e}^{-\beta\left(E_0+x^+(\xi_r)-\mu\right)}\right]. \tag{159}$$

Multiplying out these terms, one sees that indeed the sum over total particle number is preserved, as each $x(\xi_i)$ in the product contributes one fermion.

It is important to note that if in the sum over N, a single value $\bar{N}$ is predominant over all others, then

$$\mathcal{Z}(T,V,\mu) = \mathrm{e}^{\mu\beta\bar{N}} Z(T,V,\bar{N}). \tag{160}$$

This is certainly the case when N grows very large, and this will be assumed to be the case here. Henceforth, the insignificant terms in the sum over N will be dropped. The immediate effect of this is to allow the factorization of E_0 terms from (159):

$$\mathrm{e}^{-\beta\bar{N}E_0}\left[1+\mathrm{e}^{-\beta\left(x^+(\xi_1)-\mu\right)}\right]\left[1+\mathrm{e}^{-\beta\left(x^-(\xi_2)-\mu\right)}\right]...\left[1+\mathrm{e}^{-\beta\left(x^+(\xi_r)-\mu\right)}\right]. \tag{161}$$

Or,

$$\mathrm{Tr}\,\mathrm{e}^{-\beta(H'-\mu\bar{N})}=\mathrm{e}^{-\beta\bar{N}E_0}\prod_{\xi,\xi'}\left[1+\mathrm{e}^{-\beta\left(x^+(\xi)-\mu\right)}\right]\left[1+\mathrm{e}^{-\beta\left(x^-(\xi')-\mu\right)}\right]. \tag{162}$$

The total particle number, having been allowed to vary, has once again been fixed. The average occupation number for a particle state is given by differentiating the logarithm of the partition function for the energy of said particle state. Using the shorthand $x^{\pm}(\xi_i)\rightarrow x_i^{\pm}$, this may be expressed as

$$\begin{aligned}
\bar{n}_i &= -\beta^{-1}\frac{\partial}{\partial x_i^{\pm}}\,\mathrm{Ln}\,Z(T,V,N)\\
&= -\beta^{-1}\frac{\partial}{\partial x_i^{\pm}}\,\mathrm{Ln}\,\mathrm{e}^{-\mu\bar{N}}\mathcal{Z}(T,V,\mu)\\
&= -\beta^{-1}\frac{\partial}{\partial x_i^{\pm}}\left(-\beta\bar{N}E_0+\mathrm{Ln}\prod_{i,i'}\left[1+\mathrm{e}^{-\beta\left(x_i^+-\mu\right)}\right]\left[1+\mathrm{e}^{-\beta\left(x_{i'}^--\mu\right)}\right]\right)\\
&= \left(1+\mathrm{e}^{\beta\left(x_i^{\pm}-\mu\right)}\right)^{-1},
\end{aligned} \tag{163}$$

which is the Fermi-Dirac function, $f(x_i^{\pm})$, elsewhere appearing in this work.

The free energy may also be expressed in terms of thermodynamic quantities as

$$\mathcal{F} = \langle E \rangle - TS. \tag{164}$$

In order to reach the right-hand side of the above, the following relationships will be used:

$$\mathrm{Ln}\left(1+e^{-\beta z}\right) = -\mathrm{Ln}\left(1-f(z)\right), \text{ and} \tag{165}$$

$$\mathrm{Ln}\left(1+e^{-\beta z}\right) = -\beta z - \mathrm{Ln}\, f(z). \tag{166}$$

Adding and subtracting, one also can write

$$\mathrm{Ln}\left(1+e^{-\beta z}\right) = f(z)\,\mathrm{Ln}\left(1+e^{-\beta z}\right) + \left(1-f(z)\right)\mathrm{Ln}\left(1+e^{-\beta z}\right). \tag{167}$$

Returning to (162), the momentum dependence will now be made explicit (bar-notation is dropped):

$$\begin{aligned}
\mathcal{F} &= -\beta^{-1}\,\mathrm{Ln}\, Z(T,V,N) \\
&= -\beta^{-1}\mathrm{Ln}\,\mathrm{e}^{-\mu N}\,\mathcal{Z}(T,V,\mu) \\
&= -\beta^{-1}\mathrm{Ln}\,\mathrm{e}^{-\mu N}\,\mathrm{Tr}\,\mathrm{e}^{-\beta(H'-\mu N)} \\
&= NE_0 - \beta^{-1}\sum_{\xi}\mathrm{Ln}\,\left[1+\mathrm{e}^{-\beta\left(x^{+}(\xi)-\mu\right)}\right] - \beta^{-1}\sum_{\xi'}\mathrm{Ln}\,\left[1+\mathrm{e}^{-\beta\left(x^{-}(\xi')-\mu\right)}\right] \\
&= NE_0 - \beta^{-1}\sum_{\mathbf{k},\xi}\mathrm{Ln}\,\left[1+\mathrm{e}^{-\beta\left(x^{+}_{\mathbf{k}}(\xi)-\mu\right)}\right] - \beta^{-1}\sum_{\mathbf{k}',\xi'}\mathrm{Ln}\,\left[1+\mathrm{e}^{-\beta\left(x^{-}_{\mathbf{k}'}(\xi')-\mu\right)}\right].
\end{aligned} \tag{168}$$

Expressing the above using (167),

$$\begin{aligned}\mathcal{F} = NE_0 &+ \sum_{\mathbf{k},\xi} x^+_{\mathbf{k}}(\xi) f\left(x^+_{\mathbf{k}}(\xi)\right) + \sum_{\mathbf{k},\xi} x^-_{\mathbf{k}}(\xi) f\left(x^-_{\mathbf{k}}(\xi)\right) \\ &+ \beta^{-1} \sum_{\mathbf{k},\xi} f\left(x^+_{\mathbf{k}}(\xi)\right) \operatorname{Ln} f\left(x^+_{\mathbf{k}}(\xi)\right) \\ &+ \beta^{-1} \sum_{\mathbf{k},\xi} f\left(x^-_{\mathbf{k}}(\xi)\right) \operatorname{Ln} f\left(x^-_{\mathbf{k}}(\xi)\right) \\ &+ \beta^{-1} \sum_{\mathbf{k},\xi} \left[1 - f\left(x^+_{\mathbf{k}}(\xi)\right)\right] \operatorname{Ln} \left[1 - f\left(x^+_{\mathbf{k}}(\xi)\right)\right] \\ &+ \beta^{-1} \sum_{\mathbf{k},\xi} \left[1 - f\left(x^-_{\mathbf{k}}(\xi)\right)\right] \operatorname{Ln} \left[1 - f\left(x^-_{\mathbf{k}}(\xi)\right)\right]\end{aligned} \tag{169}$$

The terms of (169) are manifestly separated into the form of $\mathcal{F} = \langle E \rangle - TS$. In the limit $T \to 0$, the free energy reduces to the energy, and thus to the first line of (169).

APPENDIX B

ORDERING CONSTANTS

In this appendix entry, the subject of isotropy in the ordering constants will be explored. As described elsewhere, only transverse interaction terms will be considered for magnetic ordering.

In the first section, inconsistencies will be demonstrated for a $J = 3/2$ system. In the second section, expressions will be derived which will be seen to be equivalent to those derived elsewhere.

B.1 $J = \frac{3}{2}$

The ordering constants will now be defined in a manner similar to the hybridization constants, i.e., as

$$\begin{aligned} M^{+}_{\mathbf{q},j\to j+1} &= \frac{1}{N}\sum_{\mathbf{k}}\langle f^{\dagger}_{\mathbf{k}-\mathbf{q},j+1} f_{\mathbf{k},j}\rangle \;=\; \frac{1}{N}\sum_{\mathbf{k}}\langle f^{\dagger}_{\mathbf{k},j+1} f_{\mathbf{k}+\mathbf{q},j}\rangle, \\ S^{+}_{\mathbf{q},j\to j+1} &= \frac{1}{N}\sum_{\mathbf{k}}\langle c^{\dagger}_{\mathbf{k}-\mathbf{q},j+1} c_{\mathbf{k},j}\rangle \;=\; \frac{1}{N}\sum_{\mathbf{k}}\langle c^{\dagger}_{\mathbf{k},j+1} c_{\mathbf{k}+\mathbf{q},j}\rangle. \end{aligned} \tag{170}$$

By the above definition,

$$M^{+}_{\mathbf{q},j\to j+1} = \left(M^{-}_{-\mathbf{q},j+1\to j}\right)^{\dagger}, \text{ and}$$
$$S^{+}_{\mathbf{q},j\to j+1} = \left(S^{-}_{-\mathbf{q},j+1\to j}\right)^{\dagger}. \tag{171}$$

The mean-field Hamiltonian is then

$$\begin{aligned} H_{\mathbf{q}} = &\sum_{\mathbf{k},j} \varepsilon_{\mathbf{k}} c^{\dagger}_{\mathbf{k},j} c_{\mathbf{k},j} + \lambda\Big(\sum_{\mathbf{k},j} f^{\dagger}_{\mathbf{k},j} f_{\mathbf{k},j} - N\Big) \\ &- \mathcal{J} M^{+}_{\mathbf{q},j\to j+1} \sum_{\mathbf{k},j} \frac{J(J+1) - j(j+1)}{2} c^{\dagger}_{\mathbf{k}+\mathbf{q},j} c_{\mathbf{k},j+1} \\ &- \mathcal{J} S^{+}_{\mathbf{q},j\to j+1} \sum_{\mathbf{k},j} \frac{J(J+1) - j(j+1)}{2} f^{\dagger}_{\mathbf{k}+\mathbf{q},j} f_{\mathbf{k},j+1} \\ &+ (2J+1) N \mathcal{J} \sum_{j} \frac{J(J+1) - j(j+1)}{2} M^{+}_{\mathbf{q},j\to j+1} S^{-}_{\mathbf{q},j+1\to j} \\ &+ \text{H.C.} \end{aligned} \tag{172}$$

As in (69) and (70), the state vector and Hamiltonian matrix can be written, for the conduction band, as

$$\begin{bmatrix} c^{\dagger}_{\mathbf{k},\frac{3}{2}} & c^{\dagger}_{\mathbf{k}+\mathbf{q},\frac{1}{2}} & c^{\dagger}_{\mathbf{k}+2\mathbf{q},-\frac{1}{2}} c^{\dagger}_{\mathbf{k}+3\mathbf{q},-\frac{3}{2}} \end{bmatrix} \tag{173}$$

and

$$\begin{pmatrix} \varepsilon_{\mathbf{k}} & -\frac{3}{2}\mathcal{J} M^{-}_{-\mathbf{q},\frac{3}{2}\to\frac{1}{2}} & 0 & 0 \\ -\frac{3}{2}\mathcal{J} M^{+}_{\mathbf{q},\frac{1}{2}\to\frac{3}{2}} & \varepsilon_{\mathbf{k}+\mathbf{q}} & -2\mathcal{J} M^{-}_{-\mathbf{q},\frac{1}{2}\to-\frac{1}{2}} & 0 \\ 0 & -2\mathcal{J} M^{+}_{\mathbf{q},-\frac{1}{2}\to\frac{1}{2}} & \varepsilon_{\mathbf{k}+2\mathbf{q}} & -\frac{3}{2}\mathcal{J} M^{-}_{-\mathbf{q},-\frac{1}{2}\to-\frac{3}{2}} \\ 0 & 0 & -\frac{3}{2}\mathcal{J} M^{+}_{\mathbf{q},-\frac{3}{2}\to-\frac{1}{2}} & \varepsilon_{\mathbf{k}+3\mathbf{q}}. \end{pmatrix} \tag{174}$$

The above matrix retains explicitly the J_z dependence of the ordering constants. Similarly, one can write a vector of f-operators and a matrix of λ and S terms, just as in (71) and (72), but retaining the $j \to j'$ transitions.

Example Green's functions will now be written for (172):

$$
\begin{aligned}
&D(\mathbf{k},\mathbf{q})\,\langle\langle c_{\mathbf{k},\frac{3}{2}} | c^{\dagger}_{\mathbf{k}',j'}\rangle\rangle_{i\Omega_n} \quad = \\
&\delta_{\frac{3}{2},j'}\delta(\mathbf{k}-\mathbf{k}')\Bigg((i\Omega_n-\varepsilon_{\mathbf{k}+\mathbf{q}})\left[(i\Omega_n-\varepsilon_{\mathbf{k}+2\mathbf{q}})(i\Omega_n-\varepsilon_{\mathbf{k}+3\mathbf{q}})-\frac{9}{4}\mathcal{J}^2|M_{\mathbf{q},-\frac{1}{2}\to-\frac{3}{2}}|^2\right] \\
&\qquad\qquad -4\mathcal{J}^2|M_{\mathbf{q},-\frac{1}{2}\to\frac{1}{2}}|^2(i\Omega_n-\varepsilon_{\mathbf{k}+3\mathbf{q}})\Bigg) \\
&-\delta_{\frac{1}{2},j'}\delta(\mathbf{k}+\mathbf{q}-\mathbf{k}')\frac{3}{2}\mathcal{J}M^{-}_{\mathbf{q},\frac{3}{2}\to\frac{1}{2}}\left[(i\Omega_n-\varepsilon_{\mathbf{k}+2\mathbf{q}})(i\Omega_n-\varepsilon_{\mathbf{k}+3\mathbf{q}})-\frac{9}{4}\mathcal{J}^2|M_{\mathbf{q},-\frac{1}{2}\to-\frac{3}{2}}|^2\right] \\
&+\delta_{-\frac{1}{2},j'}\delta(\mathbf{k}+2\mathbf{q}-\mathbf{k}')3\mathcal{J}^2M^{-}_{\mathbf{q},\frac{3}{2}\to\frac{1}{2}}M^{-}_{\mathbf{q},\frac{1}{2}\to-\frac{1}{2}}(i\Omega_n-\varepsilon_{\mathbf{k}+3\mathbf{q}}) \\
&-\delta_{-\frac{3}{2},j'}\delta(\mathbf{k}+3\mathbf{q}-\mathbf{k}')\frac{9}{2}\mathcal{J}^3M^{-}_{\mathbf{q},\frac{3}{2}\to\frac{1}{2}}M^{-}_{\mathbf{q},\frac{1}{2}\to-\frac{1}{2}}M^{-}_{\mathbf{q},-\frac{1}{2}\to-\frac{3}{2}}\,, \qquad (175)
\end{aligned}
$$

$$
\begin{aligned}
&D(\mathbf{k}-\mathbf{q},\mathbf{q})\,\langle\langle c_{\mathbf{k},\frac{1}{2}} | c^{\dagger}_{\mathbf{k}',j'}\rangle\rangle_{i\Omega_n} \quad = \\
&\delta_{\frac{1}{2},j'}\delta(\mathbf{k}-\mathbf{k}')(i\Omega_n-\varepsilon_{\mathbf{k}-\mathbf{q}})\left[(i\Omega_n-\varepsilon_{\mathbf{k}+\mathbf{q}})(i\Omega_n-\varepsilon_{\mathbf{k}+2\mathbf{q}})-\frac{9}{4}\mathcal{J}^2|M_{\mathbf{q},-\frac{1}{2}\to-\frac{3}{2}}|^2\right] \\
&-\delta_{\frac{3}{2},j'}\delta(\mathbf{k}-\mathbf{q}-\mathbf{k}')\frac{3}{2}\mathcal{J}M^{+}_{\mathbf{q},\frac{1}{2}\to\frac{3}{2}}\left[(i\Omega_n-\varepsilon_{\mathbf{k}+\mathbf{q}})(i\Omega_n-\varepsilon_{\mathbf{k}+2\mathbf{q}})-\frac{9}{4}\mathcal{J}^2|M_{\mathbf{q},-\frac{1}{2}\to-\frac{3}{2}}|^2\right] \\
&-\delta_{-\frac{1}{2},j'}\delta(\mathbf{k}+\mathbf{q}-\mathbf{k}')2\mathcal{J}M^{-}_{\mathbf{q},\frac{1}{2}\to-\frac{1}{2}}(i\Omega_n-\varepsilon_{\mathbf{k}+2\mathbf{q}})(i\Omega_n-\varepsilon_{\mathbf{k}-\mathbf{q}}) \\
&+\delta_{-\frac{3}{2},j'}\delta(\mathbf{k}+2\mathbf{q}-\mathbf{k}')3\mathcal{J}^2M^{-}_{\mathbf{q},\frac{1}{2}\to-\frac{1}{2}}M^{-}_{\mathbf{q},-\frac{1}{2}\to-\frac{3}{2}}(i\Omega_n-\varepsilon_{\mathbf{k}-\mathbf{q}})\,, \qquad (176)
\end{aligned}
$$

The denominator D is given by:

$$\begin{aligned} D(\mathbf{k},\mathbf{q}) = &(i\Omega_n - \varepsilon_{\mathbf{k}})(i\Omega_n - \varepsilon_{\mathbf{k}+\mathbf{q}})(i\Omega_n - \varepsilon_{\mathbf{k}+2\mathbf{q}})(i\Omega_n - \varepsilon_{\mathbf{k}+3\mathbf{q}}) \\ &-\mathcal{J}^2\left[\frac{9}{4}|M_{\mathbf{q},-\frac{1}{2}\to-\frac{3}{2}}|^2(i\Omega_n - \varepsilon_{\mathbf{k}})(i\Omega_n - \varepsilon_{\mathbf{k}+\mathbf{q}})\right. \\ &\qquad \frac{9}{4}|M_{\mathbf{q},\frac{1}{2}\to\frac{3}{2}}|^2(i\Omega_n - \varepsilon_{\mathbf{k}+3\mathbf{q}})(i\Omega_n - \varepsilon_{\mathbf{k}+2\mathbf{q}}) \\ &\qquad \left. 4|M_{\mathbf{q},-\frac{1}{2}\to\frac{1}{2}}|^2(i\Omega_n - \varepsilon_{\mathbf{k}+3\mathbf{q}})(i\Omega_n - \varepsilon_{\mathbf{k}})\right] \\ &+\frac{81}{16}\mathcal{J}^4|M_{\mathbf{q},-\frac{1}{2}\to-\frac{3}{2}}|^2|M_{\mathbf{q},\frac{1}{2}\to\frac{3}{2}}|^2. \end{aligned} \tag{177}$$

The corresponding functions for the f-f operators are had by replacing every ε term with λ and every M by S.

The J_z-dependence of the ordering constants will now be dropped. One may immediately simplify the denominator defined in (177), but the numerators of (175) and (176) differ in form even after simplification. Calculation of an ordering constant, for example $M^-_{\mathbf{q}}$, can therefore be accomplished by using either of

$$\langle\langle f_{\mathbf{k},\frac{3}{2}}|f^\dagger_{\mathbf{k}+\mathbf{q},\frac{1}{2}}\rangle\rangle_{i\Omega_n}, \text{ and } \langle\langle c_{\mathbf{k},\frac{3}{2}}|c^\dagger_{\mathbf{k}+\mathbf{q},\frac{1}{2}}\rangle\rangle_{i\Omega_n}, \tag{178}$$

or

$$\langle\langle f_{\mathbf{k},\frac{1}{2}}|f^\dagger_{\mathbf{k}+\mathbf{q},-\frac{1}{2}}\rangle\rangle_{i\Omega_n}, \text{ and } \langle\langle c_{\mathbf{k},\frac{1}{2}}|c^\dagger_{\mathbf{k}+\mathbf{q},-\frac{1}{2}}\rangle\rangle_{i\Omega_n}. \tag{179}$$

These two possible routes for an $M^-_{\mathbf{q}}$ produce two different results. Whereas in the Kondo phase, dropping the J_z-dependence of the hybridization was consistent with the creation of $2J+1$ non-interacting subsystems, in the magnetically-ordered phase it produces inconsistency.

On the path toward isotropy in the ordering constants, one might instead imagine that

$$M^{+}_{\mathbf{q},\frac{1}{2}\to\frac{3}{2}} = M^{-}_{-\mathbf{q},-\frac{1}{2}\to-\frac{3}{2}}, \tag{180}$$

which is to say that one might suppose the existence of a symmetry in the plane transverse to an external field. Identifying other such relationships,

$$\begin{aligned} M^{-}_{-\mathbf{q},\frac{3}{2}\to\frac{1}{2}} &= M^{+}_{\mathbf{q},-\frac{3}{2}\to-\frac{1}{2}}, \text{ and} \\ M^{+}_{\mathbf{q},-\frac{1}{2}\to\frac{1}{2}} &= M^{-}_{-\mathbf{q},\frac{1}{2}\to-\frac{1}{2}}; \end{aligned} \tag{181}$$

and the same will apply for the S constants. With the assumption of these symmetries, the following notation can be used:

$$\begin{aligned} M^{+}_{\mathbf{q},\frac{1}{2}\to\frac{3}{2}} &= M^{+}_{\mathbf{q},\frac{3}{2}}, \quad M^{+}_{\mathbf{q},-\frac{3}{2}\to-\frac{1}{2}} = M^{-}_{-\mathbf{q},\frac{3}{2}}, \\ M^{+}_{\mathbf{q},-\frac{1}{2}\to\frac{1}{2}} &= M^{+}_{\mathbf{q},\frac{1}{2}}, \quad \text{and so forth.} \end{aligned} \tag{182}$$

This assumption of symmetry and its concomitant short-hand notation allows for simplification of the Green's functions without producing inconsistent expressions for the ordering constants. Despite this, the self-consistency equations require greater amounts of numerical computation to solve than do the equations for the isotropic case. In view of this, the equations may be forced into even simpler forms by choosing certain ordering constants to be zero:

$$M^{+}_{\mathbf{q},\frac{3}{2}} = 0 \quad \text{leads to} \quad S^{+}_{\mathbf{q},\frac{3}{2}} = 0, \tag{183}$$

and so on. In this way, partial polarization may be used to artificially separate the system into (a) a subsystem of $J_z = \pm\frac{1}{2}$ interacting pseudofermions and a system of $J_z = \pm\frac{3}{2}$ non-interacting ones, or (b) a subsystem of $J_z = -\frac{3}{2}$ and $-\frac{1}{2}$ interacting pseudofermions

and a subsystem of $J_z = \frac{1}{2}$ and $\frac{3}{2}$ interacting ones, depending on the choice of zeroes in the ordering constants. Each case may be taken as a separate phase and included in the phase diagram in this work. Nevertheless, it is the finding of this work that at finite temperatures, both partially-polarized cases lead to lower Neel temperatures than do the isotropic case; and at zero temperature, the isotropic case is energetically favorable over the partially-polarized ones. For this reason, results for the partially-polarized anisotropic $J = \frac{3}{2}$ magnetically-ordered phase are not presented in this work.

B.2 $S = \frac{1}{2}$

In the $S = \frac{1}{2}$ magnetically-ordered system, there are only two possible changes in J_z: $-\frac{1}{2} \to \frac{1}{2}$ and $\frac{1}{2} \to -\frac{1}{2}$. Combined with the rotation matrix elements for $S = \frac{1}{2}$,

$$r_j = \sqrt{\frac{1}{2}\left(\frac{3}{2}\right) - j(j+1)} = 1 \quad \text{for } j = \pm\frac{1}{2}. \tag{184}$$

This leads the discussion down a very different path than that above for $J = \frac{3}{2}$. Beginning with the same definition of the ordering constants as in (170), and using $j = \frac{1}{2} = \uparrow$, $j = -\frac{1}{2} = \downarrow$, the linearized Hamiltonian is

$$\begin{aligned} H_{\mathbf{q}} = &\sum_{\mathbf{k},j} \varepsilon_{\mathbf{k}} c^{\dagger}_{\mathbf{k},j} c_{\mathbf{k},j} + \lambda\big(\sum_{\mathbf{k},j} f^{\dagger}_{\mathbf{k},j} f_{\mathbf{k},j} - N\big) \\ &- \frac{\mathcal{J} M^{+}_{\mathbf{q},\downarrow\to\uparrow}}{2} \sum_{\mathbf{k}} c^{\dagger}_{\mathbf{k}+\mathbf{q},\downarrow} c_{\mathbf{k},\uparrow} - \frac{\mathcal{J} S^{+}_{\mathbf{q},\downarrow\to\uparrow}}{2} \sum_{\mathbf{k}} f^{\dagger}_{\mathbf{k}+\mathbf{q},\downarrow} f_{\mathbf{k},\uparrow} \\ &+ N\mathcal{J} \sum_{j} M^{+}_{\mathbf{q},\downarrow\to\uparrow} S^{-}_{-\mathbf{q},\uparrow\to\downarrow} + \text{H.C.} \end{aligned} \tag{185}$$

With a vector

$$\psi^{\dagger}_{\mathbf{k},\mathbf{q}} = \big[c^{\dagger}_{\mathbf{k},\uparrow} c^{\dagger}_{\mathbf{k}+\mathbf{q},\downarrow} f^{\dagger}_{\mathbf{k},\uparrow} f^{\dagger}_{\mathbf{k}+\mathbf{q},\downarrow}\big], \tag{186}$$

the Hamiltonian can be expressed via the matrix

$$\mathbf{H}_{\mathbf{k},\mathbf{q}} = \begin{pmatrix} \varepsilon_{\mathbf{k}} & -\frac{1}{2}\mathcal{J}M^{-}_{-\mathbf{q},\uparrow\to\downarrow} & 0 & 0 \\ -\frac{1}{2}\mathcal{J}M^{+}_{\mathbf{q},\downarrow\to\uparrow} & \varepsilon_{\mathbf{k}+\mathbf{q}} & 0 & 0 \\ 0 & 0 & \lambda & -\frac{1}{2}\mathcal{J}S^{-}_{-\mathbf{q},\uparrow\to\downarrow} \\ 0 & 0 & -\frac{1}{2}\mathcal{J}S^{+}_{\mathbf{q},\downarrow\to\uparrow} & \lambda \end{pmatrix}. \tag{187}$$

The *c*-*c* Green's functions are

$$\begin{aligned} D(\mathbf{k},\mathbf{q})^{-1}\left\langle\left\langle c_{\mathbf{k},\uparrow}|c^{\dagger}_{\mathbf{k}',j'}\right\rangle\right\rangle_{i\Omega_n} = \quad & \delta_{\uparrow,j'}\delta(\mathbf{k}-\mathbf{k}')(i\Omega_n-\varepsilon_{\mathbf{k}+\mathbf{q}}) \\ & -\delta_{\downarrow,j'}\delta(\mathbf{k}+\mathbf{q}-\mathbf{k}')\frac{\mathcal{J}M^{-}_{-\mathbf{q},\uparrow\to\downarrow}}{2} \text{ and} \end{aligned} \tag{188}$$

$$\begin{aligned} D(\mathbf{k}-\mathbf{q},\mathbf{q})^{-1}\left\langle\left\langle c_{\mathbf{k},\downarrow}|c^{\dagger}_{\mathbf{k}',j'}\right\rangle\right\rangle_{i\Omega_n} = \quad & \delta_{\downarrow,j'}\delta(\mathbf{k}-\mathbf{k}')(i\Omega_n-\varepsilon_{\mathbf{k}-\mathbf{q}}) \\ & -\delta_{\uparrow,j'}\delta(\mathbf{k}-\mathbf{q}-\mathbf{k}')\frac{\mathcal{J}M^{+}_{\mathbf{q},\downarrow\to\uparrow}}{2}. \end{aligned} \tag{189}$$

where

$$D(\mathbf{k},\mathbf{q}) = (i\Omega_n-\varepsilon_{\mathbf{k}})(i\Omega-\varepsilon_{\mathbf{k}+\mathbf{q}}) - \frac{\mathcal{J}^2|M_{\mathbf{q}}|^2}{4}. \tag{190}$$

In the squared modulus of $M_{\mathbf{q}}$ in (190), the J_z-changes have been omitted because there is no ambiguity in them. The f-f matrices are had, as usual, by replacement of the ε terms with λ and of M with S.

The J_z-dependence of the ordering constants will now be dropped. The Hamiltonian in (187) becomes

$$\mathbf{H}_{\mathbf{k},\mathbf{q}} = \begin{pmatrix} \varepsilon_{\mathbf{k}} & -\frac{1}{2}\mathcal{J}M^{-}_{-\mathbf{q}} & 0 & 0 \\ -\frac{1}{2}\mathcal{J}M^{+}_{\mathbf{q}} & \varepsilon_{\mathbf{k}+\mathbf{q}} & 0 & 0 \\ 0 & 0 & \lambda & -\frac{1}{2}\mathcal{J}S^{-}_{-\mathbf{q}} \\ 0 & 0 & -\frac{1}{2}\mathcal{J}S^{+}_{\mathbf{q}} & \lambda \end{pmatrix}. \tag{191}$$

The above is equivalent to (118). The Green's functions become

$$\begin{aligned} D(\mathbf{k},\mathbf{q})^{-1}\left\langle\langle c_{\mathbf{k},\uparrow}|c^{\dagger}_{\mathbf{k}',j'}\rangle\right\rangle_{i\Omega_n} = \quad & \delta_{\uparrow,j'}\delta(\mathbf{k}-\mathbf{k}')(i\Omega_n-\varepsilon_{\mathbf{k}+\mathbf{q}}) \\ & -\delta_{\downarrow,j'}\delta(\mathbf{k}+\mathbf{q}-\mathbf{k}')\frac{\mathcal{J}M^{-}_{-\mathbf{q}}}{2} \text{ and} \end{aligned} \tag{192}$$

$$\begin{aligned} D(\mathbf{k}-\mathbf{q},\mathbf{q})^{-1}\left\langle\langle c_{\mathbf{k},\downarrow}|c^{\dagger}_{\mathbf{k}',j'}\rangle\right\rangle_{i\Omega_n} = \quad & \delta_{\downarrow,j'}\delta(\mathbf{k}-\mathbf{k}')(i\Omega_n-\varepsilon_{\mathbf{k}-\mathbf{q}}) \\ & -\delta_{\uparrow,j'}\delta(\mathbf{k}-\mathbf{q}-\mathbf{k}')\frac{\mathcal{J}M^{+}_{\mathbf{q}}}{2}. \end{aligned} \tag{193}$$

These functions are also equivalent to those of (126). That the ordering constants carried $\uparrow\rightarrow\downarrow$ or $\downarrow\rightarrow\uparrow$ indicators turns out to have been extraneous, since, with or without J_z-dependence, the $\pm$ of the constants could have been used without ambiguity to imply the change in J_z. In the isotropic formulation, the ordering constants are expressed via

summation as

$$S^{+}_{\mathbf{q}} = \frac{1}{N}\sum_{\mathbf{k},j} r_j \langle f^{\dagger}_{\mathbf{k},j+1} f_{\mathbf{k}+\mathbf{q},j} \rangle,$$
$$M^{-}_{-\mathbf{q}} = \frac{1}{N}\sum_{\mathbf{k},j} r_j \langle c^{\dagger}_{\mathbf{k},j} c_{\mathbf{k}-\mathbf{q},j+1} \rangle, \text{ etc..} \tag{194}$$

In the $S = \frac{1}{2}$ case, not only is summation over j replaced by only one possible choice of j, that being $-\frac{1}{2}$ or $\downarrow$, but also $r_j = 1$ for both j's. Therefore, the expressions for the ordering constants in the anisotropic $S = \frac{1}{2}$ system are equivalent to those of the isotropic $S = \frac{1}{2}$ system.